VERSÃO CORRIGIDA

TANIA GERALDINE CHURASACARI VINCES

Functional characterization of a new dark soil esterase from Amazon with hysterical behavior

Dissertation presented to the post-graduate program in Microbiology at the Institute of Biomedical Sciences at the University of São Paulo for the title of Master in Sciences

São Paulo 2020

VERSÃO CORRIGIDA

TANIA GERALDINE CHURASACARI VINCES

Caracterização funcional de uma nova esterase de solo escuro da Amazônia com comportamento histerético

Dissertação apresentada ao Programa de Pós-graduação em Microbiologia do Instituto de Ciências Biomédicas da Universidade de São Paulo, para obtenção do título de Mestre em Ciências.

São Paulo 2020

TANIA GERALDINE CHURASACARI VINCES

Functional characterization of a new dark soil esterase from Amazon with hysterical behavior

Dissertation presented to the post-graduate program in Microbiology at the Institute of Biomedical Sciences at the University of São Paulo for the title of Master in Sciences

Concentration area: Microbiology

Supervisor: Profa. Dra. Cristiane Rodrigues Guzzo Carvalho

São Paulo 2020

TANIA GERALDINE CHURASACARI VINCES

Caracterização funcional de uma nova esterase de solo escuro da Amazônia com comportamento histerético

Dissertação apresentada ao programa de pós-graduação em Microbiologia do Instituto de Ciências Biomédicas da Universidade de São Paulo para o título de Mestre em Ciências

Área de concentração: Microbiologia

Orientadora: Profa. Dra. Cristiane Rodrigues Guzzo Carvalho

São Paulo 2020

CATALOGAÇÃO NA PUBLICAÇÃO (CIP)
Serviço de Biblioteca e informação Biomédica
do Instituto de Ciências Biomédicas da Universidade de São Paulo

Ficha Catalográfica elaborada pelo(a) autor(a)

Churasacari Vinces, Tania Geraldine
Functional characterization of a new dark soil esterase from Amazon with hysterical behavior / Tania Geraldine Churasacari Vinces; orientadora Cristiane Rodrigues Guzzo Carvalho. -- São Paulo, 2020.
84 p.

Dissertação (Mestrado)) -- Universidade de São Paulo, Instituto de Ciências Biomédicas.

1. biochemical characterization. 2. enzymatic kinetics. 3. quorum quenching. I. Rodrigues Guzzo Carvalho, Cristiane, orientador. II. Título.

UNIVERSIDADE DE SÃO PAULO INSTITUTO DE CIÊNCIAS BIOMÉDICAS

Candidato(a): Tania Geraldine Churasacari Vinces

Título da dissertação: Functional characterization of a new dark soil esterase from Amazon with hysterical behavior

Orientador: Profa. Dra. Cristiane Rodrigues Guzzo Carvalho

A comissão julgadora dos trabalhos de defesa da Dissertação de Mestrado, em sessão pública realizada ...../...../ ....., considerou

( ) Aprovado(a) **( ) Reprovado(a)**

Examinador(a): Assinatura: .....
Nome: .....
Instituição: .....

Examinador(a): Assinatura: .....
Nome: .....
Instituição: .....

Examinador(a): Assinatura: .....
Nome: .....
Instituição: .....

Presidente: Assinatura: .....
Nome: .....
Instituição: .....

O presente trabalho foi realizado com apoio da PROAP/PROEX da Coordenação de Aperfeiçoamento de Pessoal de Nível Superior -Brasil (CAPES).

À minha família, meus pais Edgar e Miriam (meu anjo), meus grandes exemplos de perseverança e esforço, a vocês que me mostraram a importância da vida; aos meus irmãos Andrea e Alex que me incentivam a continuar e lutar pelos meus sonhos, obrigado por me contagiar com essa vontade de continuar e encontrar meu caminho

A mi familia, mis padres Edgar y Miriam (mi ángel), mis grandes ejemplos de perseverancia y esfuerzo, a ustedes que me mostraron lo importante de la vida; a mis hermanos Andrea y Alex quienes me animan a seguir y luchar por mis sueños, gracias por contagiarme esas ganas de seguir y encontrar mi camino

ACKNOWLEDGMENT

Agradeço aos meus pais pelo amor e apoio incondicional, pela confiança, pelas lições de vida, obrigada pai e mãe por serem meu maior exemplo de vida. Aos meus irmãos (Andrea, Alex, Blanca e Lourdes), sobrinhos, avós, tias e tios, que me incentivam a ser melhor a cada dia, isso também é para vocês.

A minha família em São Paulo:

À minha orientadora Cristiane Guzzo, por todo o apoio e oportunidades, pela orientação e conselhos, por ser além da minha orientadora uma grande amiga, muito obrigada Cris.

Minha primeira família, os meninos da Republica, obrigada Ale, Edgar, Henry, Guille Leydi, Leo, Rodrigo e Raúla por todos os momentos compartilhados ♥

À meus amigos e colegas do laboratório LEEP, Gabriel, Angel, Guilherme, Gilberto, Aureliano, Camila, Ana Paula, Vanice, Iris, Aline, Anacleto, Nathália, Daniel, Stephanie, Júlia, Gabriel, Rodolfo e Gianlucca ; obrigada por todos os momentos compartilhados, pelas longas conversas sobre literalmente qualquer assunto nos momentos de café ou bandejões, pelas nossas reuniões semanais com pizza vegetariana, pelas brincadeiras e sobre tudo pela grande e sincera amizade.

Agradecimentos especiais para Stephanie, Amzy, Cindy, Miguel y Lina, por estar tão presentes. Obrigada pelas urras! Por comemorar minhas vitórias e me encorajar nos tempos cinzentos, obrigada pelas longas ligações, pelas discussões de meus novos experimentos, pelos momentos de ocio necessários, obrigada por estar sempre presente.

A Camilo, Mario, Conchita, Valentina y Guaca que fez com que a quarentena se tornasse mais leve.

Para os professores Drs. Robson e Ethel, obrigada pelas dicas e discussões; a Marcia por facilitar nosso trabalho no laboratório.

À “Los Insectos” por sua amizade, por comemorar comigo cada nova experiência e por me encher de amor

A meus amigos do grupo de dança do IQ com quem descobri uma das melhores coisas do Brasil (o forró) e com quem o bom humor foi sempre garantido em cada aula.

Ao Prof. Chuck Farah e membros de seu laboratório, obrigada pela amizade e dicas nos experimentos, e porque estiveram dispostos a me ajudar.

Ao Prof. Sandro Marana pela ajuda nos experimentos cinéticos e as discussões.

Ao Prof. José Gregório Cabrera pela disponibilidade no uso de seus equipamentos.

Gisele y Renato, muito obrigada por toda a ajuda prestada, vocês são excepcionais!

A todas as pessoas que compartilharam seu tempo comigo desde que cheguei ao Brasil, obrigada pelos risos, experiências e aventuras.

Á PROAP/PROEX da CAPES (Coordenação de Aperfeiçoamento de Pessoal de Nível Superior -Brasil) pelo apoio financeiro, ao Instituto de Ciências Biomédicas – Departamento de Microbiologia e à Universidade de São Paulo

MUITO OBRIGADA A TODOS! ♥

RESUMO

CHURASACARI, T. **Caracterização funcional de uma nova esterase de solo escuro da Amazônia com comportamento histérico**. 2020. 67 f. Dissertacao (Mestrado em Microbiologia) – Inituto de Ciencias Biomédicas, Universidade de São Paulo, SP, 2020.

No presente estudo, caracterizamos bioquimicamente uma nova enzima com atividade esterase membro da superfamília α/β-hidrolase obtida de uma biblioteca metagenômica de solo escuro da Amazônia. Essa enzima foi nomeada como Amazonian Dark Earth Esterase 1 (Ade1). Ade1 hidrolisa ligações éster de diferentes substratos como: tributirina (cadeia alifática com 3 carbonos), Tween 20 (cadeia alifática com 11 carbonos), *p*-nitrofenil butirato (cadeia alifática com 4 carbonos), e *p*-nitrofenil octanoato (cadeia alifática com 8 carbonos) e N-hexanoil-L-homoserina lactona (C6-HSL, cadeia alifática com 6 carbonos) onde Ade1 atua interrompendo o quórum sensing pela sua capacidade de hidrolisar o autoindutor N-hexanoyl homoserine lactone, processo conhecido como quórum quenching. Dessa forma, Ade1 mostra um grau de promiscuidade em sua atividade enzimática pela sua capacidade de hidrolisar ligações ésteres de diferentes moléculas cuja estereoquímica permita coloca-la/seu ingresso no bolsillo catalítico no não seja volumosa. Ade1 é um monómero que apresento um perfil sigmoidal evidente nos ensaios de cinética, conhecido como comportamento histerético com perfil transitório tipo "burst", o que já foi reportado para outras enzimas lipolíticas. Analise de dinâmica molecular mostra que Ade1 tem dois estados conformacionais: E1 e E2 cujo equilíbrio foi dependente da concentração do substrato. Alem, a atividade enzimática de Ade1 foi influenciada pela presencia de cobalto. O estado E2 possui uma maior velocidade de hidrólise de *p*-nitrofenil octanoato do que o estado E1. Ade1 pode ser uma enzima com interesse biotecnológico por poder modular "quorum quenching" em algumas bactérias que tem C6-HSL como autoindutor.

Palavras chaves: Caraterização bioquímica, cinética enzimática, quorum quenching.

ABSTRACT

CHURASACARI, T. **Functional characterization of a new dark soil esterase from Amazon with hysterical behavior**. 2020. 67 p. Master thesis (Microbiology) – Biochemical Science Institute, University of Sao Paulo, SP, 2020.

In the present study, we biochemically characterized a new enzyme with esterase activity that is a member of the α/β-hydrolase superfamily from a metagenomic library of dark soil in the Amazon. This enzyme was named as Amazonian Dark Earth Esterase 1 (Ade1). Ade1 hydrolyses ester bonds from different substrate such as: tributyrin (aliphatic chain with 3 carbons), Tween 20 (aliphatic chain with 11 carbons), *p*-nitrophenyl butyrate (aliphatic chain with 4 carbons), and *p*-nitrophenyl octanoate (aliphatic chain with 8 carbons) and N-hexanoyl-L-homoserine lactone (C6-AHL, aliphatic chain with 6 carbons) where Ade1 interrupts the quorum sensing by its ability to hydrolyze C6-HSL autoinducer. Thus, Ade1 shows a degree of promiscuity in its enzymatic activity due to its ability to hydrolyze ester bonds of different molecules whose stereochemistry is not bulky. Ade1 is a monomer that has a sigmoidal profile evident in kinetic test, known as hysteretic behavior with a "burst" profile, which has already been reported for other lipolytic enzymes. Molecular dynamics analysis shows that Ade1 has two conformational states: E1 and E2 whose equilibrium depend on the substrate concentration. In addition, the enzymatic activity of Ade1 was influenced by the presence of cobalt. The E2 state has a higher hydrolysis rate of *p*-nitrophenyl octanoate than the E1 state. Ade1 can be an enzyme with biotechnological interest because it can modulate "quorum quenching" in some bacteria that have C6-HSL as an autoinducer.

Key words: Biochemical characterization, enzymatic kinetics, quorum quenching

LISTS OF FIGURES

LIST OF TABLES

LIST OF ABREVIATIONS AND ACRONYMS

ADE	-	Amazonian Dark earth Esterase
DNA	-	Deoxyribonucleic acid
QS	-	Quorum sensing
QQ	-	Quorum quenching
ELH	-	Enol-lactone-hydrolase
AHL	-	N-acyl-homoserine lactones
C6-HSL	-	N-hexanoyl homoserine lactone
LIST	-	Ligand-induced slow transitions
MEGA	-	Molecular Evolutionary Genetics Analysis software
2XTY	-	Yeast Extract Tryptone microbial medium
IPTG	-	Isopropyl-β-D-1-thiogalactopyranoside
DMSO	-	Dimethyl sulfoxide
p-NP	-	*p*-nitrophenyl
p-NP C4	-	*p*-nitrophenyl butyrate
p-NP C8	-	*p*-nitrophenyl octanoate
p-NP C12	-	*p*-nitrophenyl decanoate
p-NP C16	-	*p*-nitrophenyl palmitate
SEC	-	Size Exclusion Chromatography
MALS	-	Multi-angle light scattering detector
kDa	-	Kilodaltons
MW	-	Molecular weight
LAMP	-	Loop-mediated isothermal amplification
LLINs	-	Long-lasting insecticide treated bednets
RMSD	-	Root-mean-square deviation

SUMMARY

1 INTRODUCTION

1.1 Amazonian dark soil

The soil fertility is associated with the presence of great diversity of microorganisms (ZILLI; RUMJANEK; XAVIER; DA COSTA COUTINHO *et al.*, 2003). To illustrate the scale of this diversity, it is estimated that one gram of soil can contain over 10,000 species of bacteria, archaea, viruses, and eukaryotic microorganisms (TORSVIK; OVREAS, 2002). However, it is not yet been well characterized (WARD, 2002). A reason for that is the fact that, typically, only 1% of the total microbial population in a sample can be cultivated in laboratory conditions by traditional culture techniques (CURTIS; SLOAN, 2005). Nevertheless, the study of this type of environment has largely progressed from non-culture-based molecular techniques. The vast soil microbial diversity can be understood as a consequence of the multiple niches found within it: soil microorganisms are subjected to biotic stresses (as competition and parasitism) and abiotic stresses (temperature fluctuations, levels of humidity) that generate a dynamic ecosystem with different microbial functions and interactions (KAKIRDE; PARSLEY; LILES, 2010). How these multiple factors interact to the structure of the microorganism communities in the soil and how this impacts soil quality is of great interest but still a major challenge for microbiology and soil science.

In general, conventional soils from most of the Amazon rainforest is considered not very nutritious and with low fertility, and this would be related to a limited microbial diversity, however a particular type of soil called Amazon Dark Earth (ADE) is an exception. These soils are of anthropogenic origin from indigenous populations of the pre-Columbian era and present a higher content of organic matter (NAVARRETE; CANNAVAN; TAKETANI; TSAI, 2010). Specifically, ADE soils present a high concentration of carbon in the form of organic matter as result of accumulation of vegetable residues (leaves, seed shells, among others) and animal residues (bones, blood, fat, feces, shells, among others), in addition to a large amount of cinder and residues of bonfires (charcoal), and also phosphorus, calcium, magnesium, manganese, zinc, and other minor elements (DE AQUINO; MARQUES; CAMPOS; DE OLIVEIRA *et al.*, 2016). These factors may be contributing to microbial biomass. Previous studies by NAVARRETE; CANNAVAN; TAKETANI and TSAI (2010) and SILVA (2009) have explored the composition and diversity of the communities of microorganisms in ADE soils. The most abundant bacterial phyla in ADE soils were Proteobacteria (24%), Acidobacteria (10%), Actinobacteria (7%), Verrucomicrobia (8%), Firmicutes (3%), plus 36% of unclassified

bacteria (NAVARRETE; CANNAVAN; TAKETANI; TSAI, 2010), while the most abundant archaeal phyla were Crenarcheota (40%) and Euryarcheota (8%) (SILVA, 2009). Distinct environmental factors determine the metabolic activities essential for the survival of microorganisms that reside in these niches, and each species possess a great diversity of enzymes that have the potential to be used in industry. For example, the Amazon conditions ensure the presence of enzymes whose catalytic activity is highest at relatively high temperatures and acidic pH values, which can be useful for finding new enzymatic resources.

In a previous functional metagenomic study, seventy-five clones from a library of environmental DNA from Amazonian soil were found to present substantial lipolytic activity, which demonstrates the enzymatic potential of the microbial community in this region (WILLERDING; OLIVEIRA; MOREIRA; GERMANO *et al.*, 2011). In line with this approach, the genomes of uncultivated prokaryotes are known to code for a large pool of new enzymes with metabolic capabilities still completely unexplored (SIMON; DANIEL, 2011). In addition to that, in general, enzymes can present an extraordinary array of catalytic functions and substrate specificities which are often better than both synthetic and inorganic catalysts (SANGEETHA; ARULPANDI; GEETHA, 2011). Therefore, this evidences the large biotechnological potential literally hidden below ground in the Amazon, part of which we explore in-depth in this work.

1.2 Metagenomic

The study of microorganisms has become very important because they are the cause of human and animal diseases, and they also have a fundamental role in some industrial processes. Microorganisms have a great variety of forms and consist of a great variety of metabolic enzymes that allow them to colonize different ecological niches, some of them with extreme conditions. 1g of soil may contain over 100 billion microbial cells representing several thousand to over a million distinct genomic species and, only 0.1 - 1 % of microbial species are cultured by standard microbiological methods (XU, 2006), for it, is important develop and use new tools. The metagenomic technique is a tool that facilitate studying and examining the diversity of microbial communities and molecules with industrial importance, using genetic technology and bioinformatics tools. Metagenomic technique is used to find new coding genes for enzymes as proteases, lipases, amylases, alcohol oxidoreductases, antibiotics, antibiotic resistance (VOGET; LEGGEWIE; UESBECK; RAASCH *et al.*, 2003) and drugs important to the industrial (CARVALHO; CALAFATTI; MARASSI; SILVA *et al.*, 2005).

The steps generally involved in this technique are shown in **Figure 1** (THOMAS; GILBERT; MEYER, 2012) . First, taking and processing of the sample, this step is relevant, total DNA extracted must have a high quality and be representative (it must include the greatest amount of diversity present in the sample). The DNA obtained is cloned into Fosmid plasmids and thereby generate gene libraries that can be used in functional screening for metabolic activity of metagenomic clones, or sequence and annotate sequences from which it is possible to predict conserved motifs (ESCHENFELDT; STOLS; ROSENBAUM; KHAMBATTA *et al.*, 2001). The sequencing of the clones of interest can be performed by the classical Sanger method (to generate complete genomes in samples with low diversity) or next generation sequencing (NGS) by 454/Roche or Illumina/Solexa. The assembly can be based on references, where the assembly is carried out with the help of related genomes as reference with differences such as: insertion, deletion or polymorphisms; or de novo assembly, it requires assembly tools based on Brujin graphics for a large amount of data, therefore it requires more computational resources. For the annotation it is necessary to identify the genes of interest and then, by prediction, assign functions of these putative genes and taxonomic neighbors (functional annotation) using different bioinformatic tools. After a statistical analysis, the genomic data are placed in public repositories where they can be made available to other researchers.

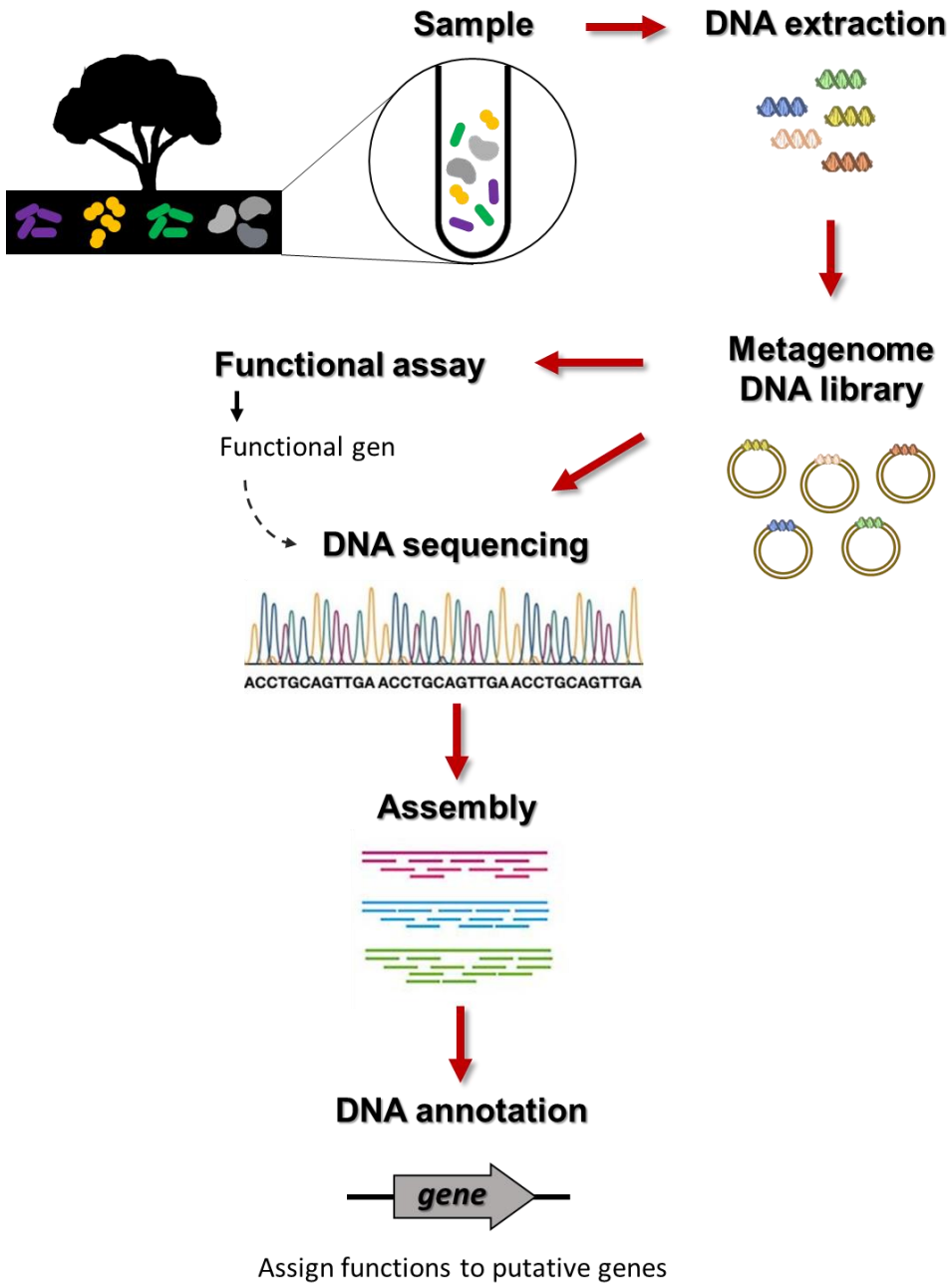

Figure 1. Metagenomic process. Sample processing, total DNA extraction and subcloning into fosmid plasmids to generate a metagenome DNA library. These clones can be used in functional screening or sequence processing and DNA assembly to annotate them and predict conserved motifs. The genomic data obtained is placed in public repositories.

1.3 Lipolytic enzyme

Lipolytic enzymes are part of the group of hydrolases, since catalysis is assisted by a water molecule (**Figure 2**). These enzymes hydrolyze ester groups of fatty acids and is composed of enzymes that have diverse amino acid sequences but related three-dimensional structure.

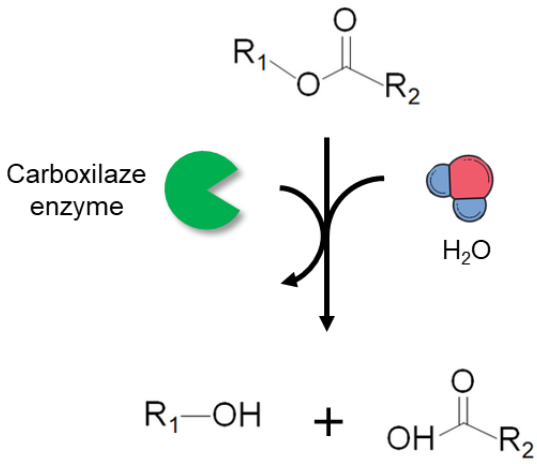

Figure 2. Carboxylase enzymes hydrolyze on carboxyl ester bond in lipids.

1.3.1 α/β-hydrolase superfamily

Lipolytic enzymes belong to the α/β-hydrolase superfamily, which present different types of catalytic activity such as carboxylic ester hydrolase, lipid hydrolase, thioester hydrolase, peptide hydrolase, halo peroxidase, dehalogenase, epoxide hydrolase, and C-C bond breaking. The α/β-hydrolases present similar tertiary structures which consist of 8 central β-strands surrounded by a variable number of α-helices (**Figure 3a**), composing two domains. The core domain is described by an 8-stranded β-sheet region surrounded by a variable number of α-helices (**Figure 3b**) (BAUER; BUCHHOLZ; PLEISS, 2020; LENFANT; HOTELIER; BOURNE; MARCHOT *et al.*, 2013; MINDREBO; NARTEY; SETO; BURKARTL *et al.*, 2016). The cap domain is composed of a variable number of α-helices (**Figure 3b**). BAINS; KAUFMAN; FARNELL and BOULANGER (2011) suggest that the cap domain is important for dimerization of two monomers and define the architecture of the active site helping in the substrate selectivity of the enzyme (MINDREBO; NARTEY; SETO; BURKARTL *et al.*, 2016). The enzymatic activity is due to the presence of a catalytic triad composed of a nucleophilic residue, a histidine, and an acidic residue. Only the histidine is invariant within the superfamily members, while the nucleophilic residue can be a serine, a cysteine, or an asparagine, and the acidic residue can be either an aspartate or a glutamate (HOLMQUIST, 2000; LEE; KWON; PARK; KIM *et al.*, 2017; MINDREBO; NARTEY; SETO; BURKARTL *et al.*, 2016; SAYER; ISUPOV; BONCH-OSMOLOVSKAYA; LITTLECHILD, 2015). Although this group of enzymes shares similar catalytic triads, they hydrolyze many different substrates and act in diverse biological contexts. The main factor contributing for the substrate specificity of each enzyme of this family could be the orientation of the additional residues

located in the pocket of the active site (FOJAN; JONSON; PETERSEN; PETERSEN, 2000). Having the same core structure and similar residues in the catalytic pocket (HOLMQUIST, 2000; MINDREBO; NARTEY; SETO; BURKARTL *et al.*, 2016), only experimental assays can be used to identify the substrates and catalytic pathways of a novel α/β-hydrolase enzyme.

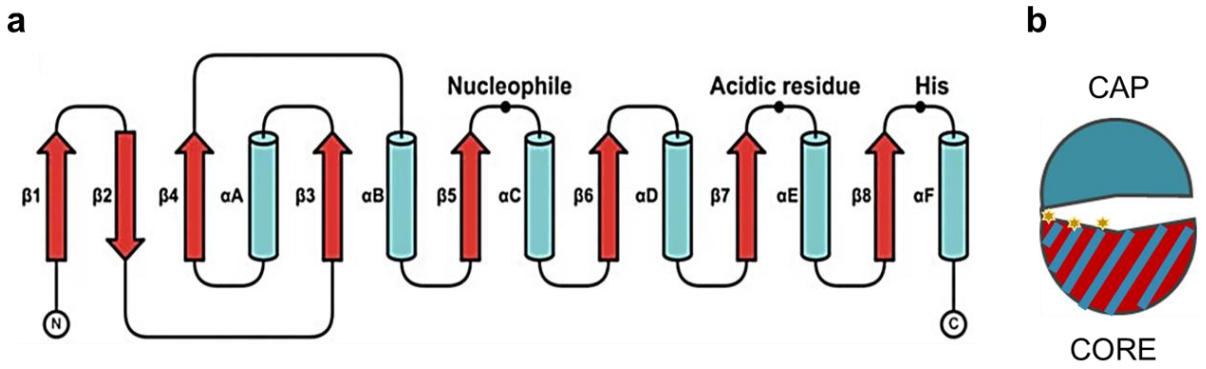

Figure 3. Schematic representation of the α/β-hydrolase fold. (a) β-sheets (1–8) are shown as red arrows and α-helices (A–F) are shown as blue cylinders. The positions of each amino acid that compose the catalytic triad is also indicated. Source: (LEVISSON; SUN; HENDRIKS; SWINKELS *et al.*, 2009). **(b)** Typical 3D representative scheme of α/β-hydrolase, signaling the CAP and CORE domains, the yellow stars, located in the catalytic pocket, represent the catalytic triad.

Lipolytic enzymes are ubiquitous (CHAHINIAN; SARDA, 2009), and can be classified in two groups: esterases (EC 3.1.1.1) and lipases (EC 3.1.1.3) (HOLMQUIST, 2000), **Figure 4**, both of which are capable of catalyzing the hydrolysis of esters into carboxylic acid and alcohol molecules, differing mainly in the size of the carbon chain of their preferred substrates (**Figure 5**). Based on their source, biochemical properties, protein fold, and the position of the catalytic triad these enzymes can be classified into one of the XXXV families (HITCH; CLAVEL, 2019).

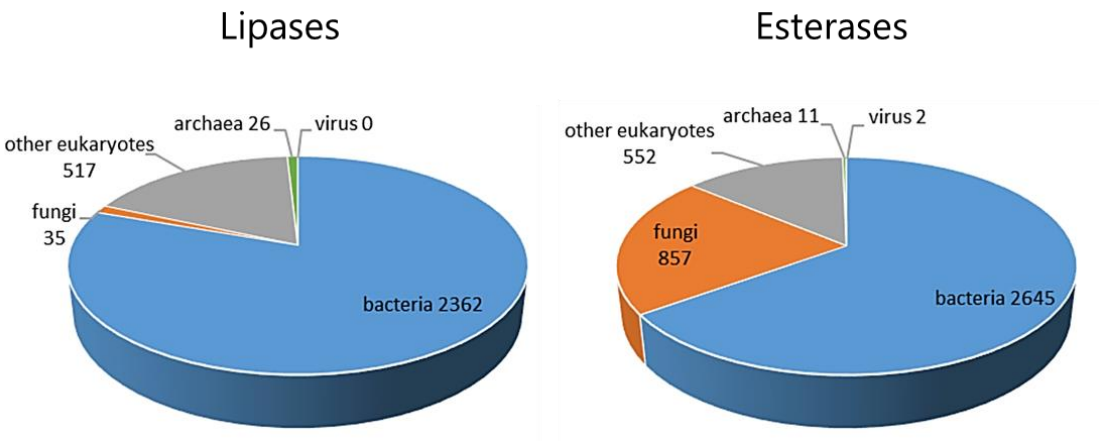

Figure 4. Lipolytic enzymes diversity. Taxonomic distribution of lipases and esterases using Brenda database (KOVACIC; BABIC; KRAUSS; JAEGER, 2019)

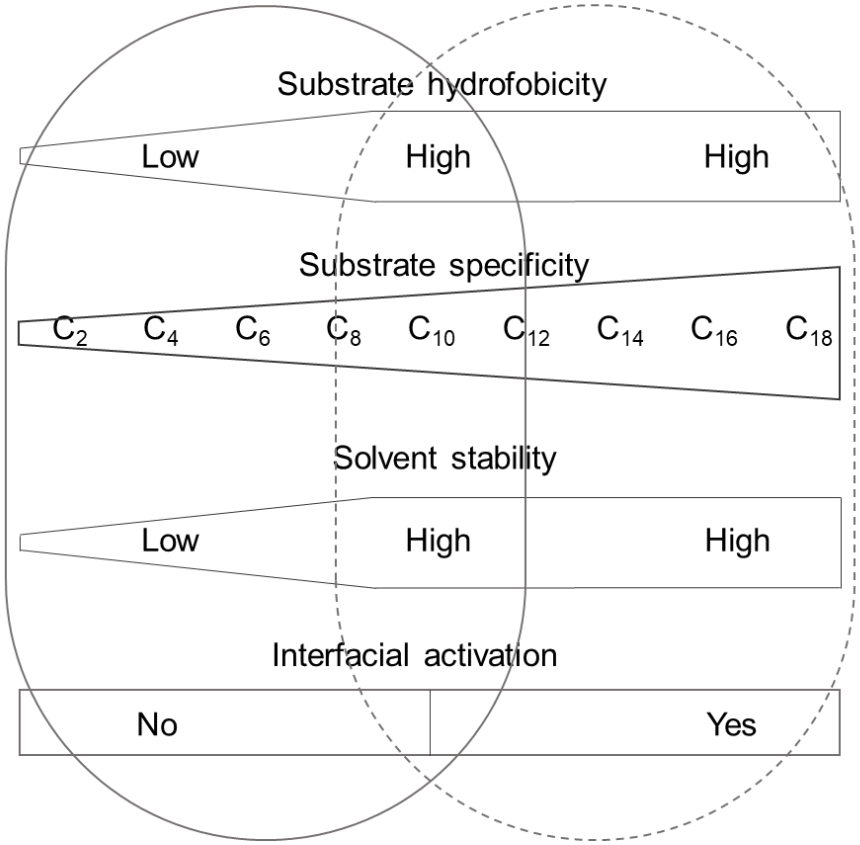

Figure 5. Lipase and esterases enzymes properties and features. (ELLEUCHE; SCHRÖDER; ANTRANIKIAN, 2016)

Lipolytic enzymes share the same physicochemical nature of their catalytic triad and present many structural similarities. These enzymes can be broadly applied in biotechnological processes due to their promiscuity, high regioselectivity, and stereoselectivity to accommodate substrate for different reactions (HOLMQUIST, 2000). Due to the characteristics that these

enzymes present, they are the third largest group with industrial importance (ELLEUCHE; SCHRÖDER; ANTRANIKIAN, 2016). Because of this, lipolytic enzymes can be used in food modifications, detergent formulations, and chemical synthesis, as well as for drug metabolism and drug detoxifications in pharmacological and clinical contexts (**Figure 6**) (MURUGAYAH; GERTH, 2019)

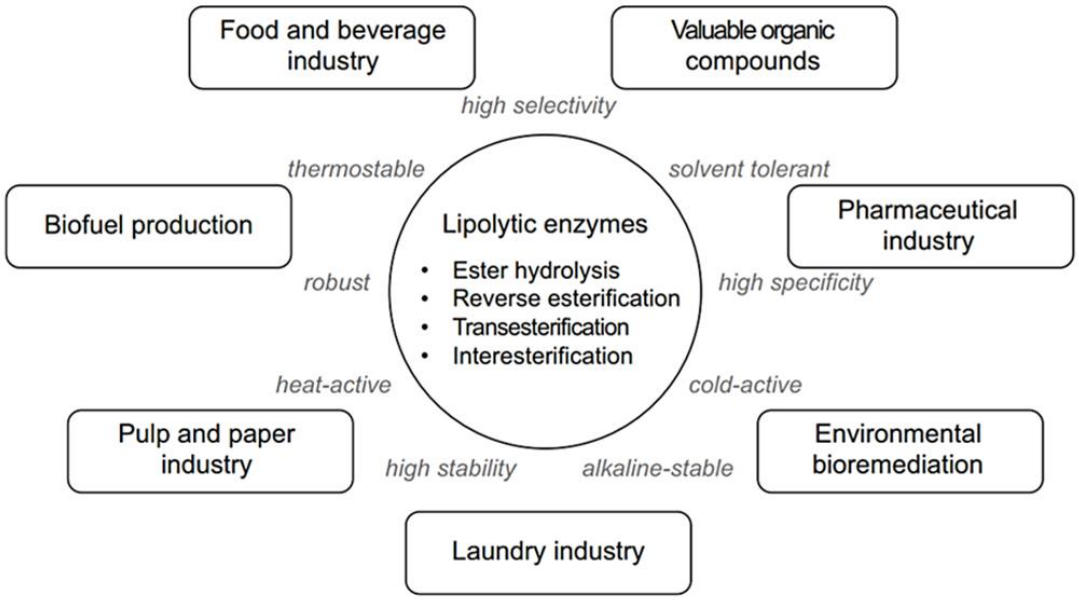

Figure 6. Industrial importance of lipolytic enzymes. Lipolytic enzyme catalyzed reactions, features and several applications (ELLEUCHE; SCHRÖDER; ANTRANIKIAN, 2016).

1.3.2 Lipases

Lipases can be distinguished from esterases by the phenomenon of interfacial activation in kinetics terms, this refer that the lipase activity increases considerably at the lipid-water interface (BRZOZOWSKI; DEREWENDA; DEREWENDA; DODSON *et al.*, 1991; VERGER, 1997). These enzymes can hydrolyze short and long chain acyl-glycerides (≥ 10 carbons) and exhibit high activity towards aggregated states of its substrates (JAEGER; STEINBUCHEL; JENDROSSEK, 1995).

1.3.3 *Esterases*

Esterases hydrolyze only short-chain esters (< 10 carbons) when its substrate is in a soluble state (ARPIGNY; JAEGER, 1999). This group of enzymes hydrolyzes ester linkages in compounds such as aryl-ester, acyl-glycerol, and carboxylic esters. Esterases are known to play important physiological roles in lipid metabolism and detoxification of xenobiotics agents in different organisms and thus are ubiquitous in nature (LEE; KWON; PARK; KIM *et al.*, 2017).

1.4 Quorum Sensing and Quorum Quenching

1.4.1 Quorum sensing

Quorum sensing (QS) is a process related to bacterial cell-to-cell communication related to bacterial cell-population density to coordinate the gene regulation and therefore the behavior to the community, changes in the cell-population density is perceived by the accumulation of signal molecule called the "autoinducer" (**Figure 7 a** and **b**) (MILLER, 2001). The autoinducer is a small signal molecule produced by bacteria that diffuses out of the bacterial cell and accumulates in the extracellular environment. QS-mediated regulation is activated by sensing high cell densities and synchronizes gene expression for coordinating inter-bacterial behavior (KALIA; PATEL; KANG; LEE, 2019; PIEWNGAM; CHIOU; CHATTERJEE; OTTO, 2020). It is also related to the regulation of biofilm formation, antibiotic resistance, bioluminescence, and bacterial virulence in different species (CHOO; RUKAYADI; HWANG, 2006; FETZNER, 2015; LIN; XU; HU; WANG *et al.*, 2003; TORRES; UROZ; SALTO; FAUCHERY *et al.*, 2017). Different types of signal molecules have been identified, but the most studied correspond to N-acyl homoserine lactone (AHL) analogs that differ in the length of their N-acyl chains (BAINS; KAUFMAN; FARNELL; BOULANGER, 2011). The side-chain length of AHL from different bacterial species is often in the range between 4 to 14 carbons connected by an ester linkage to the lactone ring. These distinct molecular structures influence the binding of the signal molecule to the receptor protein. In this manner, AHL communication systems are usually highly species-specific, but crosstalk which disturbs proper signaling may also happen (MARTINELLI; GROSSMANN; SEQUIN; BRANDL *et al.*, 2004). AHLs autoinducers regulate several functions in terrestrial and aquatic environments such as the production of exoenzymes in *Pectobacterium carotovun*, bioluminescence in *Aliivibrio fisheri*, activation of the conjugative transfer of plasmid Ti in *Agrobacterium tumefaciens*, motility in *Aeromonas hydrophyla* (TORRES; UROZ; SALTO; FAUCHERY *et al.*, 2017) and is also related with bacterial pathogenicity.

1.4.2 Quorum quenching

In nature, it has been reported the ability of different organisms (bacteria, fungi, plants, and animals) to inhibit and/or interfere with the bacterial QS, suggesting that host cells or competing organisms have developed QS-interference methods as evasion mechanisms to avoid infection or to obstruct the development of adversary microbes (TORRES; UROZ; SALTO;

FAUCHERY *et al.*, 2017). Quorum quenching (QQ) is any process involved in the disturbance of the QS through quorum sensing inhibitory molecules (QQ enzymes) or physical processes that affect the temperature and pH upon infection of animal or plant hosts, which inactivate the AHL QS signal. QQ was revealed to play a fundamental role in microbial competition (GRANDCLEMENT; TANNIERES; MORERA; DESSAUX *et al.*, 2016; MURUGAYAH; GERTH, 2019; WANG; DAI; ZHANG; HU *et al.*, 2007). One efficient way to avoid cell-to-cell communication is by the degradation or modification of autoinducers by different classes of enzymes, including lipolytic enzymes (**Table 1**). QQ enzymes have gained importance in the last years because they can be used as a strategy for the development of antibacterial, antiviral or compounds against diseases of important pathogens (GRANDCLEMENT; TANNIERES; MORERA; DESSAUX *et al.*, 2016). In this context, AHLs are one example of autoinducer well-characterized in Gram-negative bacteria that can be specifically targeted for interference by QQ (FETZNER, 2015; MURUGAYAH; GERTH, 2019). The lactonases are examples of QQ enzymes that show a high range of selectivity, from highly promiscuous, to considerably both stereo and regio-specific facilitating the correct accommodation of the substrate. Enol-lactone-hydrolases (ELH) are the more selective family, which convert the terminal cyclic structure 3-oxoadipate-enol-lactone (β-ketoadipate-enol-lactone) into β-ketoadipate as part of the β-ketoadipate pathway, where the aromatic metabolites - protocatechuate and catechol - are turned into intermediaries of the Krebs cycle (BAINS; KAUFMAN; FARNELL; BOULANGER, 2011). Another group of enzymes are Acyl homoserine lactone lactonases (AHL lactonases) that inactivate acyl homoserine lactone molecules by hydrolyzing the lactone ring (LIN; XU; HU; WANG *et al.*, 2003).

A common organism used to investigate QS and QQ in laboratory studies (also used in this work) is *Chromobacterium violaceum*, a Gram-negative bacterium which resides in the tropical and subtropical areas. This bacterium synthesizes an easily measured violet pigment – called violacein – as a result of biofilm formation by quorum sensing signaling. The autoinducer is a N-hexanoyl homoserine lactone (C6-HSL). C6-HSL binds to the transcriptional regulator (CviR) and activates the expression of the violacein biosynthetic genes (Fig. 3b) as well as other virulence factors (CHOO; RUKAYADI; HWANG, 2006). Quorum-quenching by degradation of homoserine lactones is observed in different classes of enzymes (such as lactonases, decarboxylases, acylases, and deaminases) that cleaves the molecule at different sites (**Figure 7c**) (CZAJKOWSKI; JAFRA, 2009; DONG; ZHANG, 2005).

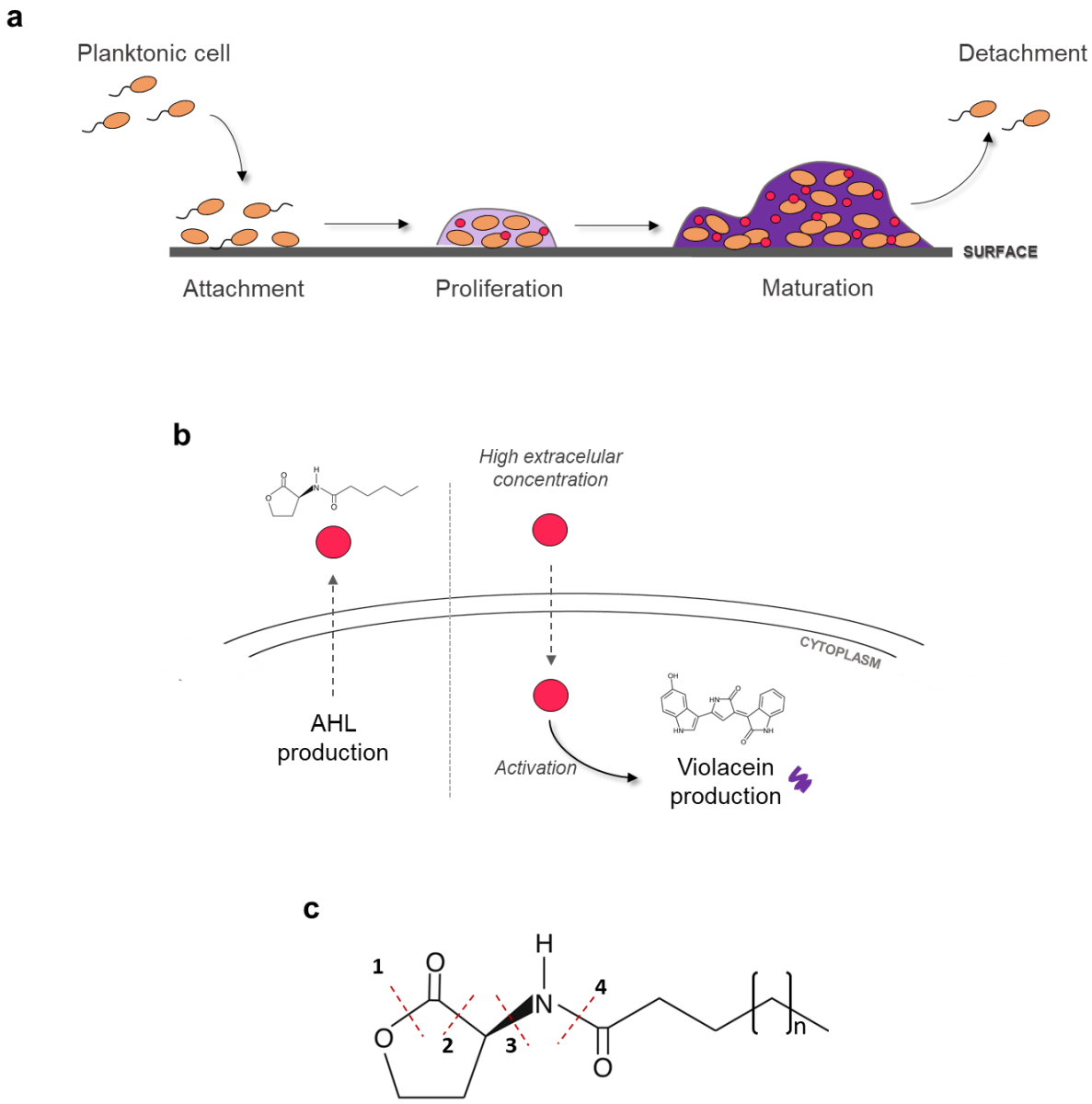

Figure 7. Quorum sensing and biofilm formation in *Chromobacterium violaceum*. (**a**), Biofilm formation, **Attachment**, the planktonic cells attach to a surface, the interaction with the surface is by protein-protein interaction; **Proliferation**, these cells divide and increase their population density, and form microcolonies; **Maturation** or colonization, the microcolony growth, bacterial cells secret extracellular matrix and virulence factors regulated by quorum sensing (QS), until some cells detach from the matrix and return to a planktonic state (JOO; OTTO, 2012). (**b**), Regulation of violacein production mediated by the autoinducer acyl homoserine lactone (AHL). AHL (red ball) is secreted out of the bacteria upon adhesion to a surface, when AHL is in high concentrations, enter into bacteria by diffusion and, activates the transcription of violacein (purple pigment). (**c**) Possible ways of enzymatic degradation of AHLs, broken lines mark the position of possible sites cleaved by the following enzymes: 1, lactonase; 2, decarboxylase; 3, deaminase and 4, acylase (CZAJKOWSKI; JAFRA, 2009).

Table 1. Quorum-quenching activity of different α/β-hydrolase members. The table has information about the enzyme, organism, biological function and if there is the presence or absence of metal during the enzymatic catalysis. There are proteins that have quorum-quenching activity.

Name	Organism	Function	Reference	metal/no metal
3-hydroxy-palmitic acid methyl ester hydrolases	metagenomic library	esterase	(LEE; KHAN; TAO; CHOI *et al.*, 2018)	no metal
XB7, XB122 and XB102	*Pseudomonas aeruginosa* and *Stenotrophomonas maltophilia*	esterase	(ACHARI; RAMESH, 2018)	Cu^{2+} and Ca^{2+} enhanced activity of quorum quenching enzymes
Est816 esterase	Turban Basin metagenomic library	esterase	(LIU; CAO; FAN; LIU *et al.*, 2016)	no metal
Porcine kidney acylase (PKA), Porcine liver esterase (PLE) and horse liver esterase (HLE)	Porcine and Horse	acylase and esterase	(KISCH; UTPATEL; HILTERHAUS; STREIT *et al.*, 2014)	no metal
Est816 esterase	Turban Basin metagenomic library	esterase	(FAN; LIU; LIU, 2012)	Ca^{2+}, activity increases slightly
QsdH	*Pseudoalteromonas byunsanensis*	esterase	(HUANG; LIN; YI; LIU *et al.*, 2012)	Zn^{2+}, Ni^{2+}, Cu^{2+}, Ba^{2+}, Mg^{2+}, Sr^{2+}, Ca^{2+} and Mg^{2+}
beta-hydroxypalmitate methyl ester hydrolase	*Ideonella* sp. 0-0013	esterase	(SHINOHARA; NAKAJIMA; UEHARA, 2007)	Fe^{2+} and Sr^{2+} inhibit the enzyme activity. Na^{+} and K^{+} promoted enzymatic activity. Zn^{2+} and Mg^{2+} do not inhibit

				the enzymatic activity.
3-hydroxy-2-methyl-4(1H)-quinolone 2,4-dioxygenase (Hod)	*Paenarthrobacter nitroguajacolicus*	oxidoreductase	(PUSTELNY; ALBERS; BULDT-KARENTZOPOULOS; PARSCHAT *et al.*, 2009)	no metal
AiiA	*Bacillus* sp. strain DMS133	esterase	(MAHMOUDI; NADERI; VENTURI, 2013)	no metal
AiiSSl – 5 EstSl – 5	*Altererythrobacter* sp. S1-5	esterase	(WANG; GUAN; PAIN; KAKSONEN *et al.*, 2019)	no metal
AHL-lactonase	*Rhodococcus* sp. BH4	esterase	(RYU; LEE; MIKOLAITYTE; KIM *et al.*, 2020)	no metal
BpiB05	metagenome-derived hydrolase	esterase	(BIJTENHOORN; SCHIPPER; HORNUNG; QUITSCHAU *et al.*, 2011)	Ca^{2+} for carrying out the catalysis
AqdC	*M. abscessus* subsp. *abscessus*	esterase	(BIRMES; SARING; HAUKE; RITZMANN *et al.*, 2019)	no metal
3-Phenyllactic acid (PLA) inhibitor	Lactobacillus species	-	(CHATTERJEE; D'MORRIS; PAUL; WARRIER *et al.*, 2017)	no metal
AiiAQSI-1	*Bacillus* sp. strain QSI-1	esterase	(ZHANG; ZHUANG; GUO; MCLEAN *et al.*,	no metal

			2019)	
EstDL30	Alluvial soil metagenomic library	esterase	(TAO; LEE; WU; KIM *et al.*, 2011)	no metal
EST816 esterase	Metagenomic library construction and AHL-lactonase screening	esterase	(LIE; MEYER; PEDERSEN, 2014)	no metal
AHL-lactonase	Human, mouse and fish	esterase	(YANG; WANG; WANG; DONG *et al.*, 2005)	Ca^{2+}
AHL lactonase	*Bacillus thuringiensis*	esterase	(LIU; MOMB; THOMAS; MOULIN *et al.*, 2008)	Zn^{2+}
Phosphotriesterase-Like Lactonases (PLLs) family	*Vulcanisaeta moutnovskia*	esterase	(HIBLOT; BZDRENGA; CHAMPION; CHABRIERE *et al.*, 2015)	Co^{2+}
N-acyl-homoserine lactone acylase	*Ralstonia solanacearum* GMI1000	acylase	(CHEN; CHEN; LIAO; LEE, 2009)	no metal
no enzymatic characterization	*Acinetobacter lactucae* strain QL-1	no enzymatic characterization	(YE; ZHOU; FAN; BHATT *et al.*, 2019)	no metal
no enzymatic characterization	*Acinetobacter* sp. XN-10	no enzymatic characterization	(ZHANG; LUO; ZHANG; FAN *et al.*, 2020)	no metal

AidF	*Ochrobactrum intermedium* D-2	esterase	(FAN; YE; LI; BHATT *et al.*, 2020)	no metal
FadY	*Acinetobacter lactucae* strain QL-1	acyl-CoA synthetase	(YE; ZHOU; XU; ZHANG *et al.*, 2020)	no metal
no enzymatic characterization	no microrganism was characterized	acylase	(BAO; HOSOE; HOSOMI; TERADA, 2020)	no metal
GcL	*Geobacillus caldoxylosilyticus*	esterase	(BERGONZI; SCHWAB; ELIAS, 2016)	Co^{2+}
PFE esterase	*Burkholderia anthina* HN-8	esterase	(YE; ZHANG; FENG; FAN *et al.*, 2020)	no metal
PLL (PTE-like lactonase)	*Mycobacterium avium* subsp. *paratuberculosis* K-10	esterase	(CHOW; WU; YEW, 2009)	no metal
QsdA	*Rhodococcus erythropolis*	phosphodiesterase	(UROZ; OGER; CHAPELLE; ADELINE *et al.*, 2008)	no metal

1.5 Hysteretic behavior

An enzymatic reaction has two important components, enzyme and substrate, which will form a complex and after catalysis a product will be generated. Esterases metabolize ester groups in alcohol and a carboxylic acid, and kinetic data tend to fit the Michaelis-Menten model (ADLER; KISTIAKOWSKY, 1962; HOFFSTEE, 1952; KHUSHAIRI; SAMAD; RAHMAN; YUSSOF *et al.*, 2020; SHENOUDA; GREEN; SULTATOS, 2009; VERPOORTE; MEHTA; EDSALL, 1967; ZAINOL; ISMAIL, 2019). The Michaelis-Menten model assumes that the enzymatic activity is one enzyme, one substrate and one product. Along the enzymatic turnover, the enzyme structure conformation is restored for recognizing the substrate and performs a new catalytic cycle (QIAN; ELSON, 2002).

The cooperative activity profile is a feature of some enzymes capable of forming an oligomeric state or having multiple substrate binding sites (VIVOLI; PANG; HARMER, 2017). Interestingly, some monomeric enzymes with one substrate site, show enzymatic activity with a profile of cooperativity (sigmoidal curve) and this characteristic is due to a slow conformational change in response to the environment, substrate or product, also known as hysteresis (**Figure 8**). The conformational changes of a protein can occur from very short periods of time (nano or picoseconds) to hours (BEHZADI; HATLESKOG; RUOFF, 1999; FRIEDEN, 1979). Behzadi and collaborators determined the influence of pH on the activity of an alkaline phosphatase, they observed that the change of activity was generated by a change in the conformation of the enzyme (conformational adaptation to pH), being that when increasing the pH the enzyme presented less activity (BEHZADI; HATLESKOG; RUOFF, 1999). The hysterical behavior of certain enzymes is due to the mechanism to control the activation or inhibition of a biological pathway using only one enzyme, **Figure 9** (FRIEDEN, 1979). One example of that is the modulation of the enzymatic activity based on the oscillation of a metabolic pathway benefiting the cell (CORNISH-BOWDEN; CÁRDENAS, 1987; JIANG; LI; MORROW; POTHUKUCHY *et al.*, 2019). The hysteresis can be observed by the transient kinetics as a burst or lag in substrate utilization, most of them belong to a metabolic (some detailed examples in **Table 2**). Burst is described as a change from an initially higher rate of activity to a lower steady state rate. Lag is described as a change from a lower rate to a higher rate of activity. There are two ways that cause enzymatic hysteresis behavior: Mnemonic model and Ligand-induced slow transitions model, described below (AINSLIE; NEET; SHILL, 1972; PORTER; MILLER, 2012).

1.5.1 Mnemonic model

In mnemonic model, the enzyme can keep or "recalls" a structural memory substrate-induced by a short time after releasing the product. In this model the enzyme present two conformational state, one of low affinity state and other of high affinity state. In absence of substrate, the enzyme maintains only one conformational state. However, the presence of substrate cause a second conformational state of the enzyme (with high or low affinity) and, the two conformational states with different initial velocities are present in equilibrium in the reaction (PORTER; MILLER, 2012).

1.5.2 Ligand-induced slow transitions model

The ligand-induced slow transitions (LIST) the enzyme visits two structural conformations in absence or presence of substrate. In contrast, the presence of substrate changes the equilibrium constant of the structural conformation states. In addition, the LIST behavior can be caused not only by the substrate but also by the solvent nature or pH (FOLOGEA; KRUEGER; MAZUR; STITH *et al.*, 2011; KE; KLIBANOV, 1998; STAN; BHATT; DE CAMARGO, 2020).

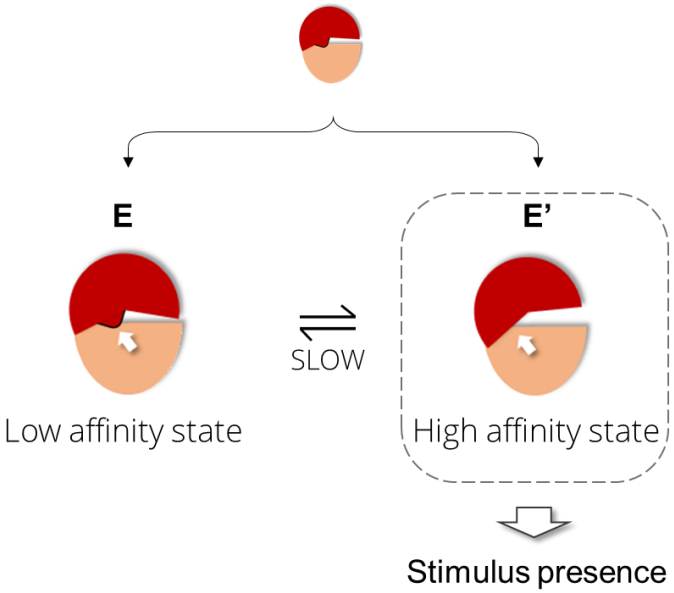

Figure 8. Hysteresis or Hysteretic behavior. When an enzyme presents two conformational states in response to a stimulus (presence or concentration of, substrate or product). Here, both states, E and E ', will be in equilibrium, being that the process of change of state, from E' to E, is slow; furthermore, the presence of E 'is conditional on the stimulus

Table 2. Different enzymes with hysteresis behavior. The table has information about the enzyme, transient behavior, organism, biological function and if there is the presence or absence of metal during the enzymatic catalysis and/or optimal pH.

Enzyme	Organism	Description	Transient behavior	pH and/or metal	Reference
Pyruvate kinase	*Bacillus licheniformis*	ATP obtention (metabolism)	Lag	Activation by Mg^{2+} (7.0 to 7.4)	(TUOMINEN; BERNLOHR, 1971)
Glutamine phosphoribosylpyro-phosphate amidotransferase	Pigeon liver	Purine biosynthesis (metabolism)	Lag	Activation by Mg^{2+} (8.0)	(ROWE; COLEMAN; WYNGAARDEN, 1970)
D-Lactate dehydrogenase	*Escherichia coli*	Fermentation – anaerobic metabolic pathway (metabolism)	Lag	(6.4 – 7.5)	(TARMY; KAPLAN, 1968)
Hexokinase B	*Saccharomyces cerevisiae*	Regulation of carbon catabolism (Metabolism)	Burst	(7.0 - 8.0)	(SHILL; NEET, 1971)
StEH1	*Solanum tuberosum*	Epoxide hydrolase	Burst	Activation by temperature change (8.0 to 9.0)	(LINDBERG; DE LA FUENTE REVENGA; WIDERSTEN, 2010)
BChE	Human	Butyrylcholinesterase (metabolism)	Burst	Activation by hydrostatic pressure, temperature, salts and pH	(MASSON; SCHOPFER; FROMENT; DEBOUZY *et al.*, 2005)
Nitrate reductase	*Cucurbita maxima*	Nitrate assimilation (metabolism)	Lag	Activation by phosphorylation state (7.5)	(LILLO; RUOFF, 1992)

Alkaline phosphatase (AP)	Calf intestine	metabolic process	?	(10.0 to 10.8)	(BEHZADI; HATLESKOG; RUOFF, 1999)
Trehalase	*Artemia salina*	Dormancy embryos	?	Intracellular pH dependent	(HAND; CARPENTER, 1986)
ProT (Protrombin)	Mamals	Blood coagulation	Lag	Activation by VWbp (Von Willebrand factor-binding protein, a glycoprotein) (7.0)	(KROH; PANIZZI; BOCK, 2009)
PFK (Phosphofructokinase)	Rat myocardium	Glycolysis (metabolism)	Lag	Alkalinization of the myocardium muscle	(HAND; CARPENTER, 1986)
ATP synthase	*Polytomella sp.*	Energy transduction in mitochondria (Oxidative phosphorylation metabolism)	Lag	Temperature (8.0)	(VILLAVICENCIO-QUEIJEIRO; PARDO; GONZÁLEZ-HALPHEN, 2015)
Oxidized fructose 1,6-bisphosphatase	Chloroplast	Glycolysis	Lag	fructose 2,6-bisphosphate (substrate analog), magnesium (7.5)	(SOULIE; RIVIERE; RICARD, 1988)
α-Acetyl-galactosaminidase	Bovine	Glycoside hydrolase	Lag	(4.7 - 5.0)	(WEISSMANN; WANG, 1971)
Homoserine dehydrogenase	*Escherichia coli*	Synthesis of L-homoserine	Burst	K^+ (6.9)	(BARBER; BRIGHT, 1968)

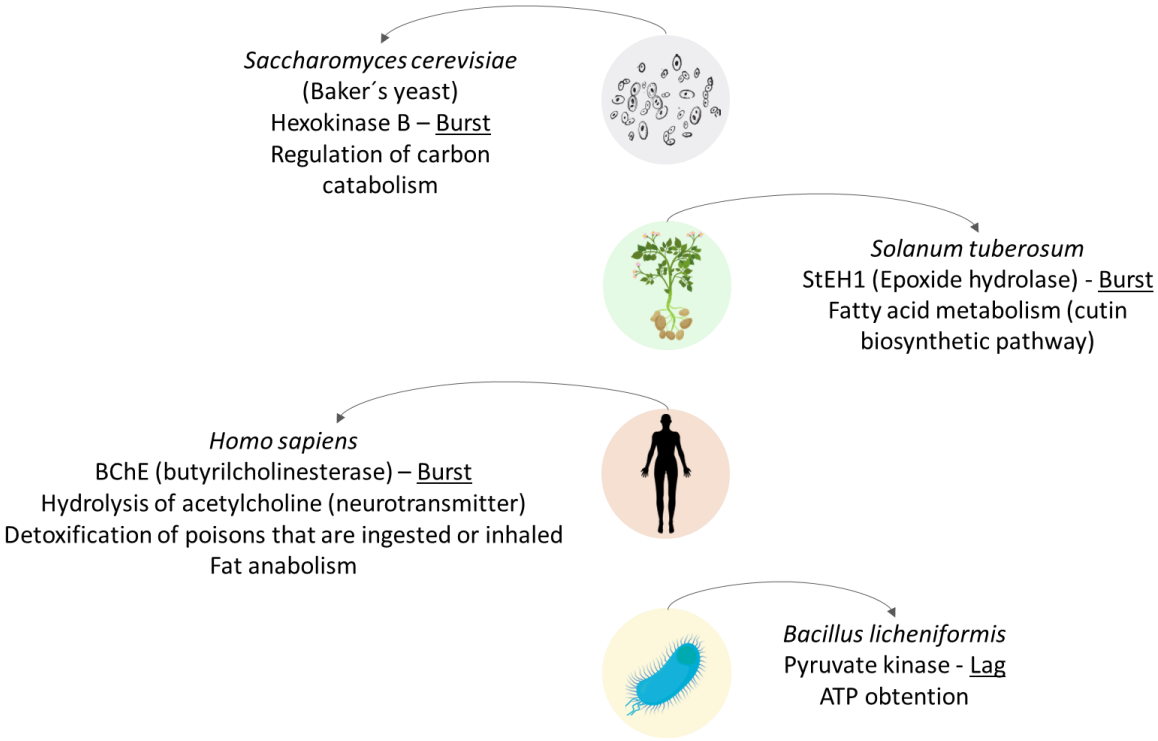

Figure 9. Examples enzymes with hysteretic behavior. Have been reported in different taxonomic groups, these enzymes participate in the regulation of different metabolic pathways in the metabolism of each organism**.**

1.6 Structural analysis of Ade1 (Amazonian Dark Earth esterase 1)

A novel lipolytic enzyme from a metagenomic library of Amazonian Dark Earth soils from the Amazonian Rainforest in Brazil, Ade1 (Amazonian Dark Earth Esterase 1), was characterized by CARVALHO (2015). Initially, the best four clones from the metagenomic library that showed triacyl-hydrolase activity were used to generate sub-libraries to identify the gene responsible for the expression of lipolytic enzymes. Using DNA sequencing with the "genome walking" technique, was identified an open reading frame (ORF) with a gene of around 804 pb, which codifies a protein of 268 residues (without a signal peptide) and theoretical molecular weight (MW) of 29.3 kDa. Ade1 was expressed, purified, and structurally characterized. Ade1 crystals diffracted at a resolution of 2.3 Å, the asymmetric unit contained four monomer units (**Figure 10 a** and **b**), and the special group was $P2_12_12_1$. The structural comparison of the Cα from structures of chains A, B, C, and D show a RMSD of 0.26 Å. This difference is located in the loop between α5 and α6 located at the beginning of the CAP domain of Ade1 (**Figure 10c**). It is an unstructured region in chain A (residues 138-140) and in chain C (residues 138 - 143).

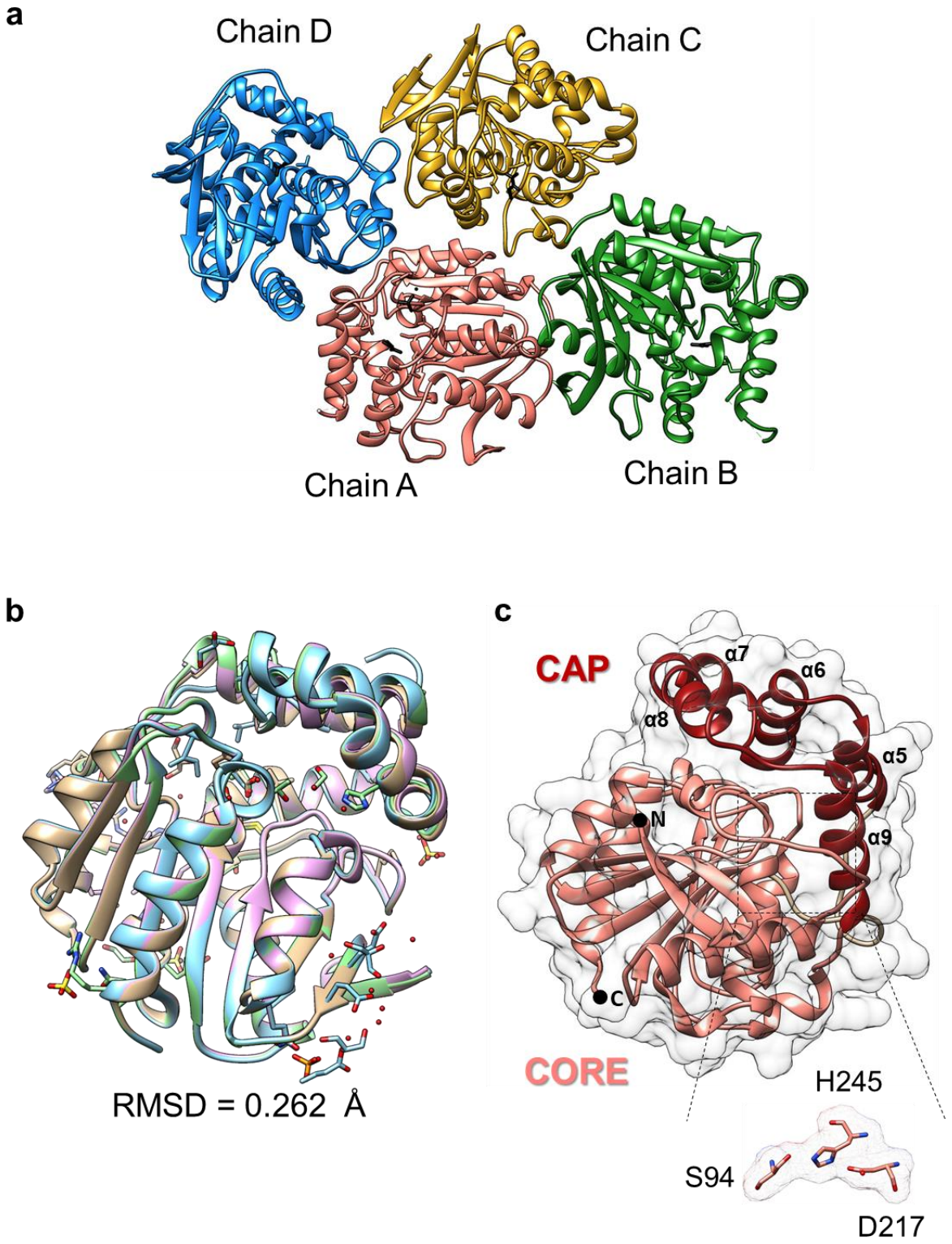

Figure 10. Ade1 structural characterization. (a) Show in ribbon four molecules contained in the asymmetric unit, chain A, B C and D, no interaction was observed between monomers. **(b)** Structural comparison of the C-alpha indicates that high similarity between the chains. **(c)** Ade1 monomer, results in dark red the Cap domain (α5 – α9), and in salmon the Core domain, highlight the catalytic triad (Ser94, His245 and D217) in the interface between these two domains, the black dots indicate the N- and C-terminal.

It was observed that Ade1 show a typical structure of an α/β-hydrolase (**Figure 10c**) with a conserved catalytic triad (Ser94, Asp217, and His245) in the core domain, while only Ser94 and His245 are exposed in the catalytic pocket. The Ser residue was found in the conserved pentapeptide motif G-X-**S**-X-G ("X" is any residue) and is important to start the catalytic cycle. Previous data classified Ade1 as a carboxylase, and two substrates were identified: tributyrin and *p*-nitrophenyl octanoate (*p*-NP C8). No influence of divalent metals ($CaCl_2$, $CoCl_2$, $MgCl_2$, $NiCl_2$) was observed in the enzymatic activity. However, when testing Zn, the activity decreased by 50%.

Two mutants were generated, S94A was used to abolish activity, and S94C was created to determine if the enzyme could acquire a cysteine hydrolase activity (dienelactone activity) (SCHLÖMANN; SCHMIDT; KNACKMUSS, 1990). None of the mutants presented any activity. Circular dichroism assays showed that in all constructions the structural conformation was preserved. Furthermore, it was observed that the Cys118 residue from the native polypeptide chain was at a distance of 2.88 Å from Cys94 in the Ade1 structure and was proposed that both could be interacting by forming a disulfide bond.

2 OBJECTIVES

In this work, we aimed to perform functional studies and kinetic characterization of a new esterase, Ade1, from an Amazon Dark Earth soil metagenomic library.

2.1 Specific objectives

- Express and purify Ade1 and its mutants ($Ade1_{S94A}$ and $Ade1_{S94C}$).
- Determine Ade1 substrates
- *In vivo* effect of Ade1 as a quorum quenching N-acyl-homoserine lactonase using *Chromobacterium violaceum.*
- Test different conditions to determine the optimal Ade1 kinetics parameters.

3 MATERIALS AND METHODS

3.1 Ade1 classification by phylogenetic analysis.

Amino acid sequence of Ade1 was subjected to protein phylogenetic analysis to classify it using the lipolytic enzyme data list constructed by HITCH and CLAVEL (2019), who divided bacterial lipolytic enzymes by sequence similarities and function into thirty-five families. Multiple sequence alignments (one per family and Ade1) were performed using the Clustal Omega program (SIEVERS; HIGGINS, 2018), the multiple sequence alignment obtained were trimming using Trimal -gt 0.5 to remove sections that have up to 50% gaps. It was visually examined and edited using the Jalview 2.11.0 program. A phylogenetic tree was constructed with the neighbor-joining method using 1,000 bootstraps replicated by means of Molecular Evolutionary Genetics Analysis software (MEGA-X, version 5) for determining the relationship between Ade1 and bacterial lipolytic enzymes. All primary sequences used, except Ade1, were obtained from the UniProt database.

3.2 $Ade1_{WT}$, $Ade1_{S94C}$ and $Ade1_{S94A}$ mutant's clones.

The $Ade1_{WT}$, $Ade1_{S94A}$ and $Ade1_{S94C}$ plasmids were designed and constructed from samples of Amazonian soil in the student's doctoral thesis work of Cecília Carvalho (CARVALHO, 2015) at the Protein Structure and Evolution Laboratory. The constructions were cloned into pET-28a vectors to add a 6×His-tag at the N-terminus of each protein, to facilitate the purification step.

3.3 Expression and of Ade1 and Ade1 mutants.

Ade1 and its mutants ($Ade1_{S94A}$ and $Ade1_{S94C}$) were expressed in *E. coli* strain BL21(DE3) RP (Stratagene). Cells were grown at 37 °C in 2XTY medium (16 $g.l^{-1}$ of bacto-tryptone, 10 $g.l^{-1}$ of yeast extract and 5 $g.l^{-1}$ sodium chloride) supplemented with kanamycin 50 $\mu g.ml^{-1}$ (Gibco) and chloramphenicol 30 $\mu g.ml^{-1}$ (Sigma Aldrich) Expression of recombinant Ade1 was induced up to OD600 1, adding 1 mM isopropyl-β-D-1-thiogalactopyranoside (IPTG) and maintained in growth by 4 h at 37°C. Bacterial cells were collected by centrifugation and resuspended in lysis buffer (50 mM Tris-HCl pH 7.5, 100 mM NaCl, 20% (w/v) sucrose, 10% glycerol (v/v), 0.03% (v/v) Triton X-100, and 0.03% (v/v) Tween 20) and then lysed by sonication. Ade1 was purified by affinity chromatography using a HisTrap Chelating HP column (GE Healthcare Life Sciences) previously equilibrated with Elution Buffer A (50 mM Tris-HCl pH 7.5, 100 mM NaCl, and 20 mM imidazole). Bound proteins were eluted in a range between 20- and 500-mM

imidazole. Elution fractions were analyzed by 15% SDS-PAGE. All elution fractions containing Ade1 were concentrated through Amicon Ultra-4 Centrifugal filters (Merck Millipore) with a 3 kDa membrane cutoff. In order to remove the high concentrations of imidazole and salts, the protein solution was dialyzed in 10 mM Tris-HCl pH 7.5 and 10 mM NaCl.

3.4 Lipolytic activity of Ade1 using Petri dishes.

Lipolytic activity (esterase or lipase) was tested using *E. coli* BL21(DE3) RP cells containing the expression vector for Ade1 and Ade1 mutants. The assays were performed using 10 µl cell culture (OD_{600} 0.8) on the top of LB solid medium supplemented with kanamycin 50 $\mu g.ml^{-1}$ (Gibco), chloramphenicol 30 $\mu g.ml^{-1}$ (Sigma Aldrich) and 0.5% (v/v) tributyrin (with a chain size of four carbons) or 0.5 % (v/v) triolein (with a chain size of eighteen carbons), in the presence of 1 mM IPTG. Tributyrin and triolein were emulsified in the medium by sonication. Petri dishes were incubated at 37 °C for 36 hours for observing the substrate hydrolysis. All assays were performed in triplicates.

3.5 Tweenase activity.

Tweenase test was performed with an LB solid medium containing a final concentration of 4 mM $CaCl_2$, supplemented with 1% (v/v) of Tween 20 or Tween 80. A volume of 10 µl (1 $mg.ml^{-1}$) of each purified protein ($Ade1_{WT}$ and $Ade1_{S94C}$) was applied on top of the solid medium and incubated at 37 °C for 24 hours to observe the precipitation of the reaction products (fatty acids) with the Ca^{2+} in the medium (LEE; KARBUL; CITARTAN; GOPINATH *et al.*, 2015; RAMNATH; SITHOLE; GOVINDEN, 2017).

3.6 *In vivo* activity of Ade1 as acyl-homoserine lactonase.

Acyl-homoserine lactonase (C6-HSL) hydrolase *in vivo* activity was tested using *Chromobacterium violaceum* ATCC 12472. This bacterium produces homoserine lactones (AHL), that mediate quorum sensing and activate violacein production, a purple compound measurable by spectrophotometry (WANG; GUAN; PAIN; KAKSONEN *et al.*, 2019). The amount of violacein in the culture medium was used as an indirect measure of HSL concentration. The assay was performed measuring the violacein production in the presence and absence of recombinant Ade1. The assay was performed using two different Ade1 concentrations (100 $\mu g.ml^{-1}$ and 300 $\mu g.ml^{-1}$) in 20 ml of LB culture medium containing *C.*

violaceum with initial OD_{600} of 0.1. Cultures were incubated at 30 °C for 24 h at 150 rpm and aliquots of 100 µl were taken every 1 h. Each aliquot was centrifuged at 1300 rpm for 4 min and the pellet was resuspended in 100 µl of DMSO to extract the total violacein. Afterward, new centrifugation was done at 1,300 rpm for 4 minutes to eliminate the residual bacteria. The samples were then used to measure the absorbance at OD_{585} (WANG; GUAN; PAIN; KAKSONEN *et al.*, 2019). All measurements were performed in triplicates.

3.7 *In vitro* effect of Ade1 in cocaine hydrolysis.

The cocaine hydrolysis by Ade1 enzyme was tested using two different protein concentrations (200 nM and 800 nM final concentration). Cocaine at the concentration of 1.98 mmol/L was dissolved in a buffer containing 100 mM Tris-HCl pH 8.0, 50 mM NaCl, Ade1 in a final volume of 1 500 µl. The reaction was incubated overnight at 30 °C. The reaction was stopped by adding 500 µl of glycine buffer at pH 2.0. The products of the enzymatic reaction were identified by liquid chromatography mass spectroscopy MS/MS and processed by Mauricio Yonamine's laboratory at the Department of Clinical and Toxicological Analysis of the Faculty of Pharmaceutical Sciences of USP.

3.8. Esterase kinetics assays by colorimetric measurements.

In order to determine the optimal enzymatic condition of Ade1, different substrates were tested considering lengths of aliphatic carbon chains (*p*-nitrophenyl butyrate, *p*-nitrophenyl octanoate, *p*-nitrophenyl laurate, and *p*-nitrophenyl palmitate). They were dissolved in methanol and diluted ranging the concentrations from 20 to 150 nM. To verify the optimum pH of Ade1 for hydrolyzing the *p*-nitrophenyl octanoate, pH was ranged from 4.0 to 9.0. Furthermore, we monitored if the presence of different divalent metals (Ca^{2+}, Co^{2+}, Mg^{2+}, Ni^{2+}, and Zn^{2+} at final concentrations of 0, 3 and 6 mM) could affect the enzymatic catalysis. All experiments were performed at different reaction buffers (100 mM Tris-HCl, 50 mM NaCl, 0.5% (v/v) Triton X-100, ranging the pH from 4.0 to 9.0) 600 µM *p*-nitrophenyl octanoate and Ade1. All enzymatic assays were performed in 96 well microplates at 30 °C. Kinetic reactions were started from the automated addition of Ade1, keeping as final condition was 100 mM Tris-HCl pH 8.0, 50 mM NaCl, 0.5% (v/v) Triton X-100, 600 µM p-nitrophenyl octanoate and 36 nM Ade1. Reaction product, *p*-nitrophenyl ester, was measured at absorbance 347 nm along 20 s for a total time of 5 minutes using a Synergy H1 Hybrid Multi-Mode Microplate Reader (BioTek, Winooski, VT, USA). Calibration curves were performed using different concentrations of *p*-nitrophenyl ester.

Measurement of absorbance was kept in the same conditions performed in the Ade1 kinetic assays. Linear regression and standard deviation calculations were performed for determining the initial reaction velocities through reaction production as time function. Michaelis-Menten and Hill-Langmuir models were compared for finding the best representation of the experimental data using the extra sum-of-squares F test in the Graph Path PRISM program. All kinetic assays were performed in triplicates.

3.9 Determination of Ade1 molecular weight by Multi-angle light scattering coupled with size exclusion chromatography (SEC-MALS)

The oligomeric state and molecular weight of Ade1 were determined through Multi-angle light scattering coupled with size exclusion chromatography (SEC-MALS). This assay was performed loading 500 µl of Ade1 (2 $mg.ml^{-1}$) in the presence and absence of 6 mM Co^{2+} into a Superdex 200 10/300 GL column (GE Healthcare) pre-equilibrated in 50 mM Tris-HCl pH 8, and 400 mM NaCl and the column was coupled to a miniDAWN TREOS multi-angles light scattering detector/multi-angle light scattering detector (MALS) and a Optilab TrRX refractive index detector/refractive index detector. All reactions were kept on ice for 1 h before being applied to the size exclusion column. The reactions were eluted at 0.5 $ml.min^{-1}$ at 23 °C. Data was analyzed using OriginLab software. The assays were performed in triplicate.

3.10 System setup for molecular dynamics simulations.

Next, we ran molecular dynamics simulations to study the structural aspects of wild-type and $Ade1_{S94C}$. Ade1 structure (PDB ID: 6EB3) was prepared using the UCSF chimera tool (PETTERSEN; GODDARD; HUANG; COUCH *et al.*, 2004) by removing co-crystallized hetero groups and water molecules. $Ade1_{S94C}$ was obtained from a site-directed mutation in wild-type Ade1 using the Maestro software (academic v. 2020-1). From the Ade1 structure, protonation states of ionizable residues were computed in an aqueous implicitly environment at pH 8.0 from the Maestro software academic v. 2020-1 using PROPKA module. Then, all glutamic and aspartic residues were represented as unprotonated; H12, H47, H106, H125, H163, H165, H245 were designed as a δ-tautomer; H89, H172, and H189 were modeled as an ε-tautomer; all glutamic residues were kept with neutral charge; arginine and lysine residues were assumed with a positive charge; the N- and C-terminal, corresponding to M1 and V268, were converted to charged groups. To build a holo-state of Ade1 and $Ade1_{S94C}$, we docked the substrate into the binding site using as reference the crystal reaction product. To that end, we

obtained the three-structure representation of the substrate tributyrin employing the conjugate gradient algorithm associated with the Merck molecular force field (MMFF94s) using Avogadro software v. 1.2.1. Subsequently, the substrate was submitted to a genetic algorithm (GA) for performing the molecular docking into binding pockets of Ade1 and $Ade1_{S94C}$ using the genetic optimization for ligand docking software (GOLD, v. 2019-2). The poses were evaluated by a force field-based fitness function (gold score) and selected for molecular dynamics studies.

All molecular dynamics runs were performed in the Groningen machine for chemical simulation software (GROMACS, v. 5.1.5) using optimized potentials for liquid simulations for all atoms (OPLS-AA) force field. Substrate topology was built in LigParGen web-based service and the 1.14*CM1A charges were kept on substrate atoms. All systems were then explicitly solvated with TIP3P water models in a cubic box and neutralized with the addition of 5 sodium ions and minimized until to reach a maximum force of 10.0 $kJ.mol^{-1}$ or a maximum number of steps in 5000. Final dimensions were approximately 72.6 × 72.6 × 72.6 Å, including 5 sodium ions and around 11000 *TIP3P* waters. The systems were equilibrated consecutively in isothermal-isochoric (NVT) and isothermal-isobaric (1 bar; NpT) ensembles, both at temperature 300 K for 1 ns. All simulations were then performed in a periodic cubic box considering the minimum distance of 1.0 nm between any protein atom and cubic box walls. Molecular dynamics runs were performed for 100 ns. Finally, to determine the size of the angle formed between the core and cap domains, we used the coordinates formed by the main chain oxygen atoms from the V127, L27, and M194 residues. Distance calculation, hydrogen bonding occupancy percentage, root-mean-square deviation (RMSD) and root-mean-square fluctuation (RMSF) were determined using the GROMACS modules and virtual molecular dynamics (VMD; v. 1.9.1).

4 RESULTS AND DISCUSSION

4.1 Bioinformatic analysis of a novel esterase enzyme

In order to classify the Ade1 family, we performed a phylogenetic tree analysis using 35 lipolytic enzyme families (HITCH; CLAVEL, 2019) (**Figure 11a**). In particular, they belong to the family V, presenting a conserved motif GX**S**XGG (NACKE; WILL; HERZOG; NOWKA *et al.*, 2011) (**Figure 11b**). Members of family V are found in mesophilic bacteria (*Pseudomonas oleovorans*, *Haemophilus influenzae*, *Acetobacter pasteurianus*) as well as in cold-adapted (*Moraxella* sp., *Psyhrobacter immobilis*) or heat-adapted (*Sulfolobus acidocaldarius*) bacteria (ARPIGNY; JAEGER, 1999). These members share sequence similarity ranging between 20 to 25 % with non-lipolytic enzymes. Among these are the epoxide hydrolases, dehalogenases, and haloperoxidase, which also have an α/β-hydrolase fold (MISAWA; CHION; ARCHER; WOODLAND *et al.*, 1998; VERSCHUEREN; SELJEE; ROZEBOOM; KALK *et al.*, 1993).

In other hand, we perform multiple sequence alignment with Ade1 orthologous proteins that identified conserved residues (numbering corresponding to the Ade1 protein and the bold residues are from the catalytic triad): $Y_{13}E_{14}x_2G_{17}$, $G_{19}xP_{21}$, G_{27}, W_{35}, $Y_{52}D_{53}N_{54}R_{55}G_{56}XG_{58}$, P_{63}, Y_{67}, $A_{73}xD_{75}$, $A_{88}x_3G_{92}x\mathbf{S_{94}}xG_{96}G_{97}x_2A_{100}Q_{101}$, $L_{114}xL_{116}x_2T_{119}x_2G_{122}G_{123}$, A_{192}, $I_{205}x_2P_{208}xL_{210}x_3G_{214}x_2\mathbf{D_{217}}$, $P_{221}x_2N_{224}$, $A_{229}x_2I_{232}$, $\mathbf{H_{245}}$, and F_{262} (**Figure 12**). Mapping these conserved residues on the Ade1 structure, we observed that most of them are located in the core domain (**Figure 13a**). However, the G_{122}, G_{123}, and A_{192} residues are located in the cap domain. G_{122} and G_{123} residues may be related to increasing the flexibility in the cap domain allowing its opening and closing. Interestingly, G_{17}, G_{19}, P_{21}, G_{58}, P_{63}, P_{208}, P_{221}, and G_{123} are conserved and are exposed to the solvent (**Figure 13b**). In addition, G_{27}, W_{35}, Y_{52}, S_{94}, and H_{245} residues are into the enzymatic pocket and are partially exposed to the solvent (except S_{94}, which is more exposed) (**Figure 13c**). Interestingly, the catalytic triad is a D_{217}, completely buried in the catalytic pocket, and helps to establish the H_{245} charge. S_{94} seems to be exposed to interact with the substrate and initiate the process of catalysis mediated by a nucleophilic attack by the serine. G_{27}, W_{35}, and Y_{52} also are conserved residues and may play a key role in the catalytic process, however to prove that new assay must be done.

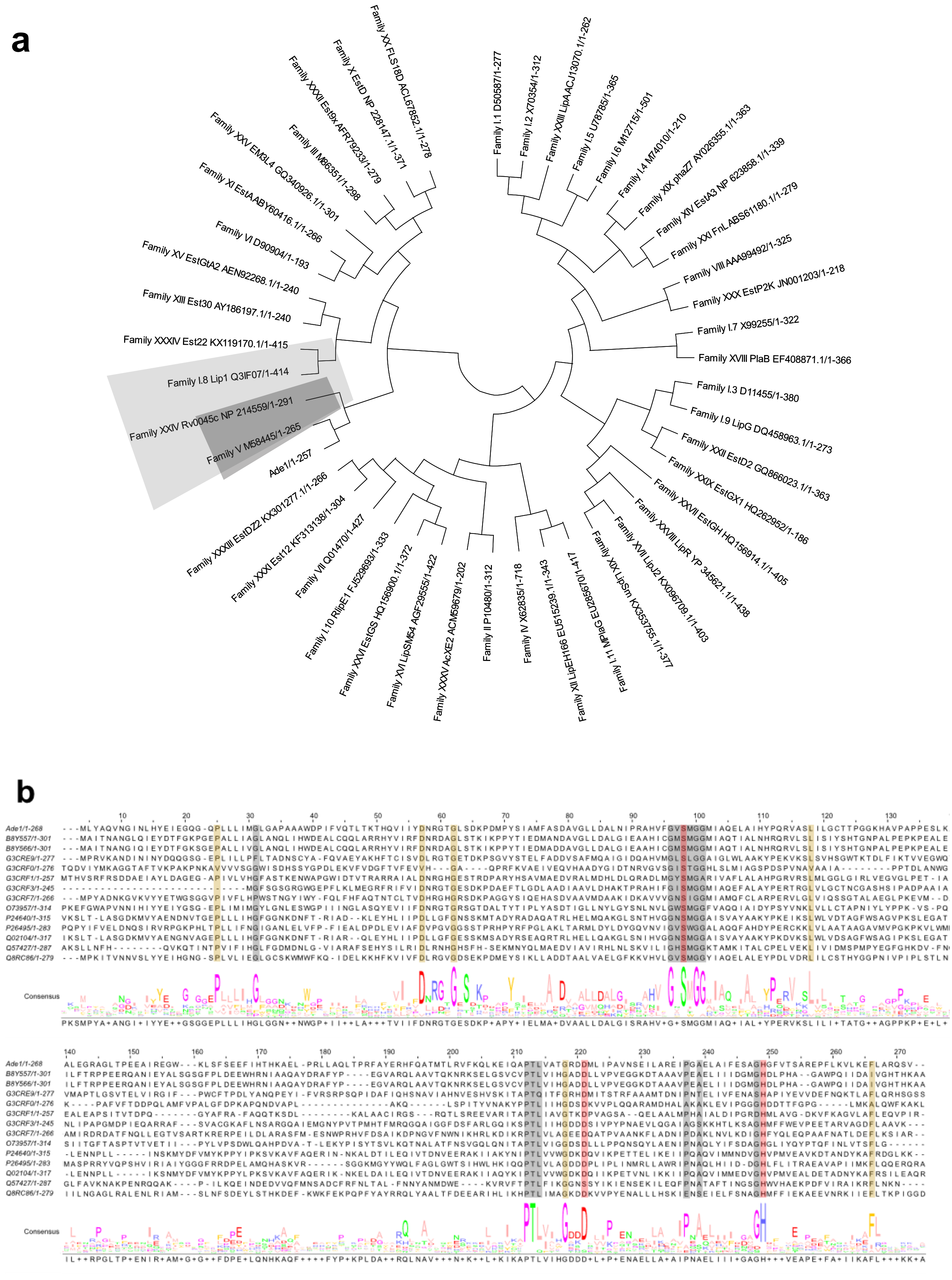
a
Family XX FLS18D ACL67852.1/1-278
Family X EstD NP 228147.1/1-371
Family XXXII Est9x AFR79233/1-279
Family III M86351/1-298
Family XXV EM3L4 GQ340926.1/1-301
Family XI EstA ABY60416.1/1-266
Family VI D90904/1-193
Family XV EstGtA2 AEN92268.1/1-240
Family XIII Est30 AY186197.1/1-240
Family XXXIV Est22 KX119170.1/1-415
Family I.8 Lip1 Q3IF07/1-414
Family XXIV Rv0045c NP 214559/1-291
Family V M58445/1-265
Ade1/1-257
Family XXXIII EstDZ2 KX301277.1/1-266
Family XXXI Est12 KF313138/1-304
Family VII Q01470/1-427
Family I.10 RlipE1 FJ529693/1-333
Family XXVI EstGS HQ156900.1/1-372
Family XVI LipSM54 AGF29555/1-422
Family XXXV AcXE2 ACM59679/1-202
Family II P10480/1-312
Family IV X62835/1-718
Family XII LipEH166 EU515239.1/1-343
Family I.11 MPlaG EU285670/1-417
Family XIX LipSm KX353755.1/1-377
Family XVII LipJ2 KX096709.1/1-403
Family XXVIII LipR YP 345621.1/1-438
Family XXVII EstGH HQ156914.1/1-405
Family XXIX EstGX1 HQ262952/1-186
Family XXII EstD2 GQ866023.1/1-363
Family I.9 LipG DQ458963.1/1-273
Family I.3 D11455/1-380
Family XVIII PlaB EF408871.1/1-366
Family I.7 X99255/1-322
Family XXX EstP2K JN001203/1-218
Family VIII AAA99492/1-325
Family XXI FnLABS61180.1/1-279
Family XIV EstA3 NP 623858.1/1-339
Family XIX phaZ7 AY026355.1/1-363
Family I.4 M74010/1-210
Family I.6 M12715/1-501
Family I.5 U78785/1-365
Family XXIII LipAACJ13070.1/1-262
Family I.2 X70354/1-312
Family I.1 D50587/1-277
b
Ade1/1-268
B8Y557/1-301
B8Y566/1-301
G3CRE9/1-277
G3CRF0/1-276
G3CRF1/1-257
G3CRF3/1-245
G3CRF7/1-266
O73957/1-314
P24640/1-315
P26495/1-283
Q02104/1-317
Q57427/1-287
Q8RC86/1-279
Consensus

Figure 11. Classification and structural characterization. (**a**) The polar tree layout representing the comparison analysis of the amino acid sequence of 35 families of lipolytic enzymes currently described by HITCH and CLAVEL (2019). The tree was constructed using the MEGA 10.1.8 program with the neighbor-joining algorithm. Each branch corresponds to one representative from each family with their respective UniProt ID. In the light gray it is shown the family groups that contained sequences more similar to Ade1; in dark gray it is shown the best candidate family to which Ade1 would belong, family V; (**b**) Multiple sequence alignment of Ade1 and proteins belonging to family V. The catalytic triad is highlighted in red; in gray are shown the motifs conserved only in family V; and in yellow are shown other conserved amino acids. B8Y557: Lip 5 from an uncultured bacterium; B8Y566: Lip 17 from an uncultured bacterium; G3CRE9: AB hydrolase-1 domain-containing protein from an uncultured organism; G3CRF0: Peptidase_S9 domain-containing protein from an uncultured organism; G3CRF1: AB hydrolase-1 domain-containing protein from an uncultured organism; G3CRF3: AB hydrolase-1 domain-containing protein from an uncultured organism; G3CRF7: AB hydrolase-1 domain-containing protein from an uncultured organism; O73957: Sal from *Sulfolobus acidocaldarius*; P24640: Lip3 from *Moraxella* sp. (strain TA144); P26495: Poly(3-hydroxy alkanoates) depolymerase from *Pseudomonas oleovorans*; Q02104: Lip 1 from *Psychrobacter immobilis*; Q57427: Putative esterase/lipase HI_0193 from *Haemophilus influenzae*; Q8RC86: Predicted hydrolase or acyltransferase from *Caldanaerobacter subterraneus* subsp. *tengcongensis*.

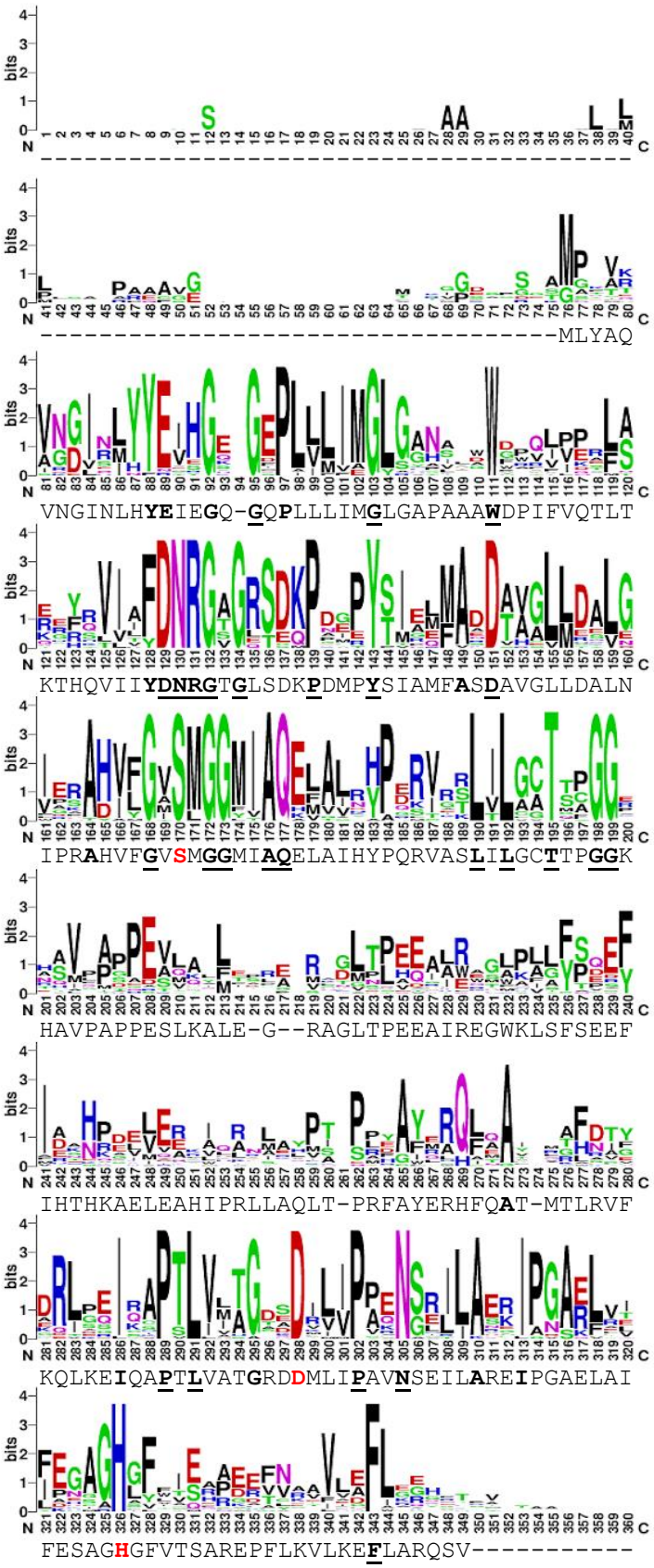

Figure 12. Multiple sequence alignment analysis of Ade1 analyzed in WEBLOGO web-based service. A multiple sequence alignment was performed with proteins that share an identity of more than 45% and coverage above 80% relative to the Ade1 sequence to make a WEBLOGO presentation. The residues in bold are highly conserved and those underlined are absolutely conserved. The catalytic triad residues are colored in red, S_{94}, D_{217} and H_{245}.

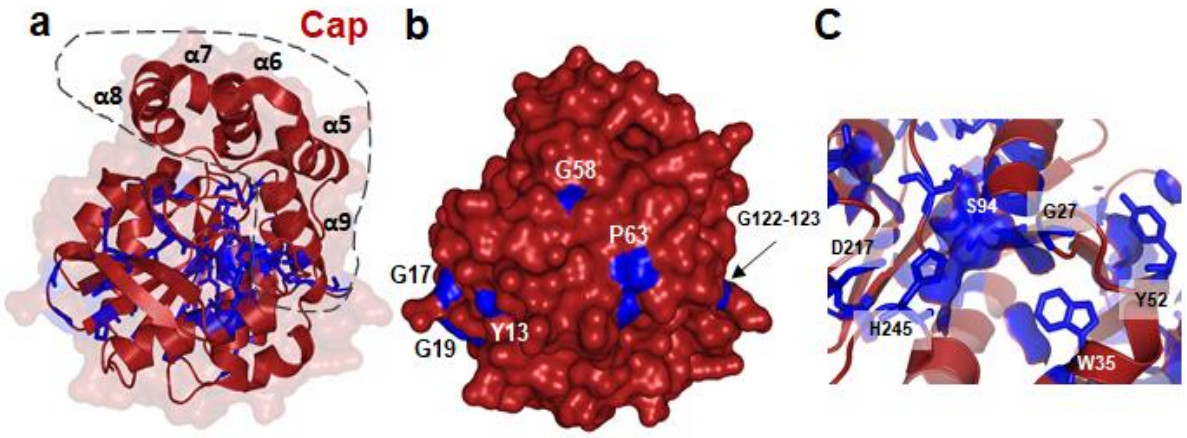

Figure 13. Ade1 conserved residues mapped on surface structure. (a) Conserved residues within Ade1 orthologues are colored in blue and are described in details in **Figure 6**. Most of them are located at the Ade1 core domain with the exception of the G_{122}, G_{123}, and A_{192} residues that are located in the cap domain. **(b)** Conserved residues in the Ade1 structure that are exposed to solvent are colored in blue. **(c)** Highlights conserved residues located in the catalytic pocket.

In order to verify the difference between Ade1 and α/β-hydrolase members, we compared the three-dimensional structures of them using DALI web-based service. Ade1 presented a structural similarity with a wide range of α/β-hydrolase family members but they present different enzymatic functions. Among them are included lactonases, peroxidases, lipases, epoxide hydrolases, peptidases, homoserine o-acetyltransferase, haloalkane dehalogenase, phospholipase, cutinase, different classes of esterases (such as arylesterase, acetylesterase, thioesterase, heroin esterase, cocaine esterase, acetylcholinesterase, sterol esterase, cholesterol esterase, carboxylesterases, and metallophore yersiniabactin (Ybt) protein) (OHLEMACHER; XU; KOBER; MALIK *et al.*, 2018) (**Table 3**). Based on that, we did not attribute a specific enzymatic function for Ade1. Thus, additional experiments are required for understanding the biochemical and biological functions of the Ade1.

Next, we investigated the structural relationships between Ade1 and structure subsets previously selected using all-against-all comparisons in the DALI-server website (**Figure 14, Table 3**). In **Figure 14a** is shown a dendrogram of these structural relationships. We identified 3 groups that do not share the same biochemical functions. Group 1 members have the same topology of Ade1 but present few structural differences in the cap domain (**Figure 14b**). Among the group 2 members, we noted differences in cap domain and insertions in the core domain relative to the structure of Ade1 (**Figure 14c**). Group 3 members are structurally more divergent than Ade1 and have significant differences in both the cap and core domain (Figure 8d). Based on that, we suggest that the structural divergence between α/β-hydrolase superfamily members

is more related with its substrate structure than with enzymatic class. Therefore, biochemical assays are key for predicting the corresponding biological function of each α/β-hydrolase family member.

Table 3. Analysis of three-dimensional structural similarities between the Ade1 structure and others deposited in public databases using DALI web-based service. The search for structural similarities used as input to the Ade1 chain B. The Table describes the main results. These results show that Ade1 shares three-dimensional structural similarities with a wide range of α/β-hydrolases members that have different enzymatic functions.

PDB ID-Chain	Z-score	RMSD (Å)	id %	Enzyme name or short description
2xua-H	34.1	2.3	27	3-OXOADIPATE ENOL-LACTONASE
3fob-A	31.6	2.4	22	BROMOPEROXIDASE
1u2e-A	31.2	2.0	26	2-HYDROXY-6-KETONONA-2,4-DIENEDIOIC ACID
1va4-A	31.0	2.4	24	ARYLESTERASE
4uhc-A	31.0	2.8	25	ESTERASE
1q0r-A	30.9	2.3	27	ACLACINOMYCIN METHYLESTERASE
4dgq-A	30.8	2.4	20	NON-HEME CHLOROPEROXIDASE
4lxh-A	30.4	2.3	23	MCP HYDROLASE
1c4x-A	30.2	2.4	21	(2-HYDROXY-6-OXO-6-PHENYLHEXA-2,4-DIENOAT
4opm-A	29.6	2.3	23	LIPASE
5ng7-A	28.9	2.1	24	EPOXIDE HYDROLASE
2vf2-A	28.7	2.5	24	2-HYDROXY-6-OXO-6-PHENYLHEXA-2,4-DIENOATE
3vvl-B	28.3	2.9	23	HOMOSERINE O-ACETYLTRANSFERASE
3kxp-A	28.0	2.3	23	ALPHA-(N-ACETYLAMINOMETHYLENE) SUCCINIC ACID
5frd-A	27.8	2.9	23	CARBOXYLESTERASE (EST-2)
1wom-A	27.5	3.0	18	SIGMA FACTOR SIGB REGULATION PROTEIN RSBQ
2oci-A	27.4	2.3	23	VALACYCLOVIR HYDROLASE
3nwo-A	27.3	2.6	22	PROLINE IMINOPEPTIDASE
1y37-A	27.2	2.6	21	FLUOROACETATE DEHALOGENASE
3kda-A	26.4	2.7	18	CFTR INHIBITORY FACTOR (CIF)
4l0c-A	26.3	2.4	25	DEFORMYLASE
6f9o-A	25.9	2.8	22	HALOALKANE DEHALOGENASE
6eic-B	25.4	2.6	19	MYCOBACTERIUM TUBERCULOSIS MONOGLYCERIDE LIPASE
6a9d-A	25.3	3.0	17	HYPOSENSITIVE TO LIGHT 7
2vav-B	25.2	3.1	20	ACETYL-COA--DEACETYLCEPHALOSPORIN C ACETYLTRANSFE
5xmw-A	24.6	2.8	18	ZEARALENONE LACTONASE

6ny9-B	23.6	2.6	18	MYCOPHENOLIC ACID ACYL-GLUCURONIDE ESTERASE
2psf-A	23.3	2.9	15	RENILLA-LUCIFERIN 2-MONOOXYGENASE
4gdm-C	23.2	3.3	15	2-SUCCINYL-6-HYDROXY-2,4-CYCLOHEXADIENE-1-CARBOXY
3qit-B	23.1	2.4	19	POLYKETIDE SYNTHASE
4qlo-A	23.1	3.6	16	HOMOSERINE O-ACETYLTRANSFERASE
3pf8-A	22.6	2.7	17	CINNAMOYL ESTERASE
6ix4-B	22.2	2.9	13	MICROSOMAL EPOXIDE HYDROLASE
2wm2-C	21.9	3.2	16	1-H-3-HYDROXY-4-OXOQUINALDINE 2,4-DIOXYGENASE
1imj-A	21.5	2.1	19	CCG1-INTERACTING FACTOR B
2o2g-A	21.3	2.3	21	DIENELACTONE HYDROLASE
3fnb-A	20.9	2.8	14	ACYLAMINOACYL PEPTIDASE SMU_737
2jbw-B	20.7	2.6	16	2,6-DIHYDROXY-PSEUDO-OXYNICOTINE HYDROLASE
6vap-A	20.6	3.2	18	THIOESTERASE
6ba8-A	20.4	3.2	14	IRON AQUISITION YERSINIABACTIN SYNTHESIS ENZYME
3o4j-C	20.3	2.8	15	ACYLAMINO-ACID-RELEASING ENZYME
1ivy-A	20.0	3.0	15	HUMAN PROTECTIVE PROTEIN
4ao8-A	19.6	2.4	16	ESTERASE
5y57-C	19.4	3.0	16	PYRETHROID HYDROLASE
3wwp-A	19.1	3.1	15	(S)-HYDROXYNITRILE LYASE
5cml-A	19.0	2.9	18	OSMC FAMILY PROTEIN
1auo-A	18.7	2.5	16	CARBOXYLESTERASE
3n2z-B	18.7	3.2	13	LYSOSOMAL PRO-X CARBOXYPEPTIDASE
3hxk-A	18.6	2.7	14	SUGAR HYDROLASE
4fhz-A	18.2	2.7	19	PHOSPHOLIPASE/CARBOXYLESTERASE
4kry-E	18.1	2.5	17	ACETYL ESTERASE
2cb9-A	18.0	3.0	11	FENGYCIN SYNTHETASE
6kd0-A	17.5	2.8	12	VIBRALACTONE CYCLASE
1lzk-A	17.4	2.9	18	HEROIN ESTERASE
3hlk-B	17.3	2.4	11	ACYL-COENZYME A THIOESTERASE 2, MITOCHONDRIAL
2h7y-A	16.6	3.0	12	TYPE I POLYKETIDE SYNTHASE PIKAIV
1jkm-B	16.4	2.8	14	BREFELDIN A ESTERASE
1jjf-A	16.1	2.6	13	ENDO-1,4-BETA-XYLANASE Z
3i2g-A	15.9	2.8	17	COCAINE ESTERASE
3iii-A	15.9	2.9	12	COCE/NOND FAMILY HYDROLASE
4xjv-A	15.9	2.8	15	S-ACYL FATTY ACID SYNTHASE THIOESTERASE, MEDIUM C
3c6b-A	15.7	2.8	17	S-FORMYLGLUTATHIONE HYDROLASE

3f98-A	15.5	2.7	14	PLATELET-ACTIVATING FACTOR ACETYLHYDROLASE
3wl5-A	15.5	3.0	10	OXIDIZED POLYVINYL ALCOHOL HYDROLASE
4j0d-A	15.5	3.3	14	TANNASE
3ils-A	15.4	3.3	13	AFLATOXIN BIOSYNTHESIS POLYKETIDE SYNTHASE
4e15-B	15.2	3.0	13	KYNURENINE FORMAMIDASE
6rt8-A	15.1	2.9	12	CATHARANTHINE SYNTHASE
3og9-A	15.0	3.2	15	PROTEIN YAHD A COPPER INDUCIBLE HYDROLASE
6rs4-B	14.8	3.0	11	TABERSONINE SYNTHASE
1cle-A	14.4	2.9	10	CHOLESTEROL ESTERASE
6eop-A	14.4	2.8	19	DIPEPTIDYL PEPTIDASE 8
3vkf-A	14.1	2.8	14	NEUROLIGIN-1
1mx9-D	13.7	3.6	18	LIVER CARBOXYLESTERASE I
5ie4-C	13.5	2.6	22	ZEARALENONE HYDROLASE
4be4-A	13.0	3.0	11	STEROL ESTERASE
5nuu-A	12.7	2.8	13	ACETYLCHOLINESTERASE
4qnn-A	11.1	3.6	13	PHOSPHOLIPASE
2czq-A	10.8	2.9	13	CUTINASE-LIKE PROTEIN
4uyz-D	10.0	3.5	9	PROTEIN NOTUM HOMOLOG
1bs9-A	9.5	3.4	13	ACETYL XYLAN ESTERASE
2xa2-A	6.9	3.4	11	TREHALOSE-SYNTHASE TRET

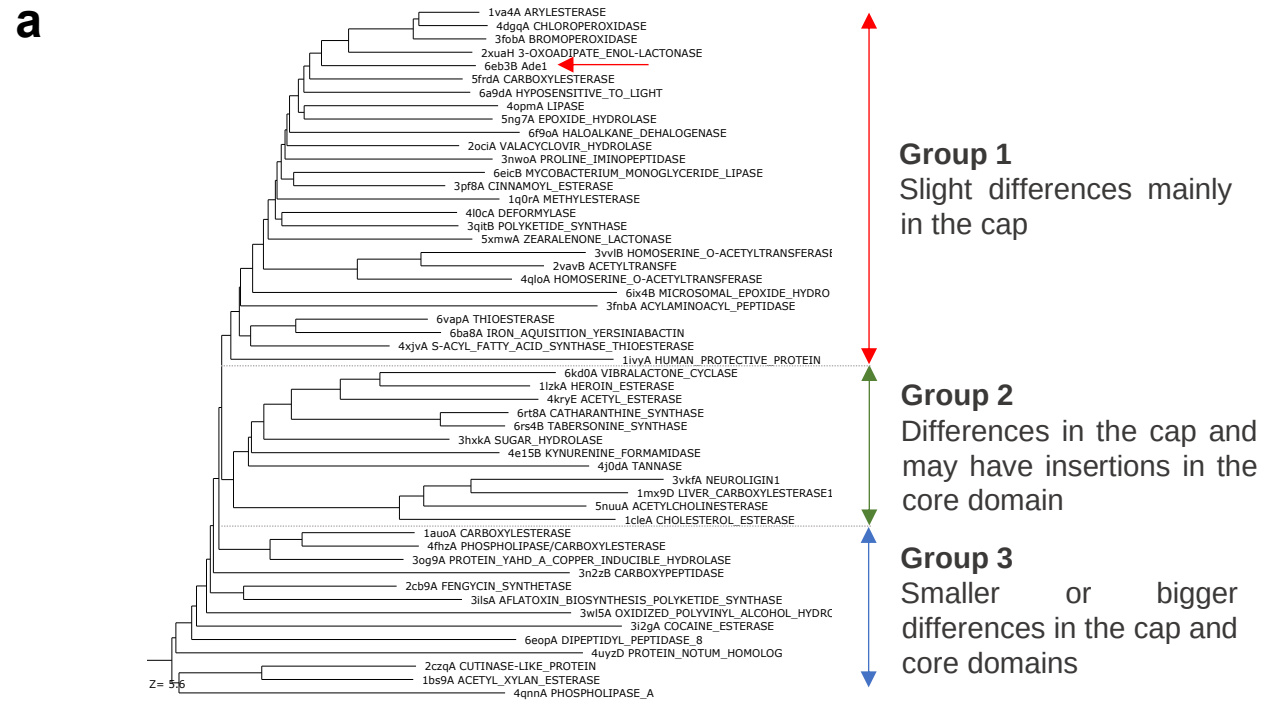
a
1va4A ARYLESTERASE
4dggA CHLOROPEROXIDASE
3fobA BROMOPEROXIDASE
2xuaH 3-OXOADIPATE_ENOL-LACTONASE
6eb3B Ade1
5frdA CARBOXYLESTERASE
6a9dA HYPOSENSITIVE_TO_LIGHT
4opmA LIPASE
5ng7A EPOXIDE_HYDROLASE
6f9oA HALOALKANE_DEHALOGENASE
2ociA VALACYCLOVIR_HYDROLASE
3nwoA PROLINE_IMINOPEPTIDASE
6eicB MYCOBACTERIUM_MONOGLYCERIDE_LIPASE
3pf8A CINNAMOYL_ESTERASE
1q0rA METHYLESTERASE
4l0cA DEFORMYLASE
3qitB POLYKETIDE_SYNTHASE
5xmwA ZEARALENONE_LACTONASE
3vvlB HOMOSERINE_O-ACETYLTRANSFERASE
2vavB ACETYLTRANSFE
4qloA HOMOSERINE_O-ACETYLTRANSFERASE
6ix4B MICROSOMAL_EPOXIDE_HYDRO
3fnbA ACYLAMINOACYL_PEPTIDASE
6vapA THIOESTERASE
6ba8A IRON_AQUISITION_YERSINIABACTIN
4xjvA S-ACYL_FATTY_ACID_SYNTHASE_THIOESTERASE
1ivyA HUMAN_PROTECTIVE_PROTEIN
6kd0A VIBRALACTONE_CYCLASE
1lzkA HEROIN_ESTERASE
4kryE ACETYL_ESTERASE
6rt8A CATHARANTHINE_SYNTHASE
6rs4B TABERSONINE_SYNTHASE
3hxkA SUGAR_HYDROLASE
4e15B KYNURENINE_FORMAMIDASE
4j0dA TANNASE
3vkfA NEUROLIGIN1
1mx9D LIVER_CARBOXYLESTERASE1
5nuuA ACETYLCHOLINESTERASE
1cleA CHOLESTEROL_ESTERASE
1auoA CARBOXYLESTERASE
4fhzA PHOSPHOLIPASE/CARBOXYLESTERASE
3og9A PROTEIN_YAHD_A_COPPER_INDUCIBLE_HYDROLASE
3n2zB CARBOXYPEPTIDASE
2cb9A FENGYCIN_SYNTHETASE
3ilsA AFLATOXIN_BIOSYNTHESIS_POLYKETIDE_SYNTHASE
3wl5A OXIDIZED_POLYVINYL_ALCOHOL_HYDRO
3i2gA COCAINE_ESTERASE
6eopA DIPEPTIDYL_PEPTIDASE_8
4uyzD PROTEIN_NOTUM_HOMOLOG
2czqA CUTINASE-LIKE_PROTEIN
1bs9A ACETYL_XYLAN_ESTERASE
4qnnA PHOSPHOLIPASE_A
Z= 5.6
Group 1
Slight differences mainly in the cap
Group 2
Differences in the cap and may have insertions in the core domain
Group 3
Smaller or bigger differences in the cap and core domains

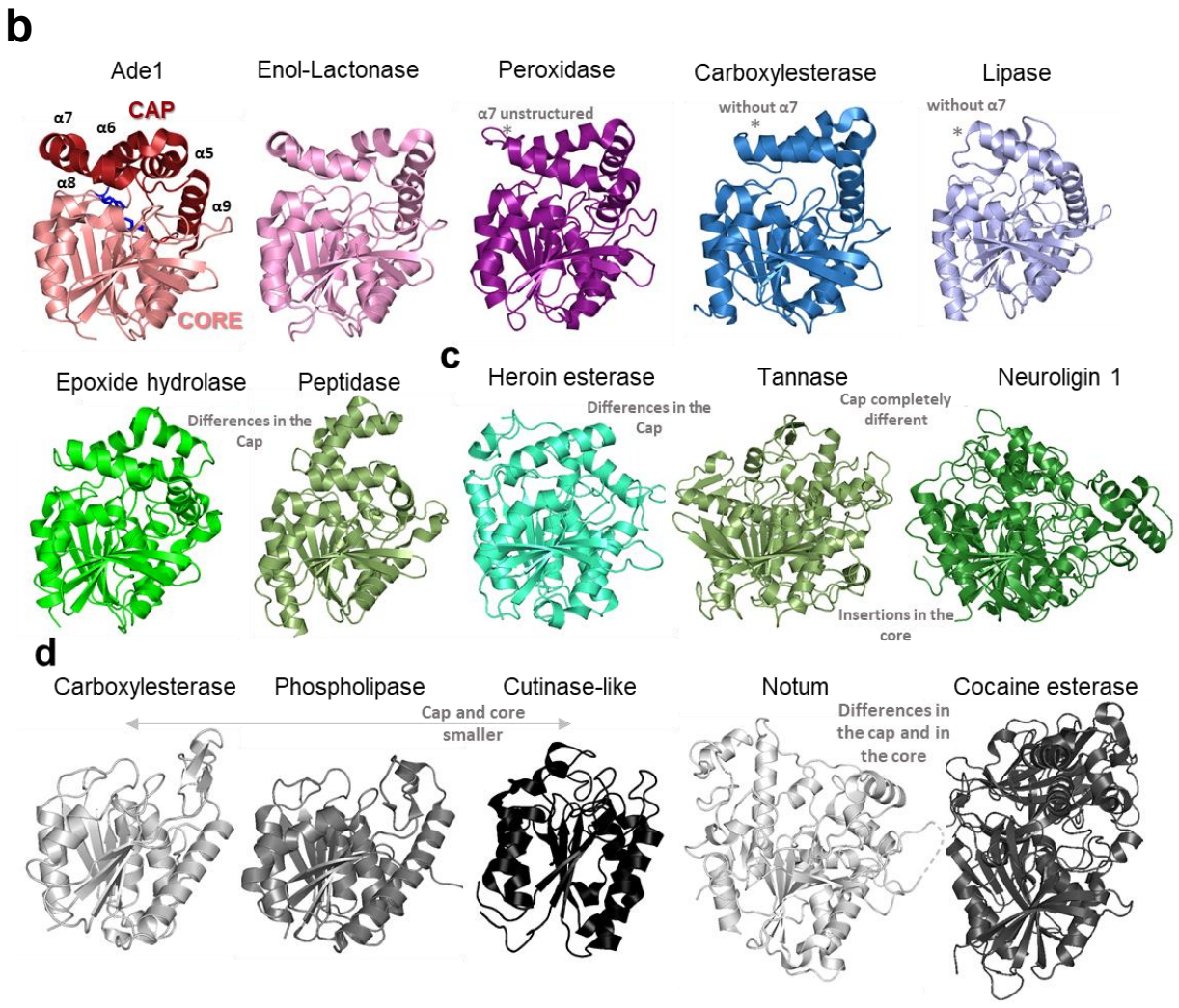
b
Ade1
Enol-Lactonase
Peroxidase
Carboxylesterase
Lipase
α7
α6
CAP
α5
α8
α9
CORE
α7 unstructured
without α7
without α7
c
Epoxide hydrolase
Peptidase
Heroin esterase
Tannase
Neuroligin 1
Differences in the Cap
Differences in the Cap
Cap completely different
Insertions in the core
d
Carboxylesterase
Phospholipase
Cutinase-like
Notum
Cocaine esterase
Cap and core smaller
Differences in the cap and in the core

Figure 14. Structural comparison of the cap domain between α/β hydrolases proteins. (a) Structural similarity dendrogram using structures similar to Ade1. The dendrogram is derived by average linkage clustering of the structural similarity matrix (Dali Z-scores). It shows three groups delimited by the double arrow (red, green, and blue, respectively). Group 1 is characterized by slight differences only in the cap domain). Group 2 has differences in the cap and could have an insertion in the core domain. Group 3 shows two sub-groups presenting smaller or bigger differences in the cap and core domains. Red arrow indicates Ade1. The painels **(b)**, **(c)**, and **(d)** show the crystal structures of different members of α/β-hydrolases representants of the group 1, 2 and 3, respectively. **(b)** Ade1 (PDB ID 6EB3, chain B), enol-lactonase (PDB ID 2XUA, chain H), peroxidase (PDB ID 4DGQ, chain A), carboxylesterase (PDB ID 5FRD, chain A), lipase (PDB ID 4OPM, chain A), epoxide hydrolase (PDB ID 5NG7, chain A), proline peptidase (PDB ID 3NWO, chain A); **(c)** heroin esterase (PDB ID 1LZK, chain A), tannase (PDB ID 4J0D, chain A), neuroligin-1 (PDB ID 3VKF, chain A); **(d)** carboxylesterase (PDB ID 1AU0, chain A), phospholipase (PDB ID 4FHZ, chain A), cutinase-like protein (PDB ID 2CZQ, chain A), notum (PDB ID 4UYZ, chain D) and cocaine esterase (PDB ID 3I2G, chain A).

4.2 Expression and purification of Ade1

The recombinant Ade1, as well as its mutants, were overexpressed in *E. coli* BL21(DE3)-RP strain (**Figure 15**). The protein expression bands of Ade1, Ade1$_{S94C}$, and Ade1$_{S94A}$ have a theoretical molecular weight of 29.3 kDa. The SDS-PAGE gel shows soluble target protein after bacterial cell lysis in 50 mM Tris-HCl pH 7.5, 100 mM NaCl, 20% (w/v) sucrose, 10% glycerol (v/v), 0.03% (v/v) Triton X-100, and 0.03% (v/v) Tween 20, and the resulting elution fractions from affinity chromatography of the recombinant proteins. After elution in the affinity column, the protein fractions were mixed and dialyzed in 10 mM Tris-HCl pH 7.5, 10 mM NaCl, and 1 mM EDTA.

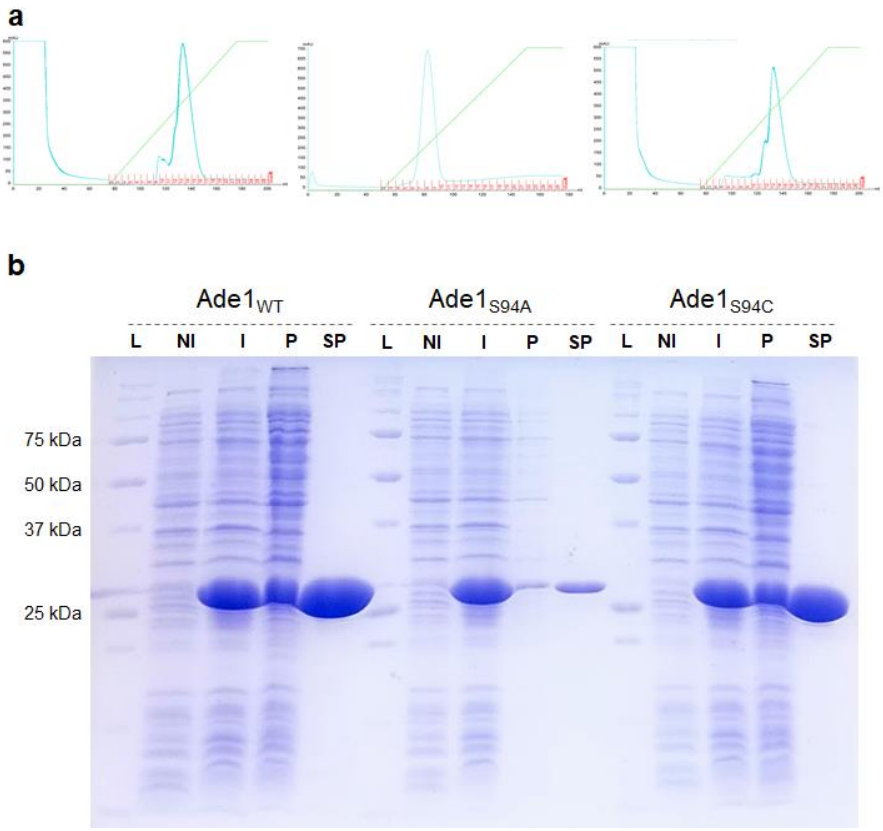

Figure 15. Expression and purification of $Ade1_{WT}$, $Ade1_{S94A}$ and $Ade1_{S94C}$. **(a)** Affinity chromatography on a 5 ml HiTrap column loaded with nickel, the green line indicates the affinity gradient and in light blue is the absorbance of the protein eluted at 280 nm, **(b)** 15% SDS-PAGE gel of the expression and affinity chromatography assay of $Ade1_{WT}$, $Ade1_{S94C}$ and $Ade1_{S94A}$ (~29 kDa). L: lader, NI: not induced, I: induced, P: pellet, SP: soluble protein.

4.2 Ade1 is a monomeric protein.

Analysis of protein-protein contacts in the protein crystal using the crystallography contacts by Protein interfaces, surfaces, and assemblies (PISA) web-based service (KRISSINEL; HENRICK, 2007) suggests that Ade1 is a monomer. Indeed, gel filtration coupled to the Multi-Angle Light Scattering detector (SEC-MALS) confirmed that Ade1 (with and without 6×His-tag) is a monomer with an experimental MW of 30 kDa (theoretical MW of 29.3 kDa, **Figure 16**). Members of the α/β-hydrolase superfamily also may oligomerize through β-strands and monomeric states are favored due to the presence of more than four α-helices in the cap domain (LAI; XU; ZHOU; LEE *et al.*, 2008). For example, PcaD has been described as a dimer in aqueous solution, in which the core domain (α1, β1, and β2) and its cap domain (α7) is involved in the protein-protein interaction (BAINS; KAUFMAN; FARNELL; BOULANGER, 2011). Therefore, structural features of the cap domain play a key role in the formation of oligomers in some members of α/β-hydrolase superfamily (FUSHINOBU; SAKU; HIDAKA; JUN *et al.*,

2002; HABE; MORII; FUSHINOBU; NAM *et al.*, 2003; SAKU; FUSHINOBU; JUN; IKEDA *et al.*, 2002).

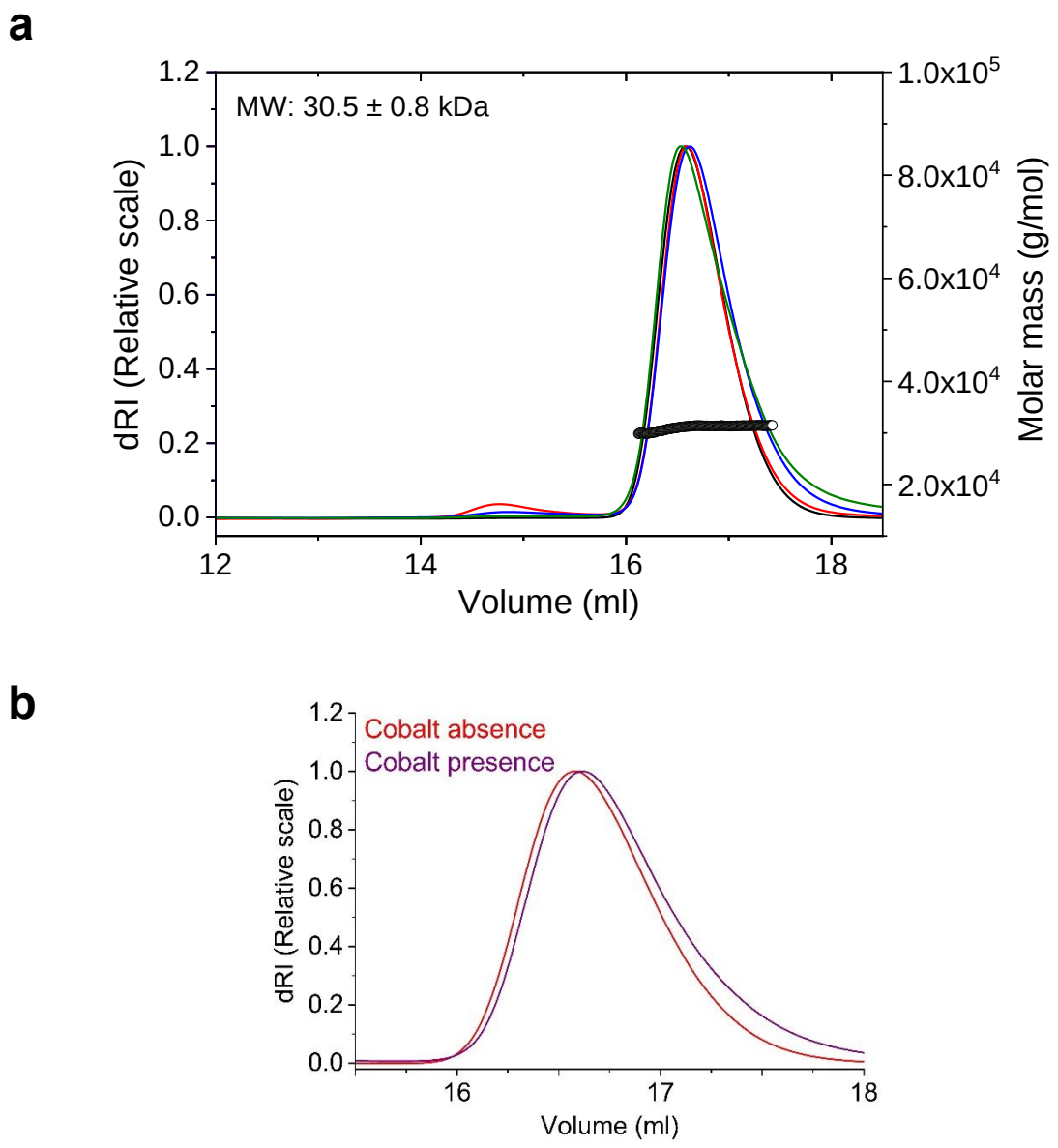

Figure 16. Molecular weight of Ade1 determined by molecular exchange chromatography coupled to a multi-angle light scattering detector (SEC-MALS). Determination of oligomeric states and molecular mass of Ade1 by molecular exchange chromatography coupled to a multi-angle light scattering detector (SEC-MALS). In this experiment was applied 550 µl of sample at 2 $g.l^{-1}$ Ade1 (Tris-HCl pH 8 50 mM and 400 mM NaCl, in absence and presence of 6 mM Co^{2+}). (**a**) Shows the profile of all runs (Ade1 in absence and presence of Co^{2+}). Only one pick of Ade1 (monomer) was observed on the chromatogram, which revealed that Ade1 has a molecular weight of 30.5 ± 0.8 kDa. (**b**) Ade1 in absence and presence of Co^{2+} (red and purple colors) show a significative shift in the curve. All runs were performed in triplicate.

4.3 Functional characterization of Ade1

4.3.1 *Biochemical studies*.

Since biochemical assays help in determining the biochemical function of Ade1 as an esterase or lipase, we evaluated its hydrolytic activity of tributyrin and triolein (**Figure 17**). As result, we did not detect a hydrolysis halo around the bacterial colony in the presence of triolein (**Figure 17b**). However, we observed a hydrolysis halo around the bacterial colony in the presence of tributyrin. Thus, we classified Ade1 as an esterase (**Figure 17a**). The cell expressing the mutants of Ade1 in the catalytic serine to alanine, $Ade1_{S94A}$, and cysteine, $Ade1_{S94C}$, did not show hydrolytic activity in the presence of tributyrin (**Figure 17a**). We also evaluated the lipolytic activity of Ade1 through precipitation tests using the Tween 20 (aliphatic chain of 11 carbons) (**Figure 17c**) and Tween 80 (aliphatic chain of 17 carbons, data not shown). As a control, we used $Ade1_{S94C}$, which did not show lipolytic activity. Comparing the experimental conditions, we detected only the degradation of Tween 20 by forming white calcium laurate crystals due to the reaction of hydrolysis products with Ca^{2+}. Taken together, Ade1 presents esterase and tweenase activities.

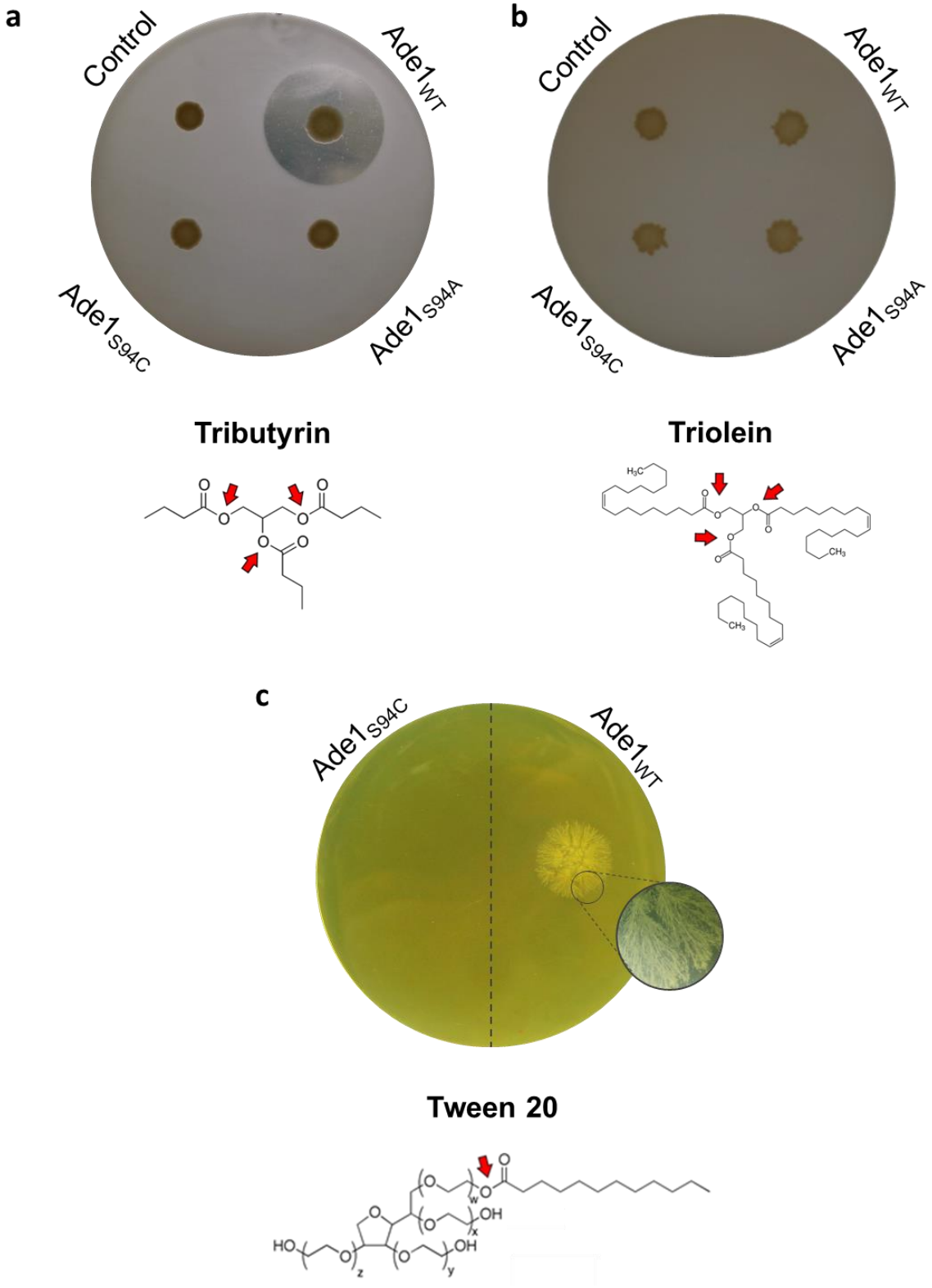

Figure 17. The hydrolytic capacity of Ade1 as an esterase. The expression of the *ade1* gene generated a translucent halo around the colony as result of the hydrolytic capacity of tributyrin and triolein, **(a)** and **(b)** respectively, added into LB culture medium suggesting that Ade1 is an esterase enzyme, as control was used *E. coli* BL21(DE3)-RP strain transformed with empty pET28a vector; **(c)** The tweenase activity test performed with $Ade1_{WT}$ and $Ade1_{S94C}$ purified recombinants after 24 hours observe insoluble crystals around the protein inoculation as results of the bind between the fatty acids liberate

by the detergent and the calcium present in the culture medium. The chemical structure of tributyrin, triolein and Tween 20 substrates is shown below respectively.

4.3.2 *Quorum quenching activity*.

Dimeric enol-lactone hydrolase (ELH) PcaD (from *Burkholderia xenovorans*) cleaves the lactone ring of 3-oxoadipate-enol-lactone (also known as β-ketoadipate-enol-lactone) in β-ketoadipate pathway (BAINS; KAUFMAN; FARNELL; BOULANGER, 2011). This molecule is converted into the formation of the succinate and acetyl CoA, which are intermediates of the Krebs cycle via β-ketoadipyl-CoA (ORNSTON, 1966). PcaD is an esterase involved in the bacterium's metabolism in the degradation of aromatic compounds (protocatechuate or catechol) for obtaining energy. It can be used as a biotechnological tool to degrade homoserine lactones by blocking quorum-sensing (BAINS; KAUFMAN; FARNELL; BOULANGER, 2011).

Since Ade1 shares 44% primary sequence similarities and high structural similarity with PcaD (RMSD of 2.3 Å, **Table 3**), we performed an assay for detecting whether Ade1 has quorum-quenching activity. To this end, we monitored the growth of *Chromobacterium violaceum* that produces a characteristic purple pigment, known as violacein, in a quorum sensing (QS) dependent way. Synthesis of violacein is activated in the presence of N-hexanoyl-L-homoserine lactone (C6-HSL), which activates QS and biosynthesis of violacein (MCCLEAN; WINSON; FISH; TAYLOR *et al.*, 1997). Thus, measurement of violacein pigment is an indirect method for detecting C6-HSL. Ade1 concentrations from 100 to 300 $\mu g.ml^{-1}$ into the medium culture, decrease significantly the violacein production by *Chromobacterium violaceum* (the area under the curve is decreased with an increase of the Ade1 concentration) (**Figure 18**). Therefore, our results suggest that Ade1 has quorum-quenching activity, possibly by hydrolysis of C6-HSL autoinducer.

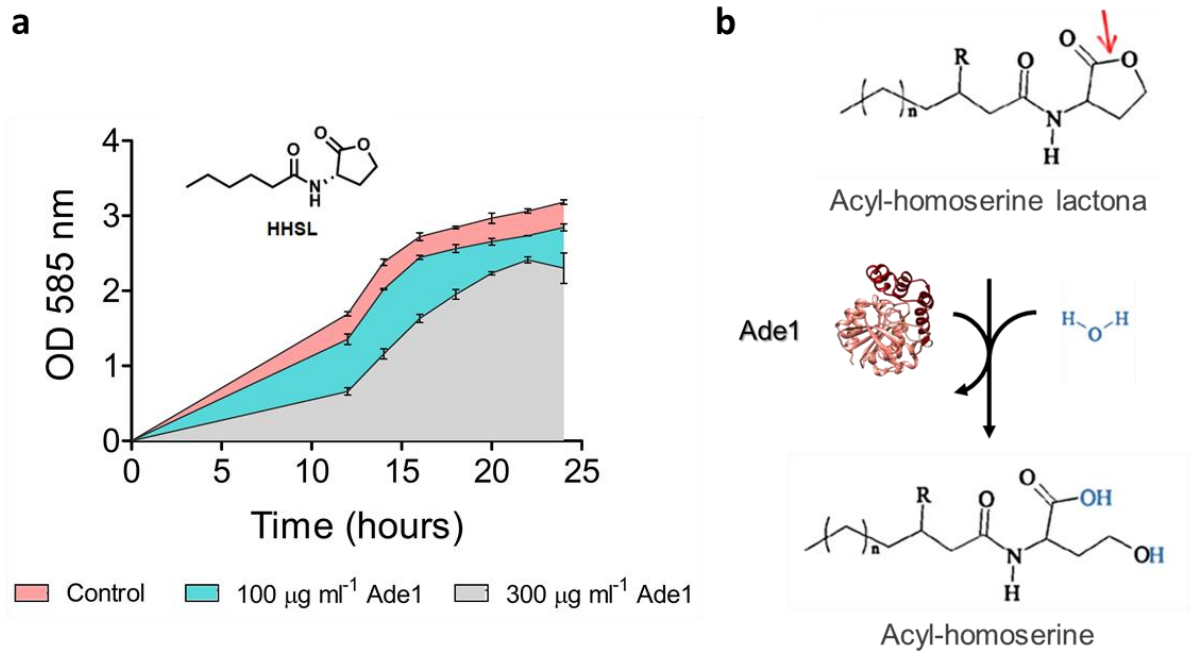

Figure 18. *In vivo* quorum quenching assay. (**a**)Inhibition of violacein production by the influence of Ade1. Violacein production was measured as an indirect measure of C6-HSL (N-hexanoyl-L-homoserine lactone) concentration. The LB culture medium with *Chromobacterium violaceum* (OD600 of 0.1) contained 100 µg ml-1 or 300 µg ml-1 of Ade1 (100 mM Tris-HCl pH 8.0 and 50 mM NaCl). The measurement of violacein in the supernatant at OD_{585} started at 12 hours after inoculation up until 24 hours. To facilitate visualization, we compare the area under the curve for each condition. Buffer was used as a negative control and each condition was tested in triplicate. (**b**) Show the hydrolysis site (red arrow) of Ade1, ring lactone from acyl-homoserine lactone molecule.

4.3.3 *In vitro effect of Ade1 in cocaine hydrolysis.*

Ade1 has a structural similarity (RMSD 2.8 Å) with a cocaine esterase enzyme (**Figure 19** and **Table 3**) that hydrolyzes pharmacologically active cocaine to a non-psychoactive metabolite (LARSEN; TURNER; STEVENS; ROSSER *et al.*, 2002). We tested the esterase activity for hydrolyzing the cocaine molecule containing the 8-methyl-8-azabicyclo[3.2.1]octane and benzyl groups in collaboration with Professor Dr. Mauricio Yonamine of the Department of Clinical and Toxicological Analysis of the Faculty of Pharmaceutical Sciences of USP. We did not observe hydrolysis of cocaine to ecgonine methyl ester and benzoic acid or benzoylecgonine (**Figure 20**). This result suggests that Ade1 not able to hydrolyze esters connected to steric bulky groups, in the conditions used.

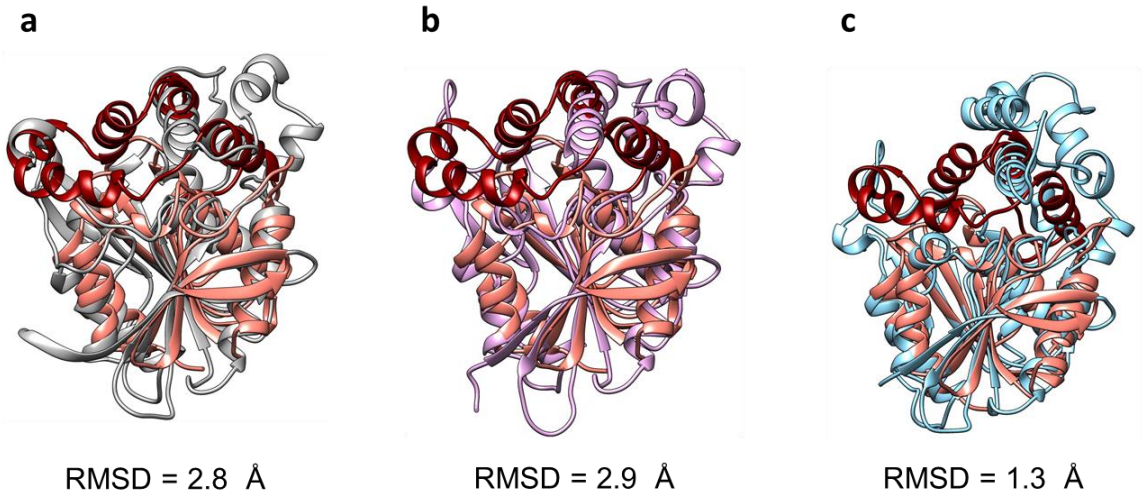

Figure 19. 3D structural alignment of Ade1 and cocaine esterases. Shows superposition between Ade1 structure (PDB ID: 6EB3) in salmon (core domain) and dark red (CAP domain) and, **(a)** cocaine esterase from *Rhodococcus sp*. (PDB ID: 3I2G, in gray), **(b)** CocE/NonD from *Staphylococcus aureus* (PDB ID: 3III, in purple), and **(c)** cocaine esterase from *Rhodococcus sp*. (PDB ID: 1L7Q, in light blue). The root-mean-square deviation (RMSD) of mainchain atoms is 2.8 Å, 2.9 Å and 1.3 Å.

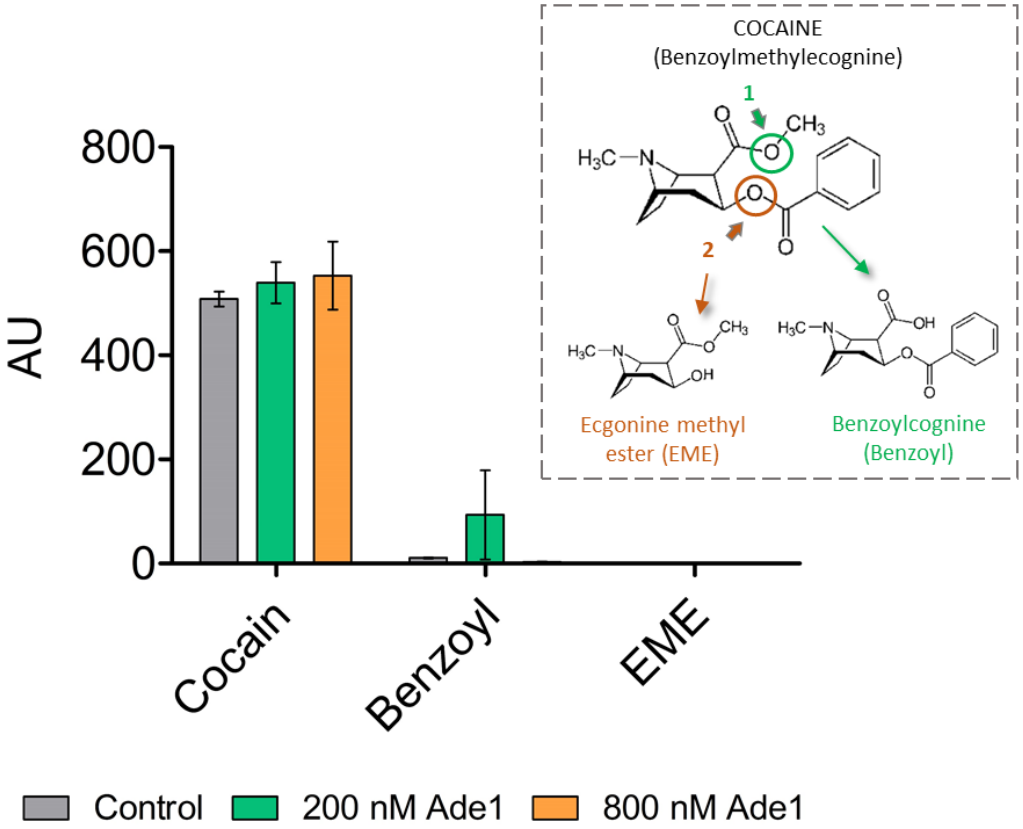

Figure 20. *In vitro* effect of Ade1 on cocaine metabolites. The hydrolysis was evidenced by comparing the formation of benzoyl and EME products with their respective control. The mix reaction contained 1.98 mmol/L cocaine in 100 mM Tris-HCl pH 8.0, 50 mM NaCl, and pure Ade1 at 200 nM and 800 nM in a final volume of 1.5 ml. The reaction was incubated overnight at 30 °C. The reaction was stopped

by adding 500 µl of glycine buffer at pH 2.0. The control consists of pure cocaine and the blank of the mix reaction without cocaine. The dotted box shows cocaine chemical structure, the arrows (1 and 2) indicate the target hydrolysis sites of esterases, and their products: EME and benzoyl molecules, ecgonine methyl ester and benzoylcognine respectively.

4.4 Ade1 kinetic characterization studies.

4.4.1 *Enzyme kinetic studies*

In order to study the esterase kinetic activity of Ade1, we performed enzymatic kinetic tests using different substrates containing *p*-nitrophenyl esters (*p*-NP) with different aliphatic group sizes (from 4 to 16 carbons) *p*-nitrophenyl butyrate, *p*-nitrophenyl octanoate, *p*-nitrophenyl laurate, and *p*-nitrophenyl palmitate. The reaction products, formation of *p*-nitrophenyl, was measured at 347 nm. Ade1 hydrolyzes only *p*-nitrophenyl butyrate and *p*-nitrophenyl octanoate (**Figure 21 a, b and c**). Ade1 catalyzes preferentially *p*-nitrophenyl octanoate in relation to *p*-nitrophenyl butyrate (**Figures 21 b** and **c**), we didn't detect significant enzymatic activity using *p*-nitrophenyl laurate and *p*-nitrophenyl palmitate. Thus, substrates with aliphatic carbon chains of more than 11 carbons did not present detectable reaction products. In addition, we tested whether $Ade1_{S94A}$ and $Ade1_{S94C}$ hydrolyze *p*-nitrophenyl octanoate and both mutants did not present any enzymatic activity (**Figure 22**).

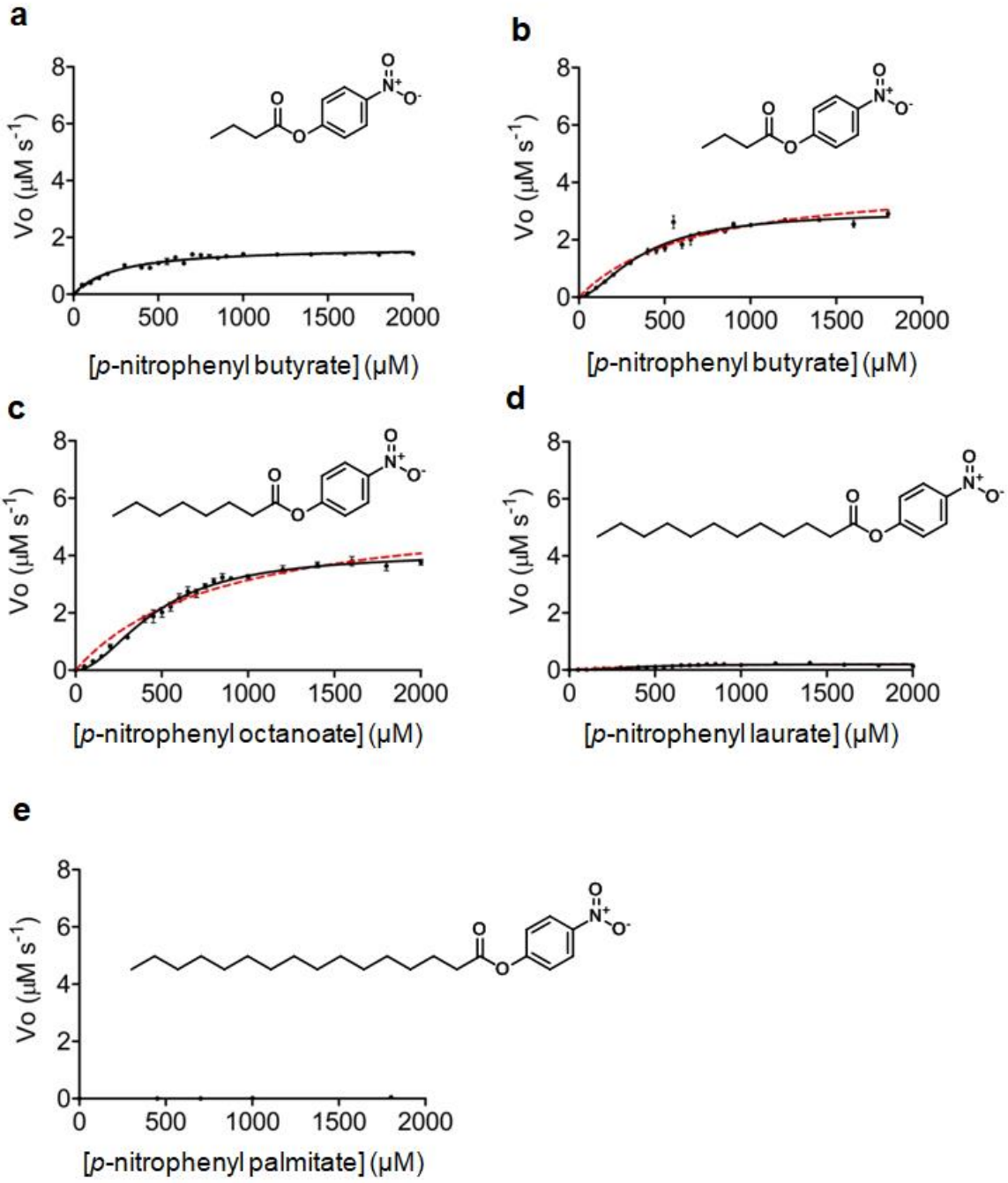

Figure 21. Enzymatic characterization. Kinetic activity of Ade1 in presence of different substrates. **(a)** *p*-nitrophenyl butyrate in presence of Triton X-100; **(b)** *p*-nitrophenyl butyrate in absence of Triton X-100. **(c)** *p*-nitrophenyl octanoate in presence of Triton X-100; **(d)** *p*-nitrophenyl laurate and **(e)** *p*-nitrophenyl palmitate, both in absence of Triton X-100. In the panels **(b)** and **(c)**, are shown two curves corresponding to Michalis-Menten (dotted lines, red color) and Hill-Langmuir (continuous lines, black color) models. The best fit to the kinetics assays (**b** and **c**) was Hill-Langmuir model to represents the experimental data (P value < 0.0001).

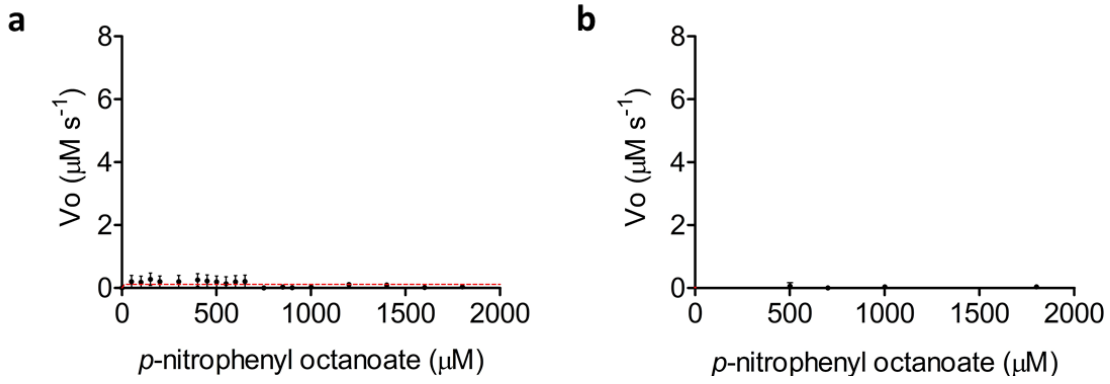

Figure 22. Ade1 mutant's kinetic activity assay. S94A and S94C mutants of Ade1 (**a** and **b** respectively**)** did not present enzymatic catalysis using *p*-nitrophenyl octanoate as substrate.

In order to determine the optimal enzymatic activity conditions of Ade1, we performed different kinetic assays using *p*-nitrophenyl octanoate as a substrate. We measured the dependence of esterase activity using different protein concentrations, from 20 to 80 nM (**Figure 23**), we did not detect significant differences in the specific activity of Ade1. After, we investigated how pH can affect the reaction velocity. Varying the pH from 4.0 to 9.0, we noted that Ade1 activity increased at pH 7.0, 8.0 and 9.0 (**Figure 24a**). We also evaluated if the presence of bivalent metals Ca^{2+}, Co^{2+}, Mg^{2+}, Ni^{2+}, and Zn^{2+} may affect the enzymatic activity. Curiously, increasing the Co^{2+} concentration from 0 to 3 and 6 mM, we observed that the reaction velocity increased from 0.75 to 2.27 and 3.65 $\mu M.s^{-1}$, respectively (**Figure 24b**). Therefore, Co^{2+} improves the Ade1 catalysis efficiency. We observed that the presence of Zn^{2+} abolished the Ade1 enzymatic activity by causing an aggregation of the protein (data not shown).

Interestingly, we observed a hyperbolic curve using *p*-nitrophenyl butyrate (**Figure 21a**) but adding 6 mM Co^{2+}, the curve changes to a sigmoidal profile. It is not expected because Ade1 is a monomer. Cooperative behavior would be observed if Co^{2+} causes an Ade1 oligomerization. Therefore, we performed SEC-MALS assays in the presence of Co^{2+} and we did not observe an oligomerization state of Ade1 (**Figure 16**). Nevertheless, this result suggests that Co^{2+} may cause a small conformational change evidenced by a significative shift in the SEC-MALS chromatography curve (**Figure 16**). In addition, the hydrolysis of *p*-nitrophenyl octanoate demonstrated a sigmoidal profile in absence and presence of Co^{2+} (**Figure 25 c** and **d**). Increasing the Co^{2+} concentration from 0 (in the presence of 5 mM EDTA) to 0.2 and 6 mM, affects the hydrolysis velocity of *p*-nitrophenyl octanoate. Furthermore, the sigmoidal curve is

more evident with 0.2 and 6 mM Co^{2+} than when compared to the condition without this metal (**Figure 25e**).

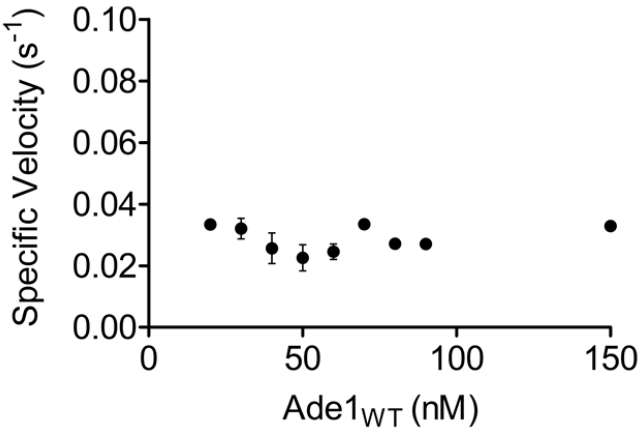

Figure 23. Effect of protein concentration on Ade1 activity. Ade1 enzymatic activity was determined as described in Materials and Methods and the Ade1 specific activity was determined as a function of protein concentration. The reactions were performed at 30 °C in 100mM Tris-HCl pH 8.0, 50 mM NaCl, 0.5% (v/v) Triton X-100, 600 µM p-NP C8, with Ade1 concentration ranging between 20 nM and 80 nM. The measured absorbance was detected through the reaction product *p*-nitrophenyl ester (p-NP) every 20 seconds for 5 minutes. Calibration curves were performed using different concentrations of *p*-nitrophenyl ester (p-NP) and measuring their absorbance at 347 nm in the same buffer conditions used for the Ade1 kinetic assays. Each assay was done in triplicate and the average values were used for constructing the kinetic curve. From the kinetic curve, standard deviations and enzymatic parameters were determined**.**

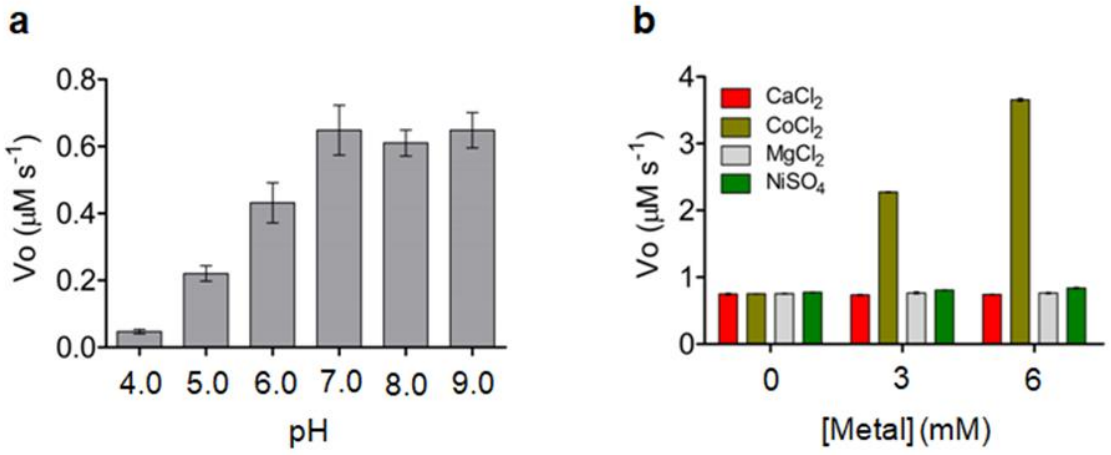

Figure 24. Biochemical assays of Ade1. (a) To determine the optimal pH, we tested different values (4.0, 5.0, 6.0, 7.0, 8.0 and 9.0) into the reaction buffer, the best condition was where the specific speed of Ade1 was higher (pH 7, 8 and 9). **(b)** Show the effect of divalent metal ions (Ca^{2+}, Co^{2+}, Mg^{2+} and Ni^{2+}) in the Ade1 activity, we use 600 µM p-NP octanoate as substrate and 36 nM Ade1 (previously dialyzed with 1 mM EDTA)

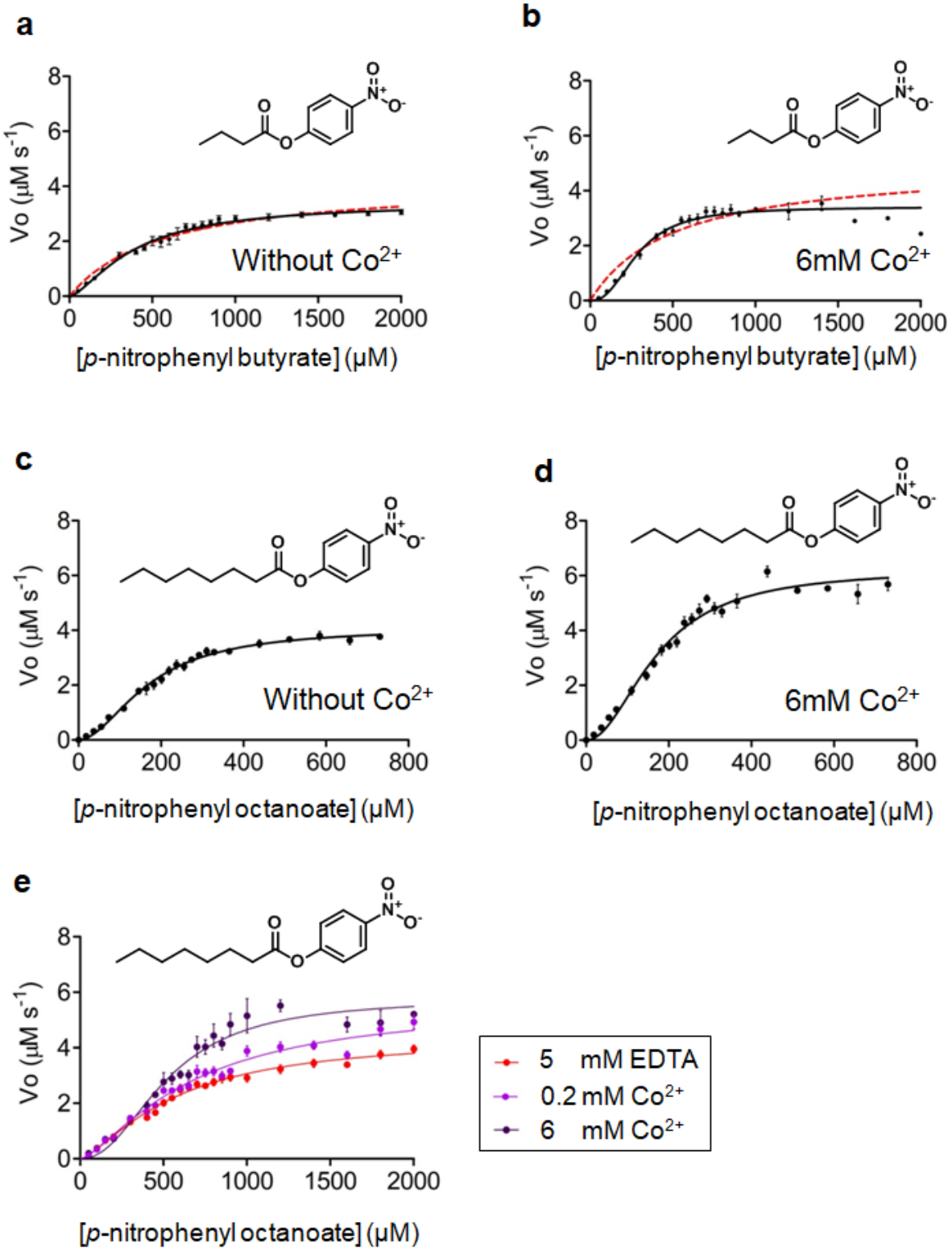

Figure 25. Hydrolysis of substrates *p*-nitrophenyl butyrate and *p*-nitrophenyl octanoate. Kinetic activity of Ade1 in presence of different substrates. *p*-nitrophenyl butyrate in absence of Triton X-100 and, **(a)** absence and **(b)** presence of 6 mM Co^{2+}. *p*-nitrophenyl octanoate in **(c)** absence and **(d)** presence of 6 mM Co^{2+}. In all kinetics assays (with exception *p*-nitrophenyl butyrate), the hypothesis test showed that Hill-Langmuir model best represents the experimental data (P-value less than 0.0001). **(e),** Initial reaction velocity of *p*-nitrophenyl octanoate at different Co^{2+} concentration (0 mM, red color; 0.2 mM, light purple; 6 mM, dark purple).

We initially hypothesized that the sigmoidal profile of the reaction velocity could be caused by the presence of Triton X-100 in the reaction buffer, where it would be generating two substrate states, both in equilibrium. In one state, the substrate would be free in aggregates into solution and the other state inserted into the micelle of Triton X-100. Thus, the enzyme binds only to substrate-free aggregates in solution (the number of monomers substrates in the aggregate, is "n"). Based on that, we propose a kinetic scheme shown in **Figure 26a**. We called this hypothesis "Substrate Effect Model" and was developed in collaboration with Professor Dr. Sandro Marana from Chemical Institute (USP).

Such an effect appears to be insignificant in the reaction when use *p*-nitrophenyl butyrate, it would have no interaction with Triton X-100 micelles (**Figure 21a**). We repeat the same assay in the absence of Triton X-100 and observed an increase in the V_{max} values (**Figure 21b**). Nevertheless, we still observe a sigmoidal effect in the enzymatic curve in the presence of Co^{2+} (**Figure 25 a** and **b**). In order to evaluate the Substrate Effect model, we detected the presence of free *p*-nitrophenyl octanoate in solution (**Figure 27**). The free substrate concentration followed a direct relationship with the total concentration of *p*-nitrophenyl octanoate present in the enzymatic reaction (**Figure 27 b**), effectively the substrate in the reaction is in two states. Another explanation for a sigmoidal profile for Ade1 enzymatic activity would be the "Hysteresis behavior model", detected for monomeric enzymes (**Figure 26b**). In this model, the enzyme is in equilibrium (K_1) between two conformational states, E1 and E2, in which K_1 could be affected due to substrate concentration. These states have different initial velocities due to their different conformational states, which each state has low or high enzymatic activities. Kinetics data of hysteretic enzymes are adequately described by the Hill-Langmuir model (COLQUHOUN, 2006; GOUTELLE; MAURIN; ROUGIER; BARBAUT *et al.*, 2008; RICARD; CORNISH-BOWDEN, 1987).

In sequence, to determine which model best explained Ade1's behavior in the reaction using *p*-nitrophenyl octanoate as substrate, we performed an extra sum-of-squares F test in the GraphPad PRISM program to compare the fits using Substrate Effect and Hysteresis models (described in **Figure 26**). The data fit significantly better with the Hysteresis models (Hill-Langmuir model), suggesting that Ade1 presents hysteresis behavior (**Figure 21 b** and **c**, *P* value < 0.0001). Based on that, we fitted our data using a hysteresis model and determined the Ade1kinetics parameters (**Table 4**). One exception is when the substrate is *p*-nitrophenyl butyrate in the presence of Triton X-100 in the reaction buffer that the kinetics data fit better with Michaelis-Menten model (**Figure 21a** and **Table 4**).

Interestingly, the presence of Co^{2+} did not affect the maximum velocity of *p*-nitrophenyl butyrate hydrolysis (3.4 ± 0.1 μM.s^{-1}) but K_{half} decreased from 392 ± 29 to 288 ± 12 μM. These results suggest that Co^{2+} increases Ade1 substrate binding affinity (**Figure 25** and **Table 4**). On the other hand, when the reaction buffer has Triton X-100, the presence of Co^{2+} increases significantly the maximum velocity of *p*-nitrophenyl butyrate hydrolysis from 1.68 ± 0.04 to 3.0 ± 0.2 μM.s^{-1}. While the K_{half} increases from 254 ± 24 to 377 ± 30 μM. These results suggest that Co^{2+} increase Ade1 substrate binding affinity in the presence of Triton X-100 (**Figure 25** and **Table 4**).

Considering the *p*-nitrophenyl octanoate hydrolysis in the presence and absence of Co^{2+}, we observed that the V_{max} increased from 4.1 ± 0.1 to 6.2 ± 0.3 μM.s^{-1}, respectively (**Figure 25** and **Table 4**). Nevertheless, K_{half} presented the same value at 171.3 ± 7.1 μM, demonstrating that the binding affinity is not affected. Therefore, in all experimental conditions tested, Co^{2+} increases the Ade1 catalytic efficiency (k_{cat}/ K_{half}, **Table 4**) because it probably causes a conformational change to a higher activity state (high catalytic efficiency).

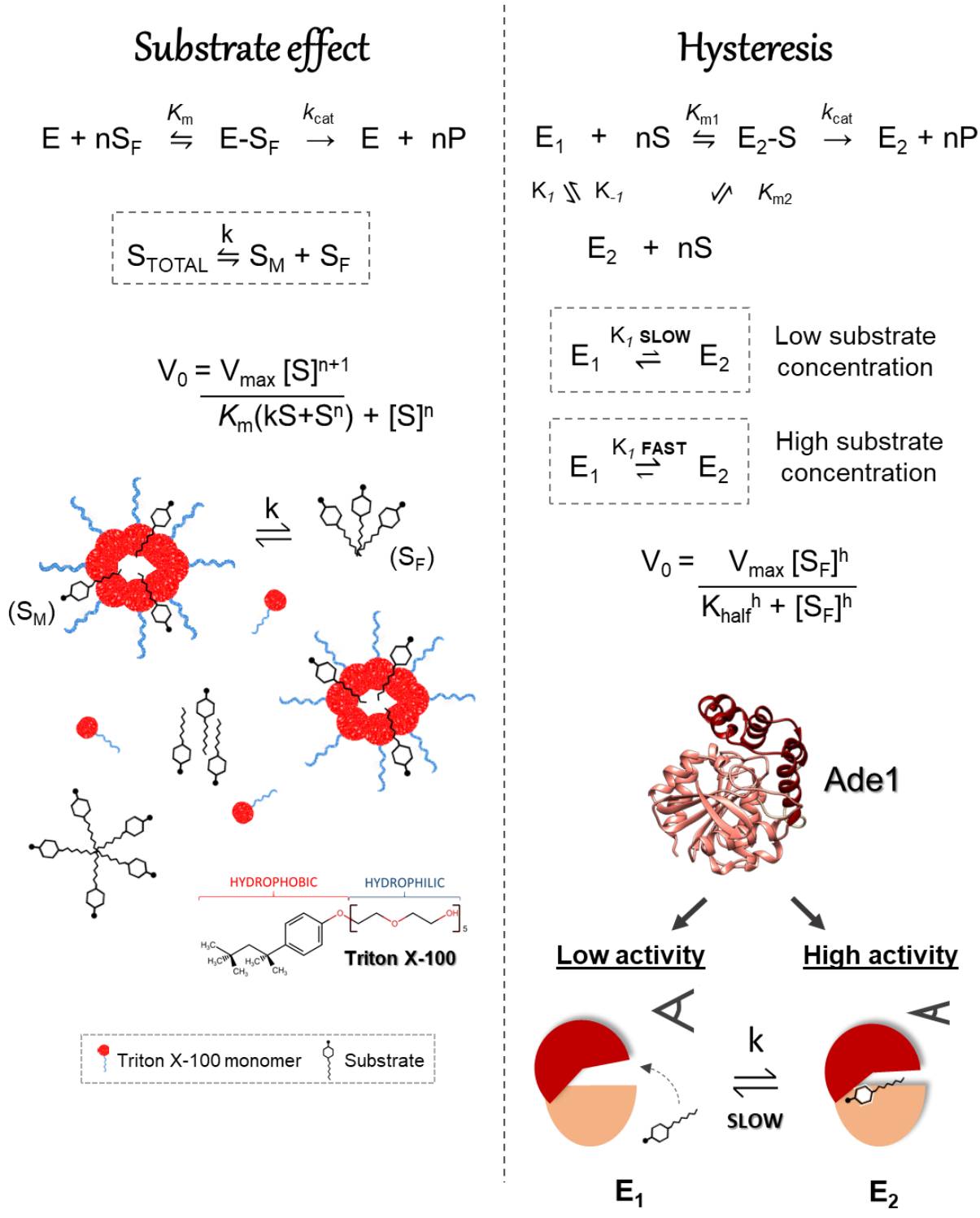

Figure 26. Schematic diagram of the hypotheses that explain the sigmoidal effect in the enzymatic kinetics. (a) Substrate effect that drives states in equilibrium SM (docked substrate into the Triton micelle) and SF (substrate outside the micelle – free substrate). It can be grouped into two or more monomers. Thus, Ade1 cleaves only the free substrate and consequently shows a non-hyperbolic curve of cooperativity (sigmoid). K is defined as a dissociation constant of the substrate inside and outside of the Triton X-100 micelles. **(b)** Hysteresis, Ade1 shows two different conformational states in equilibrium E1 (low activity) and E2 (high activity). Structural conformations, E1, and E2, which are opened and closed states, respectively. Substrate favors E2 conformation, which closes the cap domain for advancing the enzymatic catalysis (more details in **Figure 28** and **29**).

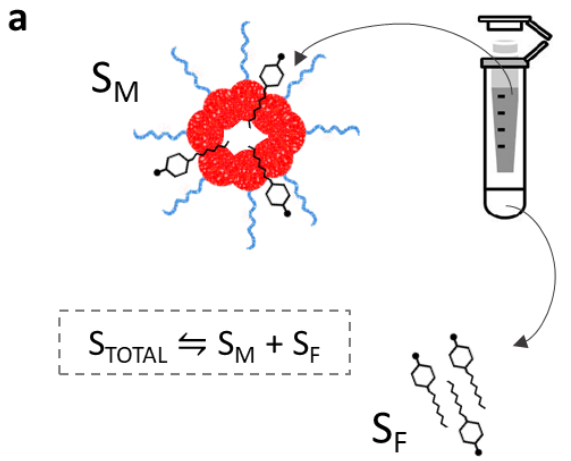

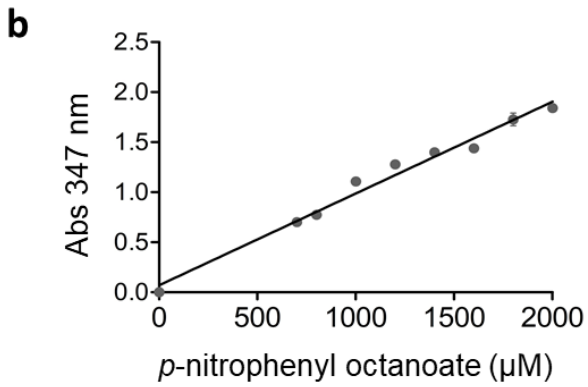

c

p-nitrophenyl octanoate (µM)	
TOTAL	FREE
700	255.71
750	273.975
800	292.24
850	310.505
900	328.77
1000	365.3
1200	438.36
1400	511.42
1600	584.48
1800	657.54
2000	730.6

Figure 27. Detection of free state substrate in the mix enzymatic reaction. (a) Represent the experimental method to determine the two proposed states of the substrate (*p*-nitrophenyl octanoate), SM and SF (explain in **Figure 26a**) in the reaction mix. The total mix reaction, without the enzyme, was incubated by 1 hour at 25 °C, then it was centrifuged in Amicon Ultra-4 Centrifugal filters (Merck Millipore 3 kDa) to remove the Triton X-100 micelles of the reaction. The filtered fraction that contained S_F was used to **(b)** Show the product vs substrate concentration plot using the filtered fraction of substrate (SF, free p-nitrophenyl octanoate). **c,** Show the total substrate used in each reaction (TOTAL) and the real substrate concentration free, found in the filtered fraction (FREE).

Table 4. Enzymatic kinetic data of Ade1. Kinetic parameters calculated from **Figure 22 b** and **c** using Hill-Langmuir or Michalis Menten model. The enzymatic assays were performed using 36 nM of Ade1. K_{half} is similar to Michaelis Menten constant (K_M).

Substrate	**V_{max} (µM s^{-1})**	**K_{half} (µM)**	**k_{cat} (s^{-1})#**	**k_{cat} / K_{half} (μM^{-1} s^{-1})**
p-nitrophenyl butyrate&	3.4 ± 0.1	391.7 ± 28.7	94.4 ± 2.8	0.241
p-nitrophenyl butyrate *&	3.4 ± 0.1	288.2 ± 12.1	94.4 ± 2.8	0.328
p-nitrophenyl butyrate!	1.68 ± 0.1	254.0 ± 24.5	46.7 ± 1.1	0.184
p-nitrophenyl butyrate *	3.0 ± 0.2	377.3 ± 30.0	83.3 ± 5.6	0.221
p-nitrophenyl octanoate	4.1 ± 0.1	171.3 ± 7.1	113.9 ± 2.8	0.665
p-nitrophenyl octanoate *	6.2 ± 0.3	171.3 ± 7.1	172.2 ± 8.3	1,005

* added 6mM Co^{2+}

& Without triton X-100 in the reaction buffer

$k_{cat} = V_{max}/[E]_{total}$

! Calculated based on Michalis Menten equation

4.4.2 *Hysteresis behavior evidence*

Hysteretic enzymes respond to substrate concentration change, which plays a key role in bacterial metabolic regulation (FRIEDEN, 1970; GOUTELLE; MAURIN; ROUGIER; BARBAUT *et al.*, 2008; RICARD; CORNISH-BOWDEN, 1987). It has been reported that the enzymatic hysteretic behavior can be dependent on both the structural aspects and the chemical nature of the substrate (MASSON; GOLDSTEIN; DEBOUZY; FROMENT *et al.*, 2004; RICARD; CORNISH-BOWDEN, 1987). It can be manifested as a transient burst or lag. In burst, it exhibits a high initial reaction velocity and then decrease and stabilize the velocity rate; in lag, it exhibits a low initial reaction velocity and, after, increases and stabilizes its velocity (EISENTHAL; DANSON, 2002). **Table 2** shows insights about different enzymes with hysteresis behavior, transient types (lag or burst), source organisms, biological functions, and if there is the presence or absence of metal during the enzymatic catalysis and/or optimal pH; thus, we noted that only 4 enzymes were attributed as a transient burst and 9 enzymes were characterized as transient lag. In general, the hysteresis behaviors of these enzymes are activated by temperature, metals, pH, or substrate type, and are directly associated with metabolic regulation.

Interestingly, we observed that Ade1 presents a transient burst profile along with the hydrolysis of the substrates p-nitrophenyl butyrate and *p*-nitrophenyl octanoate (**Figure 28**). Therefore, we classified the two conformational states, E1 and E2, which are directly associated with different initial velocities. E2 state has a bigger initial velocity than E1.

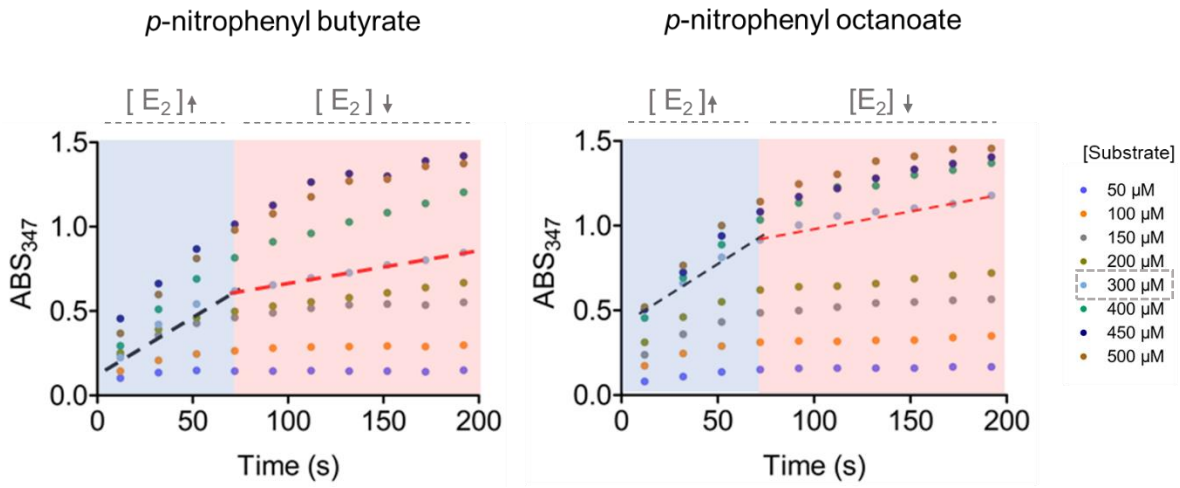

Figure 28. Ade1 kinetic activity presents a transient burst profile. Shows hydrolysis of *p*-nitrophenyl butyrate (left) and *p*-nitrophenyl octanoate (right) by Ade1 activity. According to both graphics, Ade1 has higher initial reaction velocity (black dotted lines) than steady-state velocity (red dotted lines). They are directly associated with high and low reaction velocities, respectively. Thus, Ade1 is classified as transient burst. E1 and E2 states represent the inactive and active catalytic states, respectively.

4.5 Computational simulations studies

4.5.1 *Structural analysis of the apo- and holo-states of Ade1*

In order to understand the structural changes during the Ade1 enzymatic process, we simulated it in its apo- and holo-states (using tributyrin as substrate). In **Figure 29a** is shown the root-mean-square fluctuation (RMSF) of both states of Ade1. Thus, we identified the residues 123-206 as a critical region, which involves predominantly the cap domain (residues 121-196). Interestingly, we have seen that this region is more flexible in Ade1 apo-state than in its holo-state (**Figure 29a**). An explanation for this event is that the substrate causes structural stability in the cap domain causing it to be more time in the closed conformation.

We noted that this high flexibility is associated with an opening and closing of the cap domain (enzymatic cavity) when calculating the angle formed by residues V127-L22-V194 (**Figure 29b**). Ade1 apo-state is kept the cap domain opened (~30°) from 0 to ~50 ns (corresponding to 50% of the time along MD simulation) (**Figure 29c**) and is directly associated with low conformational changes (**Figure 29d**). Afterward, Ade1 apo-state maintains its cap domain closed (~15°) from ~50 to 100 ns (**Figure 29c**), which is related to high conformational changes of the enzyme (**Figure 29d**). Conversely, Ade1 holo-state kept its cap domain during ~10 ns and, after, closed it along ~90 ns (**Figure 29e**). Such behaviors are correlated with high conformational changes of Ade1 (**Figure 29e**). These analyzes allowed us to define two states,

which are associated with the opening (E1 state) and closing (E2 state) of the cap domain. Interestingly, it has been described that MenH involved in the vitamin K biosynthetic pathway, an α/β-hydrolase, also has the same behavior of closing and opening of the cap domain (SUN; YIN; FENG; LI *et al.*, 2014). Conformational transition from open (inactive catalytic conformation) to closed (active catalytic conformation) involves movement of the cap domain. In the cap closed conformation, the side chain of the triad histidine changes for an energetically disfavored state to form the functional triad (SUN; YIN; FENG; LI *et al.*, 2014). The functional triad is activated when the histidine is closed to the nucleophilic serine to activate it to attack the substrate. Ade1 is in an equilibrium between E1 and E2 states in the absence and presence of substrate. Nevertheless, the presence of substrate changes its equilibrium constant, K_1, favoring Ade1 to be more time in the E2 state, which is consistent to a hysteresis behavior (**Figure 28** and **29**).

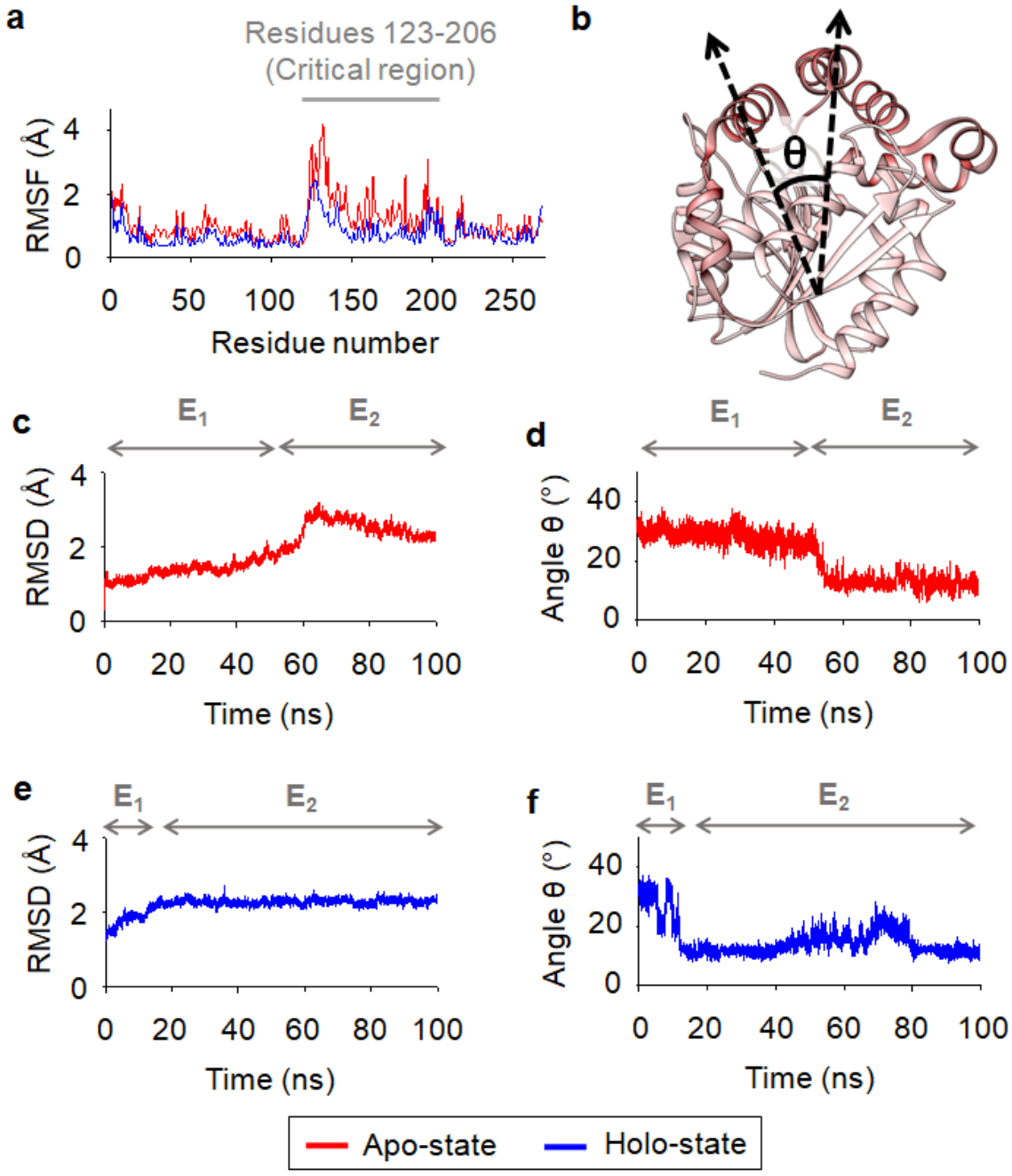

Figure 29. Substrate induces the cap domain closing for the catalysis pathway advance. The opening and closing of the cap domain are represented by the E1 and E2 states, respectively. **(a)** Esterase per-residue root-mean-square fluctuation (RMSF) plot according to color (red, apo-state; blue, holo-state). **(b)** The high fluctuation region, also called the critical region, is represented by residues 123-206. This region is highlighted in a dark red color. The closing angle (θ) was calculated using the coordinates formed by the main chain oxygen atoms of the V127, L27, and M194 residues. Closing angle plot as time function is shown on panel **(d)** and **(f)**. **(c)** Backbone root-mean-square deviation (RMSD) plot of apo-state. **(d)** Cap domain closing dynamics of Ade1 apo-state. **(e)** Backbone root-mean-square deviation (RMSD) plot of holo-state. **(f)** Cap domain closing dynamics of Ade1 holo-state.

4.5.2 *Ade1 S94 mutation to cysteine favors the E1 state (inactive catalytic conformation).*

Ade1 showed a similar structure with members of α/β-hydrolase, with cysteine hydrolase activity. Among them are the thioesterase GrgF (PDB ID: 6LZH), the nonribosomal peptide synthetase ObiF1 (PDB ID: 6N8E), and the phosphotriesterase P91 (PDB ID: 4ZI5). They are involved in the biosynthesis pathway of polyketide gregatin A (WANG; WANG; DU; LI *et al.*, 2020), in antimicrobial obafluorin biosynthetic pathway (KREITLER; GEMMELL; SCHAFFER; WENCEWICZ *et al.*, 2019), and in hydrolysis of phosphotriester hydrolysis, respectively. Therefore, it produced Ade1 mutant by changing the catalytic serine to a cysteine, $Ade1_{S94C}$, for investigating its enzymatic activity. The experimental assays show that $Ade1_{S94C}$ lost completely its enzymatic activity (**Figures 17** and **22**). In order to enhance a molecular understanding for these results, we performed molecular dynamics simulation using a $Ade1_{S94C}$ structure generated by changing the S94 to a cysteine in the wild type crystal structure. Since the structural coordinates of $Ade1_{S94C}$ presented a distance ~3 Å between C94 and C118, we initially hypothesized the activity lost would be due to the formation of a disulfide bond. To test our hypothesis, we examined if, restoring the nucleophilic nature of the thiol group of C94 in the presence of β-mercaptoethanol (reduction of disulfide bond C94-C118), we could detect any enzymatic activity. However, no activity was detected in our experimental set-up (data not shown).

To improve the molecular understanding of the inactivation caused by S94C mutant, we computed the angle formed by residues V127-L22-V194, sidechain RMSF, and backbone RMSD, and compared them to the wild type results (**Figure 30**). These results show that the structural flexibility of the cap domain of $Ade1_{S94C}$ apo-state exhibits a decrease of RMSF in relation to wild type (**Figure 30a**), suggesting that $Ade1_{S94C}$ visits mainly one structural conformation during the MD simulation. According to the RMSD plot, $Ade1_{S94C}$ is mainly in the E1 state (cap domain in the open conformation, **Figure 30b**). When compared with WT, $Ade1_{S94C}$ exhibits an enzymatic cavity essentially kept in the open conformation with an angle of ~40° (**Figure 30c**). Interestingly, we observed that the $Ade1^{S94C}$ holo-state also is affected in its RMSF (**Figure 30d**) and RMSD (**Figure 30e**) in relation to the Ade1 wild type. Sidechain RMSF, calculated using the $Ade1_{S94C}$ holo-state, revealed that the cap domain flexibility is slightly bigger than the Ade1 wild type, in mean ~0.6 Å (**Figure 30d**). Furthermore, we observed that $Ade1_{S94C}$ holo-sate is mainly in the E1 state and keeps the cap domain in an open conformation (inactive catalytic conformation) in contrast to the wild type that is mainly in the E2 state (closed conformation of the cap) (**Figure 30e**).

As a consequence, we observed a negative effect under the mutant structure, which prevented the closing of the enzymatic catalytic cavity, through the cap domain, for advancing the substrate hydrolysis (**Figure 30f**) consistent to the cap domain behavior for MenH (SUN; YIN; FENG; LI *et al.*, 2014). We also observed that Ade1$_{S94C}$ delayed 60 ns to close the cap domain when compared with WT, and it did not close completely to activate the catalytic triad (**Figure 30f**). In addition, we also have seen that there is an increase in the average distance between the mutant catalytic pair of 5.5 Å (C94 and H245) in comparison to wild type of ~3 Å (S94 and H245), causing its functional inactivation (**Figure 30 g** and **h**). This result demonstrates that the proton transfer step is disrupted between C94 and H245. These results suggest that in an eventual substrate capturing, the mutated enzyme is not able to close the cap domain for performing enzymatic catalysis progress.

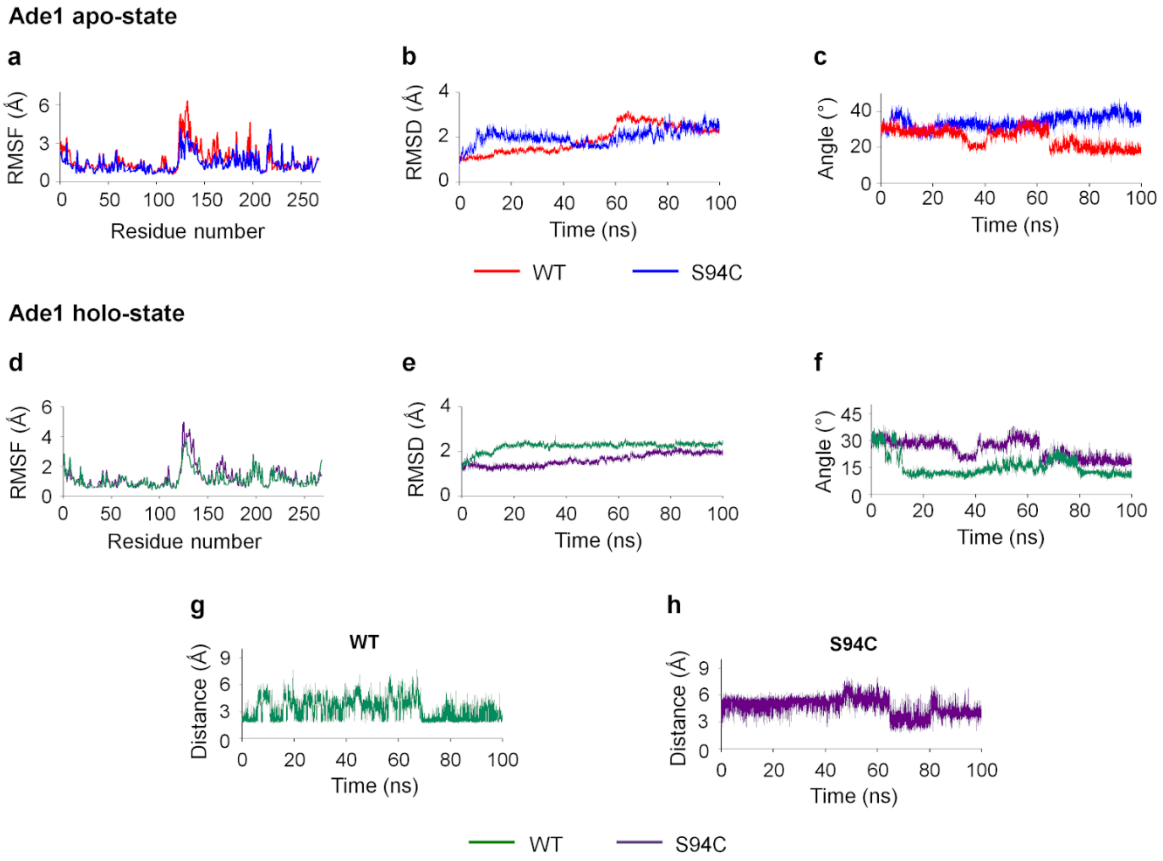

Figure 30. Structural analysis of Ade1S94C in its apo- and holo-state. Molecular dynamics simulation explains the loss of enzymatic activity of Ade1$_{S94C}$. **(a)** Side chain root-mean-square fluctuations (RMSF) of Ade1 and Ade1S94C apo-states (red and blue colors, respectively). **(b)** Backbone root-mean-square fluctuations (RMSD) of Ade1 and Ade1S94C apo-states (red and blue colors, respectively). **(c)** Closing angle (θ) was calculated using the coordinates formed by the main chain oxygen atoms of the V127, L27, and M194 residues. Closing angles of Ade1 and Ade1S94C holo-states are colored in red and blue colors, respectively. **(d)** Side chain root-mean-square fluctuations (RMSF) of Ade1 and Ade1S94C holo-states (green and purple colors, respectively). **(e)** Backbone root-mean-square fluctuations (RMSD) of Ade1 and Ade1S94C holo-states (red and blue colors,

respectively). **(f)** Closing angle of cap domain. The change from S94 to C94 prejudices the closing of the cap domain. Average distance between the pairs **(g)** S94/H245 and **(h)** C94/H245 increased from ~3 to ~5.5 Å, respectively.

5 CONCLUSIONS

Based on our results we conclude the following:

- Ade1 is a monomeric esterase.
- Ade1 is an esterase with enzymatic affinity for esters with aliphatic groups with less than 12 carbons and more than 4, such as: tributyrin (aliphatic chain with 4 carbons), Tween 20 (aliphatic chain with 12 carbons), N-hexanoyl-L-homoserine lactone (aliphatic chain with 6 carbons), activity *p*-nitrophenyl butyrate and *p*-nitrophenyl octanoate showing a degree of promiscuity in its enzymatic.
- Ade1 shows quorum-quenching activity *in vivo* against *Chromobacterium violaceum*.
- Ade1 is possibly a moonlighting protein because it could perform more than one biological function.
- Cobalt enhances Ade1 enzymatic activity while other divalent cation doesn't affect the enzymatic activity.
- We show that Ade1 has hysteresis behavior due to a presence of two conformational states, E1 and E2. Molecular dynamics simulations revealed that the E1 state has an open cap conformation (inactive catalytic conformation) while the E2 state has a closed cap domain (active catalytic conformation).
- Dynamics simulation between $Ade1_{WT}$ and $Ade1_{S94C}$, shows that the cysteine mutant favors the E1 state resulting in abolishment the experimental catalytic activity by keeping the enzyme in the open cap state (inactive catalytic conformation).

In summary, esterase are enzymes widely used in the food industry, pharmaceutical industries, and agriculture. They may also be applied in the degradation of industrial pollutants, plastics, and other toxic chemicals. Furthermore, they are also used in the synthesis of optically pure compounds, antioxidants, and perfumes (PANDA; GOWRISHANKAR, 2005). Understanding of the molecular bases, catalytic and structural mechanisms of Ade1 may be applied to other esterases of biotechnological, food, and/or pharmaceutical interest. In addition, our study enlarges the knowledge of the molecular mechanism of monomeric esterase with hysteresis behavior. Moreover, our data also suggest that Ade1 belongs to a bacterial metabolic pathway of a proteobacteria phylum bacterium

6 REFERENCES

ACHARI, G. A.; RAMESH, R. Characterization of quorum quenching enzymes from endophytic and rhizosphere colonizing bacteria. **Biocatalysis and Agricultural Biotechnology**, 13, p. 20-24, Jan 2018.

ADLER, A. J.; KISTIAKOWSKY, G. B. Kinetics of Pig Liver Esterase Catalysis. **Journal of the American Chemical Society**, 84, n. 5, p. 695-&, 1962.

AINSLIE, G. R.; NEET, K. E.; SHILL, J. P. Transients and Cooperativity - Slow Transition Model for Relating Transients and Cooperative Kinetics of Enzymes. **Journal of Biological Chemistry**, 247, n. 21, p. 7088-&, 1972.

ARPIGNY, J. L.; JAEGER, K. E. Bacterial lipolytic enzymes: classification and properties. **Biochemical Journal**, 343, p. 177-183, Oct 1 1999.

BAINS, J.; KAUFMAN, L.; FARNELL, B.; BOULANGER, M. J. A Product Analog Bound Form of 3-Oxoadipate-enol-Lactonase (PcaD) Reveals a Multifunctional Role for the Divergent Cap Domain. **Journal of Molecular Biology**, 406, n. 5, p. 649-658, Mar 11 2011.

BAO, Q.; HOSOE, A.; HOSOMI, M.; TERADA, A. Quorum quenching acylase impacts the viability and morphological change of Agrobacterium tumefaciens cells. **Journal of Bioscience and Bioengineering**, 2020.

BARBER, E. D.; BRIGHT, H. J. The rate of an allosteric process: inhibition of homoserine dehydrogenase I from E. coli by threonine. **Proceedings of the National Academy of Sciences of the United States of America**, 60, n. 4, p. 1363, 1968.

BAUER, T. L.; BUCHHOLZ, P. C. F.; PLEISS, J. The modular structure of alpha/beta-hydrolases. **Febs Journal**, 287, n. 5, p. 1035-1053, Mar 2020.

BEHZADI, A.; HATLESKOG, R.; RUOFF, P. Hysteretic enzyme adaptation to environmental pH: change in storage pH of alkaline phosphatase leads to a pH-optimum in the opposite direction to the applied change. **Biophysical chemistry**, 77, n. 2-3, p. 99-109, 1999.

BERGONZI, C.; SCHWAB, M.; ELIAS, M. The quorum-quenching lactonase from Geobacillus caldoxylosilyticus: purification, characterization, crystallization and crystallographic analysis. **Acta Crystallographica Section F: Structural Biology Communications**, 72, n. 9, p. 681-686, 2016.

BIJTENHOORN, P.; SCHIPPER, C.; HORNUNG, C.; QUITSCHAU, M. *et al.* BpiB05, a novel metagenome-derived hydrolase acting on N-acylhomoserine lactones. **Journal of Biotechnology**, 155, n. 1, p. 86-94, Aug 20 2011.

BIRMES, F. S.; SARING, R.; HAUKE, M. C.; RITZMANN, N. H. *et al.* Interference with Pseudomonas aeruginosa Quorum Sensing and Virulence by the Mycobacterial Pseudomonas Quinolone Signal Dioxygenase AqdC in Combination with the N-

Acylhomoserine Lactone Lactonase QsdA. **Infection and Immunity**, 87, n. 10, Oct 2019.

BRZOZOWSKI, A. M.; DEREWENDA, U.; DEREWENDA, Z. S.; DODSON, G. G. *et al.* A Model for Interfacial Activation in Lipases from the Structure of a Fungal Lipase-Inhibitor Complex. **Nature**, 351, n. 6326, p. 491-494, Jun 6 1991.

CARVALHO, C. F. **Caracterização funcional e estrutural de uma enzima lipolítica encontrada na biblioteca metagenômica de solo de Terra Preta de Índio**. 2015. -, Universidade de São Paulo.

CARVALHO, P. d. O.; CALAFATTI, S. A.; MARASSI, M.; SILVA, D. M. d. *et al.* Potencial de biocatálise enantiosseletiva de lipases microbianas. **Química Nova**, 2005.

COLQUHOUN, D. The quantitative analysis of drug-receptor interactions: a short history. **Trends in Pharmacological Sciences**, 27, n. 3, p. 149-157, Mar 2006.

CORNISH-BOWDEN, A.; CÁRDENAS, M. L. Co-operativity in monomeric enzymes. **Journal of theoretical biology**, 124, n. 1, p. 1-23, 1987.

CURTIS, T. P.; SLOAN, W. T. Exploring microbial diversity - A vast below. **Science**, 309, n. 5739, p. 1331-1333, Aug 26 2005.

CZAJKOWSKI, R.; JAFRA, S. Quenching of acyl-homoserine lactone-dependent quorum sensing by enzymatic disruption of signal molecules. **Acta Biochimica Polonica**, 56, n. 1, 2009.

CHAHINIAN, H.; SARDA, L. Distinction Between Esterases and Lipases: Comparative Biochemical Properties of Sequence-Related Carboxylesterases. **Protein and Peptide Letters**, 16, n. 10, p. 1149-1161, 2009.

CHATTERJEE, M.; D'MORRIS, S.; PAUL, V.; WARRIER, S. *et al.* Mechanistic understanding of Phenyllactic acid mediated inhibition of quorum sensing and biofilm development in Pseudomonas aeruginosa. **Applied Microbiology and Biotechnology**, 101, n. 22, p. 8223-8236, Nov 2017.

CHEN, C. N.; CHEN, C. J.; LIAO, C. T.; LEE, C. Y. A probable aculeacin A acylase from the Ralstonia solanacearum GMI1000 is N-acyl-homoserine lactone acylase with quorum-quenching activity. **Bmc Microbiology**, 9, May 9 2009.

CHOO, J. H.; RUKAYADI, Y.; HWANG, J. K. Inhibition of bacterial quorum sensing by vanilla extract. **Letters in Applied Microbiology**, 42, n. 6, p. 637-641, Jun 2006.

CHOW, J. Y.; WU, L.; YEW, W. S. Directed evolution of a quorum-quenching lactonase from Mycobacterium avium subsp. paratuberculosis K-10 in the amidohydrolase superfamily. **Biochemistry**, 48, n. 20, p. 4344-4353, 2009.

DE AQUINO, R. E.; MARQUES, J.; CAMPOS, M. C. C.; DE OLIVEIRA, I. A. *et al.* Characteristics of color and iron oxides of clay fraction in Archeological Dark Earth in Apui region, southern Amazonas. **Geoderma**, 262, p. 35-44, Jan 15 2016.

DONG, Y. H.; ZHANG, L. H. Quorum sensing and quorum-quenching enzymes. **Journal of Microbiology**, 43, p. 101-109, Feb 2005.

EISENTHAL, R.; DANSON, M. J. **Enzyme assays: a practical approach**. Practical Approach (Paperback), 2002. 0199638209.

ELLEUCHE, S.; SCHRÖDER, C.; ANTRANIKIAN, G. Lipolytic extremozymes from psychro-and (hyper-) thermophilic prokaryotes and their potential for industrial applications. *In*: **Biotechnology of Extremophiles:**: Springer, 2016. p. 351-374.

ESCHENFELDT, W. H.; STOLS, L.; ROSENBAUM, H.; KHAMBATTA, Z. S. *et al.* DNA from uncultured organisms as a source of 2, 5-diketo-D-gluconic acid reductases. **Applied and environmental microbiology**, 67, n. 9, p. 4206-4214, 2001.

FAN, X.; YE, T.; LI, Q.; BHATT, P. *et al.* Potential of a quorum quenching bacteria isolate Ochrobactrum intermedium D-2 against soft rot pathogen Pectobacterium carotovorum subsp. carotovorum. **Frontiers in Microbiology**, 11, p. 898, 2020.

FAN, X. J.; LIU, X. L.; LIU, Y. H. The cloning and characterization of one novel metagenome-derived thermostable esterase acting on N-acylhomoserine lactones. **Journal of Molecular Catalysis B-Enzymatic**, 83, p. 29-37, Nov 2012.

FETZNER, S. Quorum quenching enzymes. **Journal of Biotechnology**, 201, p. 2-14, Mar 27 2015.

FOJAN, P.; JONSON, P. H.; PETERSEN, M. T. N.; PETERSEN, S. B. What distinguishes an esterase from a lipase: A novel structural approach. **Biochimie**, 82, n. 11, p. 1033-1041, Nov 2000.

FOLOGEA, D.; KRUEGER, E.; MAZUR, Y. I.; STITH, C. *et al.* Bi-stability, hysteresis, and memory of voltage-gated lysenin channels. **Biochimica Et Biophysica Acta-Biomembranes**, 1808, n. 12, p. 2933-2939, Dec 2011.

FRIEDEN, C. Kinetic Aspects of Regulation of Metabolic Processes - Hysteretic Enzyme Concept. **Journal of Biological Chemistry**, 245, n. 21, p. 5788-&, 1970.

FRIEDEN, C. Slow transitions and hysteretic behavior in enzymes. **Annual review of biochemistry**, 48, n. 1, p. 471-489, 1979.

FUSHINOBU, S.; SAKU, T.; HIDAKA, M.; JUN, S. Y. *et al.* Crystal structures of a meta-cleavage product hydrolase from Pseudomonas fluorescens IP01 (CumD) complexed with cleavage products. **Protein Science**, 11, n. 9, p. 2184-2195, Sep 2002.

GOUTELLE, S.; MAURIN, M.; ROUGIER, F.; BARBAUT, X. *et al.* The Hill equation: a review of its capabilities in pharmacological modelling. **Fundamental & Clinical Pharmacology**, 22, n. 6, p. 633-648, Dec 2008.

GRANDCLEMENT, C.; TANNIERES, M.; MORERA, S.; DESSAUX, Y. *et al.* Quorum quenching: role in nature and applied developments. **Fems Microbiology Reviews**, 40, n. 1, p. 86-116, Jan 2016.

HABE, H.; MORII, K.; FUSHINOBU, S.; NAM, J. W. *et al.* Crystal structure of a histidine-tagged serine hydrolase involved in the carbazole degradation (CarC enzyme). **Biochemical and Biophysical Research Communications**, 303, n. 2, p. 631-639, Apr 4 2003.

HAND, S. C.; CARPENTER, J. F. pH-induced metabolic transitions in Artemia embryos mediated by a novel hysteretic trehalase. **Science**, 232, n. 4757, p. 1535-1537, 1986.

HIBLOT, J.; BZDRENGA, J.; CHAMPION, C.; CHABRIERE, E. *et al.* Crystal structure of VmoLac, a tentative quorum quenching lactonase from the extremophilic crenarchaeon Vulcanisaeta moutnovskia. **Scientific Reports**, 5, Feb 11 2015.

HITCH, T. C. A.; CLAVEL, T. A proposed update for the classification and description of bacterial lipolytic enzymes. **Peerj**, 7, Jul 8 2019.

HOFFSTEE, B. Specificity of esterases I. **Identification of two pancreatic aliesterases. B Biol Chem**, 199, p. 357-364, 1952.

HOLMQUIST, M. Alpha/Beta-Hydrolase Fold Enzymes: Structures, Functions and Mechanisms. **Current Protein & Peptide Science**, 1, n. 2, p. 209-235, Sep 2000.

HUANG, W.; LIN, Y. J.; YI, S. Y.; LIU, P. F. *et al.* QsdH, a Novel AHL Lactonase in the RND-Type Inner Membrane of Marine Pseudoalteromonas byunsanensis Strain 1A01261. **Plos One**, 7, n. 10, Oct 8 2012.

JAEGER, K. E.; STEINBUCHEL, A.; JENDROSSEK, D. Substrate Specificities of Bacterial Polyhydroxyalkanoate Depolymerases and Lipases - Bacterial Lipases Hydrolyze Poly(Omega-Hydroxyalkanoates). **Applied and Environmental Microbiology**, 61, n. 8, p. 3113-3118, Aug 1995.

JIANG, Y.; LI, X.; MORROW, B. R.; POTHUKUCHY, A. *et al.* Single-Molecule Mechanistic Study of Enzyme Hysteresis. **Acs Central Science**, 5, n. 10, p. 1691-1698, Oct 23 2019.

JOO, H.-S.; OTTO, M. Molecular basis of in vivo biofilm formation by bacterial pathogens. **Chemistry & biology**, 19, n. 12, p. 1503-1513, 2012.

KAKIRDE, K. S.; PARSLEY, L. C.; LILES, M. R. Size does matter: Application-driven approaches for soil metagenomics. **Soil Biology & Biochemistry**, 42, n. 11, p. 1911-1923, Nov 2010.

KALIA, V. C.; PATEL, S. K. S.; KANG, Y. C.; LEE, J. K. Quorum sensing inhibitors as antipathogens: biotechnological applications. **Biotechnology Advances**, 37, n. 1, p. 68-90, Jan-Feb 2019.

KE, T.; KLIBANOV, A. M. On enzymatic activity in organic solvents as a function of enzyme history. **Biotechnology and Bioengineering**, 57, n. 6, p. 746-750, Mar 20 1998.

KHUSHAIRI, Z. A.; SAMAD, K. A.; RAHMAN, N. A. A.; YUSSOF, H. W. *et al.* Application of Michaelis-Menten in the kinetics of oil palm frond enzymatic hydrolysis for ferulic acid production. **Sn Applied Sciences**, 2, n. 2, Feb 2020.

KISCH, J. M.; UTPATEL, C.; HILTERHAUS, L.; STREIT, W. R. *et al.* Pseudomonas aeruginosa Biofilm Growth Inhibition on Medical Plastic Materials by Immobilized Esterases and Acylase. **Chembiochem**, 15, n. 13, p. 1911-1919, Sep 5 2014.

KOVACIC, F.; BABIC, N.; KRAUSS, U.; JAEGER, K. Classification of lipolytic enzymes from bacteria. **Aerobic Utilization of Hydrocarbons, Oils, and Lipids**, 24, p. 255-289, 2019.

KREITLER, D. F.; GEMMELL, E. M.; SCHAFFER, J. E.; WENCEWICZ, T. A. *et al.* The structural basis of N-acyl-α-amino-β-lactone formation catalyzed by a nonribosomal peptide synthetase. **Nature communications**, 10, n. 1, p. 1-13, 2019.

KRISSINEL, E.; HENRICK, K. Inference of macromolecular assemblies from crystalline state. **Journal of Molecular Biology**, 372, n. 3, p. 774-797, Sep 21 2007.

KROH, H. K.; PANIZZI, P.; BOCK, P. E. Von Willebrand factor-binding protein is a hysteretic conformational activator of prothrombin. **Proceedings of the National Academy of Sciences**, 106, n. 19, p. 7786-7791, 2009.

LAI, L. S.; XU, Z. H.; ZHOU, J. H.; LEE, K. D. *et al.* Molecular basis of prodrug activation by human valacyclovirase, an alpha-amino acid ester hydrolase. **Journal of Biological Chemistry**, 283, n. 14, p. 9318-9327, Apr 4 2008.

LARSEN, N. A.; TURNER, J. M.; STEVENS, J.; ROSSER, S. J. *et al.* Crystal structure of a bacterial cocaine esterase. **Nature Structural Biology**, 9, n. 1, p. 17-21, Jan 2002.

LEE, C. W.; KWON, S.; PARK, S. H.; KIM, B. Y. *et al.* Crystal Structure and Functional Characterization of an Esterase (EaEST) from Exiguobacterium antarcticum. **Plos One**, 12, n. 1, Jan 26 2017.

LEE, L. P.; KARBUL, H. M.; CITARTAN, M.; GOPINATH, S. C. *et al.* Lipase-secreting Bacillus species in an oil-contaminated habitat: promising strains to alleviate oil pollution. **BioMed research international**, 2015, 2015.

LEE, M. H.; KHAN, R.; TAO, W.; CHOI, K. *et al.* Soil metagenome-derived 3-hydroxypalmitic acid methyl ester hydrolases suppress extracellular polysaccharide production in Ralstonia solanacearum. **Journal of Biotechnology**, 270, p. 30-38, Mar 20 2018.

LENFANT, N.; HOTELIER, T.; BOURNE, Y.; MARCHOT, P. *et al.* Proteins with an alpha/beta hydrolase fold: Relationships between subfamilies in an ever-growing superfamily. **Chemico-Biological Interactions**, 203, n. 1, p. 266-268, Mar 25 2013.

LEVISSON, M.; SUN, L.; HENDRIKS, S.; SWINKELS, P. *et al.* Crystal Structure and Biochemical Properties of a Novel Thermostable Esterase Containing an Immunoglobulin-Like Domain. **Journal of Molecular Biology**, 385, n. 3, p. 949-962, Jan 23 2009.

LIE, A.; MEYER, A. S.; PEDERSEN, L. H. Appearance and distribution of regioisomers in metallo-and serine-protease-catalysed acylation of sucrose in N, N-dimethylformamide. **Journal of Molecular Catalysis B: Enzymatic**, 106, p. 26-31, 2014.

LILLO, C.; RUOFF, P. Hysteretic behavior of nitrate reductase. Evidence of an allosteric binding site for reduced pyridine nucleotides. **Journal of Biological Chemistry**, 267, n. 19, p. 13456-13459, 1992.

LIN, Y. H.; XU, J. L.; HU, J. Y.; WANG, L. H. *et al.* Acyl-homoserine lactone acylase from Ralstonia strain XJ12B represents a novel and potent class of quorum-quenching enzymes. **Molecular Microbiology**, 47, n. 3, p. 849-860, Feb 2003.

LINDBERG, D.; DE LA FUENTE REVENGA, M.; WIDERSTEN, M. Temperature and pH dependence of enzyme-catalyzed hydrolysis of trans-methylstyrene oxide. A unifying kinetic model for observed hysteresis, cooperativity, and regioselectivity. **Biochemistry**, 49, n. 10, p. 2297-2304, 2010.

LIU, D.; MOMB, J.; THOMAS, P. W.; MOULIN, A. *et al.* Mechanism of the quorum-quenching lactonase (AiiA) from Bacillus thuringiensis. 1. Product-bound structures. **Biochemistry**, 47, n. 29, p. 7706-7714, Jul 22 2008.

LIU, X. W.; CAO, L. C.; FAN, X. J.; LIU, Y. H. *et al.* Engineering of a thermostable esterase Est816 to improve its quorum-quenching activity and the underlying structural basis. **Scientific Reports**, 6, Dec 2 2016.

MAHMOUDI, E.; NADERI, D.; VENTURI, V. AiiA lactonase disrupts N-acylhomoserine lactone and attenuates quorum-sensing-related virulence in Pectobacterium carotovorum EMPCC. **Annals of Microbiology**, 63, n. 2, p. 691-697, Jun 2013.

MARTINELLI, D.; GROSSMANN, G.; SEQUIN, U.; BRANDL, H. *et al.* Effects of natural and chemically synthesized furanones on quorum sensing in Chromobacterium violaceum. **Bmc Microbiology**, 4, Jul 2 2004.

MASSON, P.; GOLDSTEIN, B. N.; DEBOUZY, J. C.; FROMENT, M. T. *et al.* Damped oscillatory hysteretic behaviour of butyrylcholinesterase with benzoylcholine as substrate. **European Journal of Biochemistry**, 271, n. 1, p. 220-234, Jan 2004.

MASSON, P.; SCHOPFER, L. M.; FROMENT, M.-T.; DEBOUZY, J.-C. *et al.* Hysteresis of butyrylcholinesterase in the approach to steady-state kinetics. **Chemico-biological interactions**, 157, p. 143-152, 2005.

MCCLEAN, K. H.; WINSON, M. K.; FISH, L.; TAYLOR, A. *et al.* Quorum sensing and Chromobacterium violaceum: exploitation of violacein production and inhibition for the detection of N-acylhomoserine lactones. **Microbiology-Uk**, 143, p. 3703-3711, Dec 1997.

MILLER, M. B. a Bonnie L. BASSLER. **Quorum Sensing in Bacteria. Annual Review of Microbiology**, 55, n. 1, p. 165-199, 2001.

MINDREBO, J. T.; NARTEY, C. M.; SETO, Y.; BURKARTL, M. D. *et al*. Unveiling the functional diversity of the alpha/beta hydrolase superfamily in the plant kingdom (vol 41, pg 233, 2016). **Current Opinion in Structural Biology**, 41, p. 256-257, Dec 2016.

MISAWA, E.; CHION, C. K. C. C. K.; ARCHER, I. V.; WOODLAND, M. P. *et al.* Characterisation of a catabolic epoxide hydrolase from a Corynebacterium sp. **European Journal of Biochemistry**, 253, n. 1, p. 173-183, Apr 1 1998.

MURUGAYAH, S. A.; GERTH, M. L. Engineering quorum quenching enzymes: progress and perspectives. **Biochemical Society Transactions**, 47, p. 793-800, Jun 28 2019.

NACKE, H.; WILL, C.; HERZOG, S.; NOWKA, B. *et al.* Identification of novel lipolytic genes and gene families by screening of metagenomic libraries derived from soil samples of the German Biodiversity Exploratories. **FEMS microbiology ecology**, 78, n. 1, p. 188-201, 2011.

NAVARRETE, A. A.; CANNAVAN, F. S.; TAKETANI, R. G.; TSAI, S. M. A Molecular Survey of the Diversity of Microbial Communities in Different Amazonian Agricultural Model Systems. **Diversity**, 2, n. 5, p. 787-809, 2010.

OHLEMACHER, S. I.; XU, Y. Q.; KOBER, D. L.; MALIK, M. *et al.* YbtT is a low-specificity type II thioesterase that maintains production of the metallophore yersiniabactin in pathogenic enterobacteria. **Journal of Biological Chemistry**, 293, n. 51, p. 19572-19585, Dec 21 2018.

ORNSTON, L. N. The Conversion of Catechol and Protocatechuate to β-Ketoadipate by Pseudomonas putida : IV. REGULATION. **Journal of Biological Chemistry**, 241, n. 16, p. 3800-3810, August 25, 1966 1966.

PANDA, T.; GOWRISHANKAR, B. Production and applications of esterases. **Applied microbiology and biotechnology**, 67, n. 2, p. 160-169, 2005.

PETTERSEN, E. F.; GODDARD, T. D.; HUANG, C. C.; COUCH, G. S. *et al.* UCSF chimera - A visualization system for exploratory research and analysis. **Journal of Computational Chemistry**, 25, n. 13, p. 1605-1612, Oct 2004.

PIEWNGAM, P.; CHIOU, J.; CHATTERJEE, P.; OTTO, M. Alternative approaches to treat bacterial infections: targeting quorum-sensing. **Expert Review of Anti-Infective Therapy**, 18, n. 6, p. 499-510, Jun 2 2020.

PORTER, C. M.; MILLER, B. G. Cooperativity in monomeric enzymes with single ligand-binding sites. **Bioorganic Chemistry**, 43, p. 44-50, Aug 2012.

PUSTELNY, C.; ALBERS, A.; BULDT-KARENTZOPOULOS, K.; PARSCHAT, K. *et al*. Dioxygenase-Mediated Quenching of Quinolone-Dependent Quorum Sensing in Pseudomonas aeruginosa. **Chemistry & Biology**, 16, n. 12, p. 1259-1267, Dec 24 2009.

QIAN, H.; ELSON, E. L. Single-molecule enzymology: stochastic Michaelis-Menten kinetics. **Biophysical Chemistry**, 101, p. 565-576, Dec 10 2002.

RAMNATH, L.; SITHOLE, B.; GOVINDEN, R. Identification of lipolytic enzymes isolated from bacteria indigenous to Eucalyptus wood species for application in the pulping industry. **Biotechnology Reports**, 15, p. 114-124, 2017/09/01/ 2017.

RICARD, J.; CORNISH-BOWDEN, A. Co-operative and allosteric enzymes: 20 years on. **European Journal of Biochemistry**, 166, n. 2, p. 255-272, 1987.

ROWE, P. B.; COLEMAN, M. D.; WYNGAARDEN, J. B. Glutamine phosphoribosylpyrophosphate amidotransferase. Catalytic and conformation heterogeneity of the pigeon liver enzyme. **Biochemistry**, 9, n. 7, p. 1498-1505, 1970.

RYU, D. H.; LEE, S. W.; MIKOLAITYTE, V.; KIM, Y. W. *et al.* Identification of a Second Type of AHL-Lactonase from Rhodococcus sp. BH4, belonging to the alpha/beta Hydrolase Superfamily. **Journal of Microbiology and Biotechnology**, 30, n. 6, p. 937-945, Jun 2020.

SAKU, T.; FUSHINOBU, S.; JUN, S.-Y.; IKEDA, N. *et al.* Purification, characterization, and steady-state kinetics of a meta-cleavage compound hydrolase from Pseudomonas fluorescens IPO1. **Journal of Bioscience and Bioengineering**, 93, n. 6, p. 568-574, 2002/01/01/ 2002.

SANGEETHA, R.; ARULPANDI, I.; GEETHA, A. Bacterial lipases as potential industrial biocatalysts: An overview. **Research journal of microbiology**, 6, n. 1, p. 1, 2011.

SAYER, C.; ISUPOV, M. N.; BONCH-OSMOLOVSKAYA, E.; LITTLECHILD, J. A. Structural studies of a thermophilic esterase from a new Planctomycetes species, Thermogutta terrifontis. **The FEBS journal**, 282, n. 15, p. 2846-2857, 2015.

SCHLÖMANN, M.; SCHMIDT, E.; KNACKMUSS, H. Different types of dienelactone hydrolase in 4-fluorobenzoate-utilizing bacteria. **Journal of bacteriology**, 172, n. 9, p. 5112-5118, 1990.

SHENOUDA, J.; GREEN, P.; SULTATOS, L. An evaluation of the inhibition of human butyrylcholinesterase and acetylcholinesterase by the organophosphate

chlorpyrifos oxon. **Toxicology and Applied Pharmacology**, 241, n. 2, p. 135-142, Dec 1 2009.

SHILL, J.; NEET, K. A slow transient kinetic process of yeast hexokinase. **Biochemical Journal**, 123, n. 2, p. 283-285, 1971.

SHINOHARA, M.; NAKAJIMA, N.; UEHARA, Y. Purification and characterization of a novel esterase (beta-hydroxypalmitate methyl ester hydrolase) and prevention of the expression of virulence by Ralstonia solanacearum. **Journal of Applied Microbiology**, 103, n. 1, p. 152-162, Jul 2007.

SIEVERS, F.; HIGGINS, D. G. Clustal Omega for making accurate alignments of many protein sequences. **Protein Science**, 27, n. 1, p. 135-145, Jan 2018.

SILVA, L. B. d. Diversidade microbiana dos solos de Terra Preta de Índio e de Terra Mulata da Amazônia Ocidental. 2009.

SIMON, C.; DANIEL, R. Metagenomic Analyses: Past and Future Trends. **Applied and Environmental Microbiology**, 77, n. 4, p. 1153-1161, Feb 2011.

SOULIE, J. M.; RIVIERE, M.; RICARD, J. Enzymes as biosensors: 2. Hysteretic response of chloroplastic fructose-1, 6-bisphosphatase to fructose 2, 6-bisphosphate. **European journal of biochemistry**, 176, n. 1, p. 111-117, 1988.

STAN, R. C.; BHATT, D. K.; DE CAMARGO, M. M. Cellular Adaptation Relies on Regulatory Proteins Having Episodic Memory Proteins Modulate Cell Metabolism and Reproduction by Remembering, Transmitting, and Using Data on the Environment. **Bioessays**, 42, n. 1, Jan 2020.

SUN, Y. R.; YIN, S. H.; FENG, Y. T.; LI, J. *et al.* Molecular Basis of the General Base Catalysis of an alpha/beta-Hydrolase Catalytic Triad. **Journal of Biological Chemistry**, 289, n. 22, p. 15867-15879, May 30 2014.

TAO, W.; LEE, M. H.; WU, J.; KIM, N. H. *et al.* Isolation and Characterization of a Family VII Esterase Derived from Alluvial Soil Metagenomic Library. **Journal of Microbiology**, 49, n. 2, p. 178-185, Apr 2011.

TARMY, E.; KAPLAN, N. O. Kinetics of Escherichia coli B D-lactate dehydrogenase and evidence for pyruvate-controlled change in conformation. **Journal of Biological Chemistry**, 243, n. 10, p. 2587-2596, 1968.

THOMAS, T.; GILBERT, J.; MEYER, F. Metagenomics-a guide from sampling to data analysis. **Microbial informatics and experimentation**, 2, n. 1, p. 3, 2012.

TORRES, M.; UROZ, S.; SALTO, R.; FAUCHERY, L. *et al.* HqiA, a novel quorum-quenching enzyme which expands the AHL lactonase family. **Scientific Reports**, 7, Apr 19 2017.

TORSVIK, V.; OVREAS, L. Microbial diversity and function in soil: from genes to ecosystems. **Current Opinion in Microbiology**, 5, n. 3, p. 240-245, Jun 2002.

TUOMINEN, F. W.; BERNLOHR, R. W. Pyruvate Kinase of the Spore-forming Bacterium, Bacillus licheniformis II. KINETIC PROPERTIES. **Journal of Biological Chemistry**, 246, n. 6, p. 1746-1755, 1971.

UROZ, S.; OGER, P. M.; CHAPELLE, E.; ADELINE, M.-T. *et al.* A Rhodococcus qsdA-encoded enzyme defines a novel class of large-spectrum quorum-quenching lactonases. **Applied and environmental microbiology**, 74, n. 5, p. 1357-1366, 2008.

VERGER, R. 'Interfacial activation' of lipases: Facts and artifacts. **Trends in Biotechnology**, 15, n. 1, p. 32-38, Jan 1997.

VERPOORTE, J. A.; MEHTA, S.; EDSALL, J. T. Esterase Activities of Human Carbonic Anhydrases B and C. **Journal of Biological Chemistry**, 242, n. 18, p. 4221-+, 1967.

VERSCHUEREN, K. H. G.; SELJEE, F.; ROZEBOOM, H. J.; KALK, K. H. *et al.* Crystallographic Analysis of the Catalytic Mechanism of Haloalkane Dehalogenase. **Nature**, 363, n. 6431, p. 693-698, Jun 24 1993.

VILLAVICENCIO-QUEIJEIRO, A.; PARDO, J. P.; GONZÁLEZ-HALPHEN, D. Kinetic and hysteretic behavior of ATP hydrolysis of the highly stable dimeric ATP synthase of Polytomella sp. **Archives of biochemistry and biophysics**, 575, p. 30-37, 2015.

VIVOLI, M.; PANG, J. Y.; HARMER, N. J. A half-site multimeric enzyme achieves its cooperativity without conformational changes. **Scientific Reports**, 7, Nov 28 2017.

VOGET, S.; LEGGEWIE, C.; UESBECK, A.; RAASCH, C. *et al.* Prospecting for novel biocatalysts in a soil metagenome. **Applied and environmental microbiology**, 69, n. 10, p. 6235-6242, 2003.

WANG, T. N.; GUAN, Q. T.; PAIN, A.; KAKSONEN, A. H. *et al.* Discovering, Characterizing, and Applying Acyl Homoserine Lactone-Quenching Enzymes to Mitigate Microbe-Associated Problems Under Saline Conditions. **Frontiers in Microbiology**, 10, Apr 17 2019.

WANG, W.-G.; WANG, H.; DU, L.-Q.; LI, M. *et al.* Molecular Basis for the Biosynthesis of an Unusual Chain-Fused Polyketide, Gregatin A. **Journal of the American Chemical Society**, 142, n. 18, p. 8464-8472, 2020.

WANG, Y.; DAI, Y.; ZHANG, Y.; HU, Y. B. *et al.* Effects of quorum sensing autoinducer degradation gene on virulence and biofilm formation of Pseudomonas aeruginosa. **Science in China Series C-Life Sciences**, 50, n. 3, p. 385-391, Jun 2007.

WARD, B. B. How many species of prokaryotes are there? **Proceedings of the National Academy of Sciences of the United States of America**, 99, n. 16, p. 10234-10236, Aug 6 2002.

WEISSMANN, B.; WANG, C.-T. Association-dissociation and abnormal kinetics of bovine. alpha.-acetylgalactosaminidase. **Biochemistry**, 10, n. 6, p. 1067-1072, 1971.

WILLERDING, A. L.; OLIVEIRA, L. A. d.; MOREIRA, F. W.; GERMANO, M. G. *et al.* Lipase Activity among Bacteria Isolated from Amazonian Soils. **Enzyme Research**, 2011, p. 720194, 2011/10/09 2011.

XU, J. Invited review: microbial ecology in the age of genomics and metagenomics: concepts, tools, and recent advances. **Molecular ecology**, 15, n. 7, p. 1713-1731, 2006.

YANG, F.; WANG, L. H.; WANG, J.; DONG, Y. H. *et al.* Quorum quenching enzyme activity is widely conserved in the sera of mammalian species. **Febs Letters**, 579, n. 17, p. 3713-3717, Jul 4 2005.

YE, T.; ZHANG, W.; FENG, Z.; FAN, X. *et al.* Characterization of a Novel Quorum-Quenching Bacterial Strain, Burkholderia anthina HN-8, and Its Biocontrol Potential against Black Rot Disease Caused by Xanthomonas campestris pv. campestris. **Microorganisms**, 8, n. 10, p. 1485, 2020.

YE, T.; ZHOU, T.; FAN, X. H.; BHATT, P. *et al.* Acinetobacter lactucae Strain QL-1, a Novel Quorum Quenching Candidate Against Bacterial Pathogen Xanthomonas campestris pv. campestris. **Frontiers in Microbiology**, 10, Dec 17 2019.

YE, T.; ZHOU, T.; XU, X.; ZHANG, W. *et al.* Whole-genome sequencing analysis of quorum quenching bacterial strain Acinetobacter lactucae QL-1 identifies the FadY enzyme for degradation of the diffusible signal factor. **International journal of molecular sciences**, 21, n. 18, p. 6729, 2020.

ZAINOL, N.; ISMAIL, S. N. Evaluation of Enzyme Kinetic Parameters to Produce Methanol Using Michaelis-Menten Equation. **Bulletin of Chemical Reaction Engineering and Catalysis**, 14, n. 2, p. 436-442, Aug 2019.

ZHANG, B.; ZHUANG, X.; GUO, L.; MCLEAN, R. J. C. *et al.* Recombinant N-acyl homoserine lactone-Lactonase AiiAQSI-1 Attenuates Aeromonas hydrophila Virulence Factors, Biofilm Formation and Reduces Mortality in Crucian Carp. **Marine Drugs**, 17, n. 9, p. 499, 2019.

ZHANG, W.; LUO, Q.; ZHANG, Y.; FAN, X. *et al.* Quorum Quenching in a Novel Acinetobacter sp. XN-10 Bacterial Strain against Pectobacterium carotovorum subsp. carotovorum. **Microorganisms**, 8, n. 8, p. 1100, 2020.

ZILLI, J. É.; RUMJANEK, N. G.; XAVIER, G. R.; DA COSTA COUTINHO, H. L. *et al.* Diversidade microbiana como indicador de qualidade do solo. **Cadernos de Ciência & Tecnologia**, 20, n. 3, p. 391-411, 2003.